University of Thessaly
School of Engineering
Department of Mechanical Engineering

Energy balance and cycle-to-cycle pressure variation in a single cylinder diesel engine

Thesis
Submitted in partial fulfillment of the requirements for the degree of Master of Science of the Department of Mechanical Engineering University of Thessaly

BY

Dimitrios K. Tsokolis
Dipl. Chemical Engineer

Advisory Committee:
Prof. A. M. Stamatellos, supervisor
Assoc. Prof. N. Pelekasis
Assis. Prof. A. Stamatis

Volos 2012

Abstract

Steady state in-cylinder pressure measurements of a single cylinder diesel engine operating on neat diesel fuel have been conducted during September – December 2011 in the Laboratory of Thermodynamics and Thermal Engines, Department of Mechanical Engineering, University of Thessaly. Our engine operated on 2000, 2200, 2400, 2600, 2800, 2900 and 3100 rpm with no load or one, two, three resistances operating. Our purpose was to investigate the engine's P-V diagrams under steady state operating conditions. Thus, various values have been measured (e.g A/F, exhaust temperature, fuel consumption etc), the engine's efficiency and pie charts have been calculated and a COV study was performed. The major observation of this thesis was a pressure instability during the engine's combustion phase, that seemed to be affected from rpm and have been attributed to our experimental setup.

Acknowledgements

For the fulfillment of this thesis, I would like to thank the various people contributed, each one in a different way. Professor Anastasios Stamatellos for his scientific advices for this thesis and his support this one-and-a-half year this Master program lasted, Associate Professor Nikolaos Pelekasis for his remarks and Assistant Professor Anastasios Stamatis for both his scientific and friendly advices over me. Also I would like to thank the PhD candidate Dimitrios Tziourtzoumis for his opinions in this thesis and for being a pleasant company during the experiments and the other two members of the Laboratory of Thermodynamics and Thermal Engines, undergraduate student Fotis Bouroutzikas and PhD candidate Diamantis Bakalis. Last, I would like to thank Lefteris Benos, Petros Christodoulou and Nikos Polychronopoulos for making this Master program memorable and a once in a lifetime experience.

Contents

List of figures

List of tables

Nomenclature

Symbols

F	Force
f	Frequency
h_a	Specific air enthalpy
h_e	Exhaust enthalpy
$\dot{H}_{e,ic}$	Exhaust enthalpy loss due to incomplete combustion
h_f	Specific fuel enthalpy
$\bar{h}^o_{RP}$	Enthalpy of combustion
I	Current
$\dot{m}_a$	Mass air enthalpy
$\dot{m}_f$	Mass fuel flow rate
N	Crankshaft rotational speed
$\dot{n}_F$	Molar flow rate of the fuel
P	Cylinder pressure
P_b	Engine's brake power
P_f	Engine's friction power
$P_{generator}$	Power produced at the generator
P_i	Power per cylinder per i cycle
$\dot{Q}_{cool}$	Heat transfer rate to the cooling medium
$\dot{Q}_{CV}$	Heat flow rate to the control volume
Q_{LHV}	Fuel's lower heating value
$\dot{Q}_{misc}$	Heat rejected to the oil plus convection and radiation from the engine's external surface
R	Connecting rod length/crank radius
r_c	Compression ratio
T	Torque
U	Voltage
V or V_c	Volume, cylinder volume
V_d	Displaced cylinder volume
$W_{c,i}$	Work per i cycle

$\dot{W}_{CV}$	Power obtained from the control volume
η	Generator's mechanical efficiency

Acronyms

A/F	Air to fuel ratio
bTDC	Before top dead center
CFD	Computational fluid dynamics
CA	Crank angle
COV	Coefficient of variation
DI	Direct injection
DPF	Diesel particulate filter
IC	Internal combustion
IDI	Indirect injection
imep	Indicated mean effective pressure
LNV	Lowest normalized value
LTTE	Laboratory of thermodynamics and thermal engines
MTV	Mollecular tagging velocimetry
PI	Proportional-integral
PM	Particulate matter
RANS	Reynolds averaged Navier-Stokes
rpm	Revolutions per minute
TDC	Top dead center
UEGO	Universal exhaust gas oxygen

1 Introduction

Combustion is the act or process of burning something. We can also define combustion as the chemical reaction of a particular substance, usually a fuel, with an oxidant (in most cases atmospheric oxygen).

The combustion process in internal combustion engines takes places in the engine's cylinder. It is of paramount importance for a combustion researcher to investigate the in-cylinder pressure in order to further understand the combustion [1] because in-cylinder pressure and combustion are closely correlated. This fact makes the in-cylinder pressure one of the most important measurable quantities in internal combustion engines [2].

The investigation of the variations taking place during the individual combustion cycles showed that for successive operating cycles, considerable pressure variations exist. These variations affect the performance characteristics of the engine making them a large domain of scientific interest.

To adapt the investigation of pressure variation in the current research trends in automobile, it is advanced to operate an engine on biodiesel fuel apart from diesel fuel.

1.1 Starting point and objectives of this thesis

Zeibekis was the first one in the Laboratory of Thermodynamics and Thermal Engines (LTTE) who set up the engine in which the experiments of the current thesis took place. Zeibekis set up the engine, mapped it and measured the loading-regeneration characteristics of the diesel particulate filter (DPF) equipped on the engine [3]. Furthermore, Melissourgos developed a LabView code for a P-V diagram in the same engine [4].

In order to better understand the combustion in the same engine it has been asked to the author of this thesis to investigate the cycle-to-cycle pressure variation when the engine operated on diesel fuel.

Starting from the previous work done [3, 4], after its evaluation and set the engine with all its components working properly, the most crucial part of this thesis was the development of a code for the isolation of a combustion cycle from the experimental data.

1.2 Overview of this thesis

Chapter 2 contains brief information about the diesel engine (history, operation, basic relations) and a study of specialized literature on cyclic variations. Chapter 3 presents analytically the experimental setup and the testing procedure and chapter 4 includes the results and their explanation. Finally, the conclusions made from this work plus suggestions for further investigation on the engine are discussed in chapter 5.

2 Literature study

2.1 Diesel engine background information

2.1.1 Brief history of diesel engine

The compression ignition engine made its appearance in 1892 when Rudolf Diesel filled a patent for "a new rational engine" and granted it one year later for the "Working Method and Design for Combustion Engines". After four years developing his idea, in 1987 Diesel presented his results at the Association of German Engineers. He demonstrated a heat engine with efficiency reaching 26.2% [5]. From that day, diesel engine never stopped evolving, raising its efficiency, lowering its size, reducing its emissions etc.

2.1.2 Engine operation

The diesel engine is a device which converts fuel energy to mechanical energy. The fuel energy is converted to thermal energy via combustion and the thermal energy to mechanical energy through expansion. A piston placed in a cylinder moves up and down and transmits the useful work from combustion. This is achieved from a procedure which consists of four strokes (at least the majority of internal combustion engines) of the piston, the four stroke cycle. The four strokes are (Figure 2.1):

1. *The intake stroke*, where the fresh mixture enters the cylinder.
2. *The compression stroke*, where the piston compresses the mixture inside the cylinder. In this stroke, the combustion is initiated.
3. *The power/expansion stroke*, where the mixture burns and the temperature and pressure of the mixture rise pushing the piston down, producing work.

4. *The exhaust stroke*, where the remaining gases exit the cylinder [6].

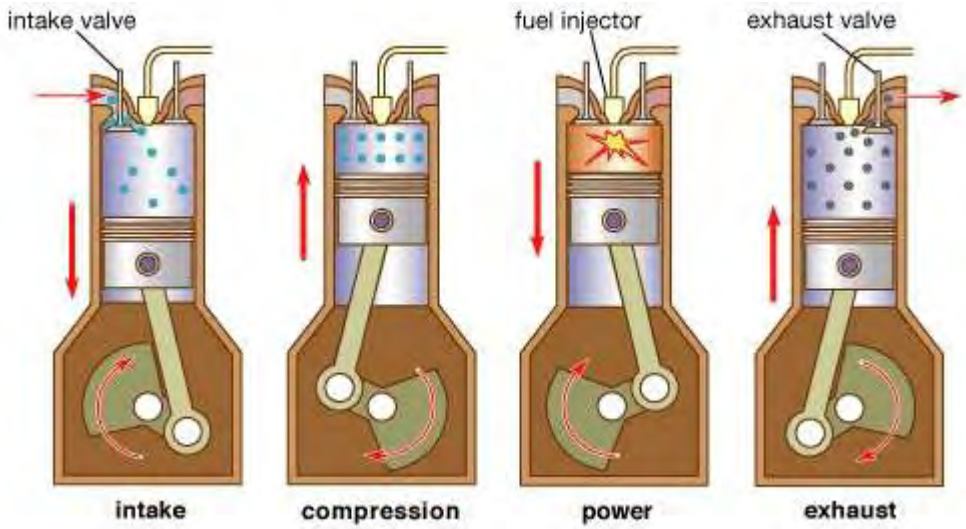

Figure 2.1: The four stroke operating cycle [7].

The basic operating principal of the diesel engine can be summed up as follows. Air enters the cylinder through the intake valve and is been compressed. That compression raises the air's pressure and temperature. Then the fuel from the injector enters the cylinder and vaporizes and mixes with the in cylinder air. At this state, the air's temperature and pressure are above the fuel's ignition point. Thus, after a short delay the combustion between the air-fuel mixture occurs (Figure 2.1).

2.1.3 Basic relations for calculations

In order to study our engine it is essential to know the equations governing its operation. The equations are common and widespread in bibliography [5, 6, 8].
Assuming we measure the in-cylinder pressure at various crank angle (θ), we can calculate the cylinder volume V at each crank angle from

$$\frac{V}{V_c} = 1 + \frac{(r_c - 1)}{2}\left[R + 1 - \cos\theta - \left(R^2 - \sin^2\theta \right)^{1/2} \right] \quad (1)$$

or equally from

$$V = \frac{V_d}{r_c - 1} + \frac{V_d}{2}\left[R + 1 - \cos\theta - \left(R^2 - \sin^2\theta \right)^{1/2} \right] \quad (2)$$

where V_c is the clearance volume, r_c is the engine's compression ratio, R the connecting rod length to crank radius and V_d the cylinder's displaced volume.

The indicated work per cycle and cylinder ($W_{c,i}$) can be calculated from the integration of a typical P-V diagram from experimental data:

$$W_{c,i} = \oint P dV \quad (3)$$

A P-V diagram from experimental data is shown in Figure 2.2.

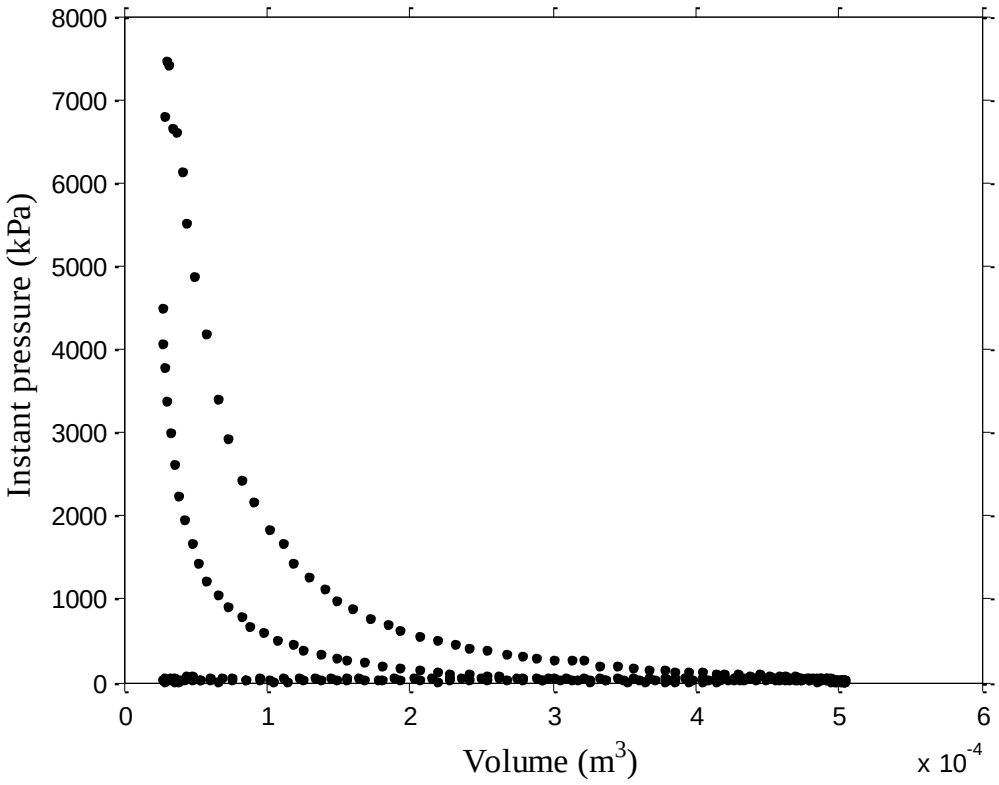

Figure 2.2: Typical P-V diagram from the experimental data of this thesis. The area enclosed is the indicated work per combustion cycle and cylinder.

The power per cylinder (P_i) for a four stroke engine is given by

$$P_i = \frac{W_{c,i} N}{2} \quad (4)$$

where N is the crankshaft rotational speed and the imep by

$$imep = \frac{2P_i}{V_d N} \tag{5}$$

Engine torque (T) can be calculated with a dynamometer connected to the engine's crankshaft from the equation

$$\mathrm{T} = Fb \tag{6}$$

If a dynamometer is not available, we can calculate the engine's power by connecting to the crankshaft an electric generator and following proportional methodology.
The crankshaft rotational speed will be equal to the electric current ($N = 60 \cdot f$). Thus, the engine's power will be:

$$P_b = \frac{P_{generator}}{\eta} \tag{7}$$

where η is the generator's mechanical efficiency. $P_{generator}$ is also equal to

$$P_{generator} = UI \tag{8}$$

With U the voltage used by the generator and I the current. The torque now will be

$$T = \frac{P_b}{2\pi N} \tag{9}$$

2.2 Cyclic variations

Combustion cycles in an IC engine are not the same. Combustion is different for consecutive cycles and from cylinder to cylinder. One can easily notice that by plotting cylinder pressure measurements vs time. Pressure integrals magnitude will

not be the same as well as the integrals' peak will be at slightly different time intervals.

This variation in measurements may be caused by the turbulent phenomena of gas motion inside the cylinder, or by the air/fuel mass supplied to the cylinder, or by the mixture composition in the case of a spark ignition engine, or by the bad mixture of exhaust gas residuals with the fresh unburned mixture [6, 9-12]. Note that in compression ignition engines, combustion is more stable than spark ignition engines [12], so we expect from CI engines less variances in its various magnitudes.

The evaluation of the cyclic variability can be done from the investigation of the coefficient of variation in imep (COV_{imep}) given by the equation:

$$COV_{imep} = \frac{\sqrt{\frac{1}{n-1}\sum_{i=1}^{n}\left(imep_i - \overline{imep}\right)^2}}{\overline{imep}} \times 100\% \qquad (10)$$

where $imep_i$ is the indicated mean effective pressure in the i cycle and $\overline{imep}$ is the average indicated mean effective pressure at a specific crank angle for all the i cycles. COV_{imep} is considered to be an important magnitude because when it exceed 10 %, the vehicle appears to have drivability problems [1, 6].

The number of cycles used by researchers to calculate *COV* and $\overline{imep}$ varies, so the question of how many iterations are needed for reliable results is essential. Ceviz et al. [2] performed a series of in-cylinder pressure measurements and by calculating COV_{imep} and through a series of statistical computations he concluded that 50 cycles are enough for reliable results in a diesel engine. In our experiments the minimum combustion cycles we used were 630.

The most similar study to this thesis performed by Zervas in 2004 [9] but the operating diesel engine is adapted for natural gas feed. Zervas represents *COV* and pressure vs crank angle diagrams. He claims that these curves can be used in order to find the beginning and end of combustion as well as the points where the mass burned fraction is 50%. He also concludes that the peak interval of the *COV* curve can be used as a criterion for the cyclic dispersion.

In 1992 Kouremenos et al. [13] performed a stochastic-experimental investigation of the pressure variation. Their investigation consists of the manipulation of pressure

results of 650 successive cycles for the maximum pressure, the maximum rate of pressure rise and the crank angle in which these phenomena occur. By analyzing the pressure in the pipe line in conjunction to the ignition delay, they concluded that the fuel pump system does not influence the pressure variation.

Another stochastic-experimental investigation, but different than the previous one, performed in 2008 by Rakopoulos et al. [14]. They tested a single cylinder 'Hydra' engine in the DI naturally aspired diesel engine mode on diesel and biodiesel fuel operation (15% v/v blends) in 2000 rpm. Apart from the imep and $imep_{max}$, they analyzed the maximum pressure rate and also the dynamic injection timing and ignition delay. When they used biodiesel mixtures, the observed that the maximum cylinder pressure remained almost constant, the $imep_{max}$ and ignition delay increased and the fuel injection pressure diagrams were delayed. Also, by their analysis it is indicated the randomness of the phenomena governing an engine operation. Their most remarkable conclusion at their research (as denoted by them) is that the fuel pump system did not affect the cyclic pressure variation, operated in all kinds of fuel does not influence the cyclic pressure variation, verifying Kouremenos [13] work.

Another one that performs a comparative study between diesel and biodiesel fuel is Ozkan [15]. Ozkan investigates the *COV* of ignition at various operating conditions (1000-4000 rpm with 500 rpm intervals) in a four cylinder turbocharged IDI diesel engine. Ozkan observed the ignition delay when operated on biodiesel and it is shown that the evaporation percentage of biodiesel is lower than that of diesel, based on crank angle. Thus, the rate of combustion of biodiesel is lower than that of diesel. Furthermore, Ozkan observed a decrease of the in cylinder maximum pressure 5.2% at 2000 rpm and 6.4% at 3500 rpm, but similarity in *COV*.

Similarly to Ozkan, Barboza [16] represented the effect of injector opening pressure and injection timing variations on a B20 fuel. He tested three injection timings (20^o, 23^o and 26^o bTDC) and four injector opening pressure at 180, 200, 220 and 240 bar. The lowest cyclic variations among them found to be at 26^o bTDC and at 220 bar injector opening pressure.

Han investigated in 2000 and 2001 [1, 17] the cyclic variations in spark ignition engines under idling operation. In 2000 he investigated the in cylinder imep variation and tried to correlate it with the lowest normalized value (LNV), while in 2001 he concluded that the *COV* of burn angle is minimum at 5^o bTDC, while the COV_{imep}

reaches its maximum value and the *COV* of burn angle increases with an advance in spark timing.

In addition to the experiments, theoretical approach of the *COV* is essential. Cosadia et al. [18] investigated the in cylinder variations of the swirling flow in a transparent motored diesel engine. Moreover, Po et al. [19] provided an indirect PI control-oriented model for the engine's torque balance, which is connected to the in-cylinder measured pressure. The PI control transplanted into an engine system and the test results agreed with the model.

Similarly to Po et al [19], Galloni [20] measured the cyclic variations at part load conditions in a SI engine. He performed a CFD analysis by means of a RANS (Reynolds-averaged Navier-Stokes) approach, calculating the residual gas mass fraction (*EGR*), the gaseous air-fuel ratio (φ) and the turbulent intensity (u') at the spark time. They found that the COV_{imep}, thus the cyclic variations, decreases as the laminar speed and the turbulence intensity of the flame increase.

Finally, Mittal and Schock [21] studied the influence of charge motion control on the in-cylinder flow. They used molecular tagging velocimetry (MTV) to obtain the measurements and probability density functions to quantify the cyclic variations. Because of the increasing demand on alternative fuel research, more interest has grown for the investigation of variances in engines when they operate on alternative fuel [22-26].

Wang et al. [22] studied the cyclic variations of a spark ignition engine fueled with natural gas-hydrogen blends, Ma et al [23] studied the effects of hydrogen addition in a lean burn natural gas spark ignition engine and Zheng et al. [24] tested a direct injection operating on natural gas. What is more, Sen et al. [25] investigated the dynamics of cycle to cycle variations in a natural gas direct injection spark ignition engine. Last, Tang et al. [26] tested the cyclic variability of a non road diesel engine operated on diesel and biodiesel blends.

2.3 Engine energy balance

2.3.1 Theory

In order to investigate an engine, it is essential to perform an energy balance study apart from simply checking its basic characteristic quantities (engine speed, bmep, power, torque, fuel consumption, heating values etc).

To begin with, we perform a first law energy balance to the control volume of Figure 2.3 for a steady state operation.

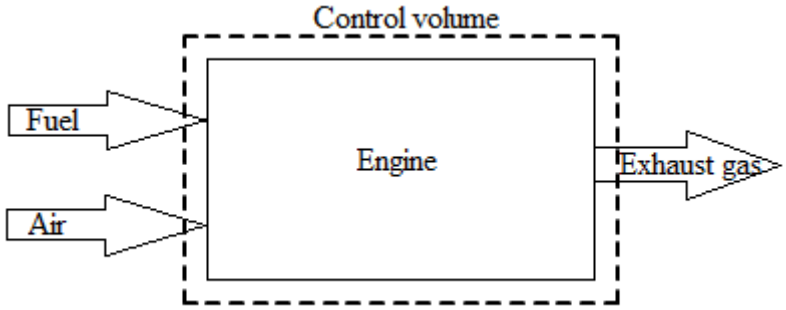

Figure 2.3: Control volume for the energy balance.

The assumptions been made are the following:

1. The engine runs at steady state.
2. The control volume includes the engine and the dynamometer (or any device acting as dynamometer, an electric generator for instance).
3. The combustion air and the exhaust gas form ideal gas mixtures.
4. Potential and kinetic effects of the incoming and outgoing fluid streams are ignored.

The same apparatus in its various forms is followed by other researchers [27-34], whose results will be discussed in the next sections. The energy conservation equation is

$$\dot{m}_f h_f + \dot{m}_a h_a = P_b + \dot{Q}_{cool} + \dot{Q}_{misc} + (\dot{m}_f + \dot{m}_a) h_e \qquad (11)$$

$\dot{m}_f$, h_f and $\dot{m}_a$, h_a are the mass flow rate and specific enthalpy of the fuel and air respectively, P_b is the engine's brake power, $\dot{Q}_{cool}$ is the heat transfer rate to the cooling medium, $\dot{Q}_{misc}$ is the heat rejected to the oil plus convection and radiation from

the engine's external surface and h_e is the exhaust enthalpy. Assuming that the exhaust enthalpy is expressed by h_e (T) = $h_{e,s}$ + h_e (298K), then the energy conservation equation is

$$P_b + \dot{Q}_{cool} + \dot{Q}_{misc} + \dot{H}_{e,ic} + \dot{m}h_{e,s} = \dot{m}_f Q_{LHV} \tag{12}$$

where $\dot{H}_{e,ic}$ is the exhaust enthalpy loss due to the incomplete combustion and Q_{LHV} is the fuel's lower heating value. It is indicated in bibliography that the input energy in internal combustion engines ($\dot{m}_f Q_{LHV}$) is divided into three, almost equal parts: the useful work (P_b), the energy transferred to the coolant ($\dot{Q}_{cool}$) and the exhaust losses, in which we include the losses due to friction. Typical values of the above magnitudes are given by Heywood [6]. For a diesel engine the useful work varies between 34-38 %, the energy transferred to coolant is 16-35 % and the exhaust losses about 22-35 % [6].

Alternatively the equation used by other researchers instead of Equation (8) in its final form is

$$\frac{\dot{Q}_{CV}}{\dot{n}_F} - \frac{\dot{W}_{CV}}{\dot{n}_F} = \bar{h}^o_{RP} + \sum_P n_e \left(\Delta\bar{h}\right)_e - \sum_R n_i \left(\Delta\bar{h}\right)_i \tag{13}$$

$\dot{Q}_{CV}$ is the heat flow rate to the control volume, $\dot{n}_F$ the molar flow rate of the fuel, $\dot{W}_{CV}$ the power obtained from the control volume, $\bar{h}^o_{RP}$ the enthalpy of combustion and n coefficients in the reaction equation of products and reactants.

The two different forms of the energy balance described above are exactly the same. The right side of Equation (10) can be evaluated from experimental data [35]. In this thesis we start our calculations for the energy balance from Equation (8).

2.3.2 Previous research work

In this section, previous research work concerning energy balance will be discussed. Diesel and gasoline engines have been used and tested. All experiments conducted on four-stroke engines either single-cylinder, three-cylinder, four-cylinder or six-cylinder, turbo charged or naturally aspired. The displacement of the engines varied

from 1 to 6 L, the engine operation from 1100 to 3500 rpm and the maximum indicated power output observed was 58.88 kW. For the gasoline engine, the compression ratio was 8:1, while in the diesel engines was between 15.6:1 and 21.3:1.

2.3.2.1 Energy balance in gasoline engines

Two research teams have conducted experiments on gasoline engines, Burhis with Leduc and Sayin.

The former performed an energy and exergy balance study on a gasoline and a diesel engine. Their aim was to estimate the difference between energy and exergy under heat recovery restrictions. The engine they tested was a three-cylinder, downsized, low friction, naturally aspired gasoline engine, with 1 L displacement. The engine operated at 2000 rpm and 3500 rpm. They concluded that when bmep increases, so does exergy and the recoverable energy/recoverable exergy ratio. They state that the efficiency of the engine can increase at a 15 % when heat recovery is concerned, which leads to a 25 % exergy recovery efficiency. Similar results they found about their diesel engine (common rail, displacement 1.6 L, operation at 1500 and 2300 rpm) with the increase in the output work can reach 10 % [32].

The latter tested a four-stroke, four-cylinder, spark ignition gasoline engine (1.6 L displacement) on various fuels. Specifically, he used a 91-RON (research octane number), a 93-RON and a 95.3-RON gasoline. The engine originally required a 91-RON mixture. In each test, the engine torque kept constant at 20 or 40 Nm, while the engine speed varied from 1200 to 2400 rpm rising 400 rpm per test. They summed up that when they used 93-RON and 95.3-RON than 91-RON gasoline, the engine operated less energy efficiently. Furthermore, they observed that when they used higher octane rating than the indicated the exergetic efficiency lowered. They also concluded that in higher engine speed, almost all energetic and exergetic performance parameters increased because of the better homogenization of the fuel mixture. Last, any inefficiency is because of the various irreversibilities taking place in the engine [28].

2.3.2.2 Energy balance in low heat rejection diesel engines

Ciniviz and Taymaz experimented on low heat rejection (LHR) diesel engines.

Ciniviz experimented on a direct injection (DI) turbocharged diesel engine, four-cylinder, displacement 4 L and r_c=17.251. He tested his engine at 1400 and 2800 rpm. In his experiments, engine power, torque and effective efficiency were higher when operating on diesel fuel [27].

What is more, Taymaz applied a 0.5 mm thickness coating on a six cylinder, DI, turbocharged, inter-cooled diesel engine and the heat loss to the coolant was 23, 34 and 46 % for high, medium and low load (27, 68 and 109 kW respectively), while in the standard engine the heat loss to the coolant found 27, 36 and 49 % respectively. The insulation caused a raise in the temperature of the cylinder wall, which resulted in higher exhaust gas temperature and energy. This also caused a drop in the volumetric efficiency. According to Taymaz, the heat loss to the exhaust system was 3, 4 and 8 % higher in the LHR engine for low, medium and high load respectively. Last, he observed that the thermal efficiency raise is not proportional to the reduction of the heat rejection in the combustion chamber [34].

2.3.2.3 Thermal and energy balance operating on alternative fuel

Ajav et al in 2000 published their work. They researched on a single cylinder diesel engine, 1.1 L displacement, r_c=15.6 and operated at 1500 rpm. Their aim was to investigate medium sized compression ignition engines, due to the lack of available information governing thermal balance. They compared No.2 diesel with 5, 10, 15, 20 % ethanol-diesel blends. The percentage of useful work for the engine when operated with No.2 diesel was 28.68 %, while for the ethanol-diesel blends was 28.73, 31.06, 31.95 and 32.89 respectively. It is obvious that when the percentage of the ethanol increased, so did the useful work. They observed that when the engine operated with the 5 and 10 % blends, the thermal balance did not differ in the 5 % level of significance. On the other hand, in the 5 % level of significance the differences were considerable in the 15 and 20 % blends [33].

Wallace made a thorough investigation of a four-cylinder turbocharged diesel engine (r_c=21.3, 2.3 L displacement) operated on No.2 diesel and a B100 blend. The difference between the two fuels for power out, coolant and exhaust were in absolute values 0.4, 0.1 and 0.3 % respectively [30].

2.3.2.4 Energy and exergy balance

Sekmen with Yilbasi and Canakci with Hosoz performed an energy and exergy balance study rather than a simple energy balance study.

The former experimented on a four-cylinder, turbocharged, naturally aspired diesel engine at 2000 rpm and 100 Nm [29].

The latter tested a four-cylinder, turbocharged diesel engine at 1400 rpm. The distribution of the fuel energy for the pure diesel was brake work was 36.7 %, heat loss was 40.4 % and exhaust loss was 22.9 %.

The similarity in percentages with Sekmen's and Yilbasi's energy balance is obvious. When the engine operated in biodiesel heat loss and brake work were bigger and exhaust loss smaller.

All in all, after the exergy term introduced, a simple energy balance study in an engine considered inadequate. Instead, researchers performed an energy and exergy balance in engines to better test the performance and efficiency of the engine. In this thesis, exergy analysis, entropy balances, or second-law analysis are not discussed, but proposed as future work. Examples of second law analysis can be found in bibliography [36-38].

2.4 Adding to the body of knowledge

From the study of the literature review mentioned above, governing cyclic variations, it can be noticed that most researchers put their efforts on experimenting in specific engine speed and load, usually where the engine appears to have its maximum torque. this thesis, the investigation includes operation in various engine speeds and loads in order to create a spectrum for single cylinder engines.

Another way this thesis adds to the overall body of knowledge is that it serves as a source of validation for diesel fuel. Although experiments took place in our engine in the past, the innovation of this thesis is that we used all the previous knowledge on this engine and merged it in a way to fit our goals and expectations. Not only did we correct and evolve the LabView codes used in the past [4], but also we created new Matlab codes for cycle to cycle calculations.

3 Experimental setup and testing procedure

The overall schematic experimental setup of this thesis is shown in Figure 3.1. Our setup contains an engine, an electric generator connected to a four-resistance device, a fuel tank deposited on an electric scale, four thermocouples, an in-cylinder pressure sensor layout, a diesel particulate filter (DPF), a universal exhaust gas oxygen sensor (UEGO), another pressure sensor to measure the pressure drop at the DPF, two desktop computers and a laptop. Each component or device (except the DPF) shown in Figure 3.1 will be discussed later on this chapter. The reason we exclude the description of the DPF is because is not in the area of interest of this thesis. Parallel to the experiments of this thesis, PhD candidate Dimitrios Tziourtzoumis, performed DPF experiments

The setup is located in the Laboratory of Thermodynamics and Thermal Engines, Department of Mechanical Engineering of University of Thessaly. All tests performed there with the help of PhD candidate Dimitrios Tziourtzoumis and the under-graduate student Fotis Bouroutzikas.

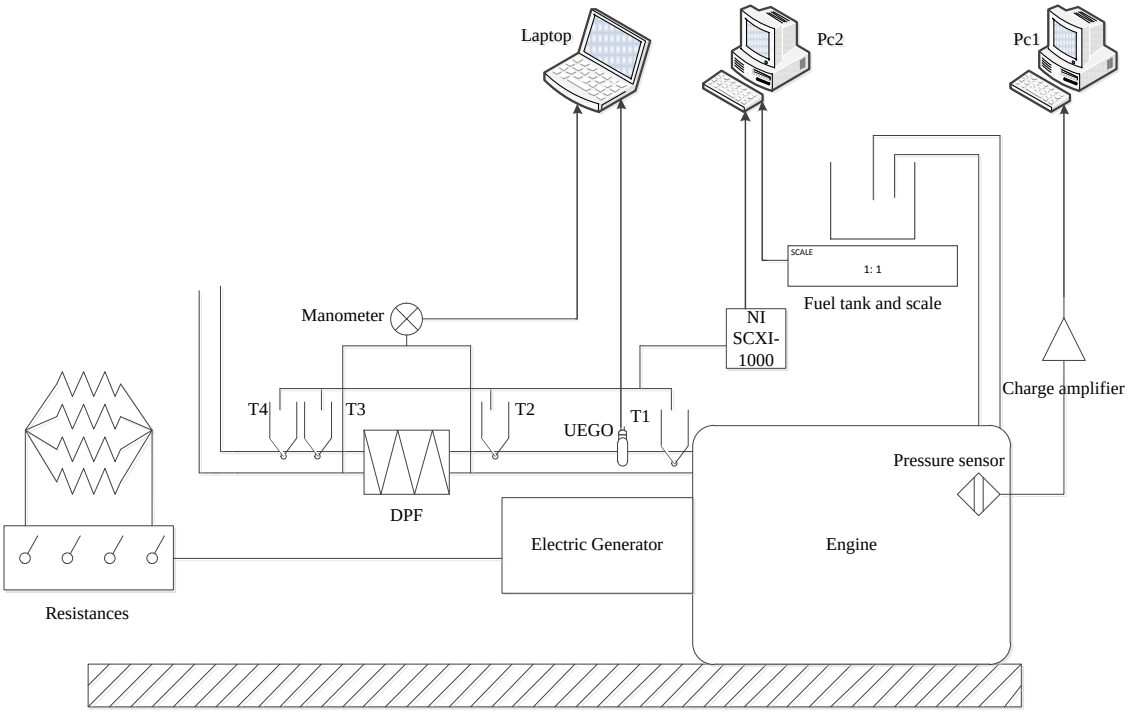

Figure 3.1: Schematic of experimental setup.

3.1 Engine

The engine of this study is Ruggerini RF91 (Figure 3.2), a single cylinder, four-stroke, diesel fueled, compression ignition engine. Its specifications are shown in Table 3.1 and its performance curves in APPENDIX A. Also its spare parts catalogue can be found in Reference 39 [39]. Operating manual does not exist on the internet database except other RF series. This happens because Ruggerini Motori has been bought by Lombardini, so the model RF91 is no longer been produced [40]. A model similar to our engine (15 LD 440) can be found in Reference 40.

3.2 Properties of fuel and blending

The fuel we used in our experiments were supplied by 'ELINOIL – HELLENIC PETROLEUM COMPANY S. A' (Volos factory) [41]. Their properties are shown briefly in Table 3.2, along with the corresponding range of variation of each parameter in the different fuel types used in Europe and North America [42, 43]. Our case study diesel fuel meets the European standards EN 590 and has been used in other laboratory experiments [44].

3.3 Electric generator

For the epiboly of load in the engine we used the electric generator MS 100LG of Nuova Saccardo Motori (Figure 3.3). More information about the generator can be found at References 45 and 46 [45, 46]. The characteristics of the generator are shown in Table 3.3.

The generator is connected to a 4-resistance device, each one 1.5 kW, indicated load (Figure 3.4). By activating the resistances from their switch, we add load to the engine. In the devise, there are 2 fuses, each one 25 A and connected to 2 resistances.

3.4 Measurement equipment

The magnitudes that we measured in our experiments and the equipment we used are shown in table 3.4. In Figure 3.5 is shown the laboratory environment.

Table 3.1: General specifications of Ruggerini RF91 engine.

Item	Specification
Trademark / type	Ruggerini / RF91
Principle of operation	DI, naturally aspired, four stroke, diesel
Cylinders	1
Bore	90 mm
Stroke	75 mm
Displacement	477 cm^3
Compression ratio	18.5
Maximum power	8.1 kW at 3600 rpm
Maximum torque	25 Nm at 2500 rpm

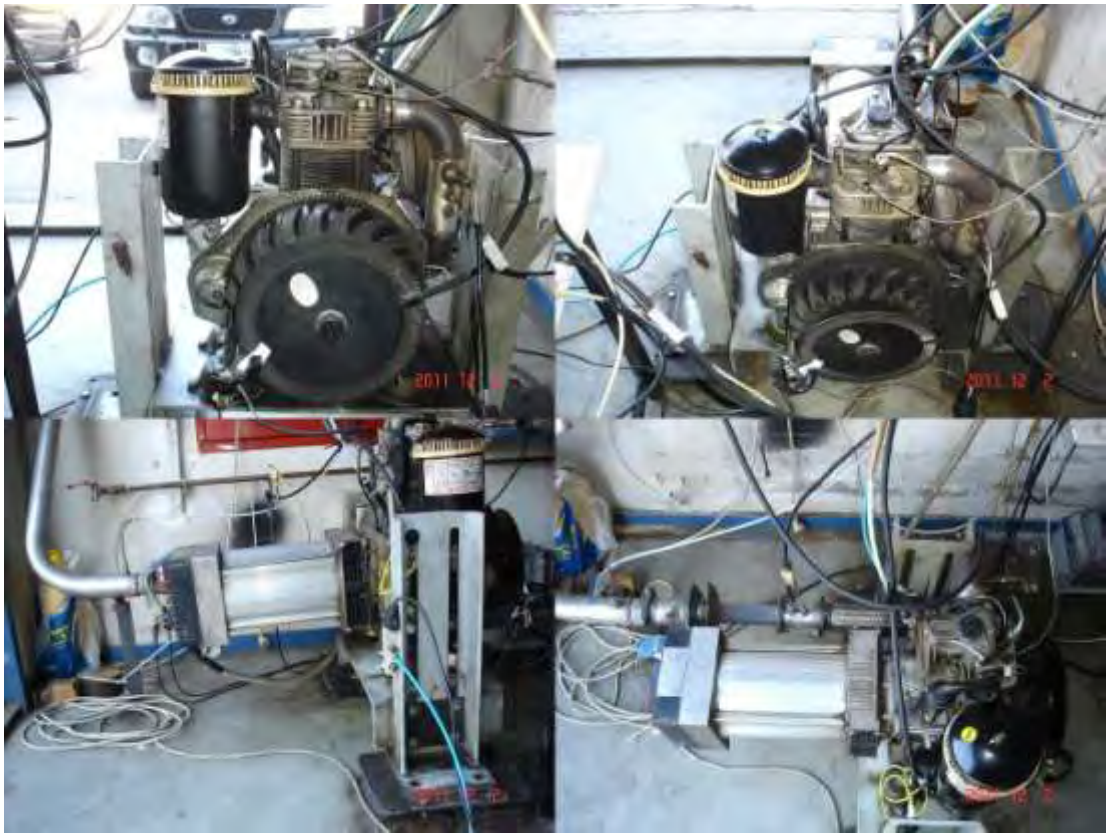

Figure 3.2: Test engine Ruggerini RF91 under various angle.

Table 3.2: Diesel fuel properties.

Properties/Range	Diesel (range)	Case study diesel
Density (15 °C) [kg/m^3]	815-845	825
Viscosity (40 °C) [cSt]	2-3.5	2.5
Cetane number	40-55	50
Cold filter plugging point	-25 to 0	-12
Gross heating value [MJ/kg]	-	46.1
Lower heating value [MJ/kg]	42.5-44	43.3
Sulfur content [ppm]	10-500	50

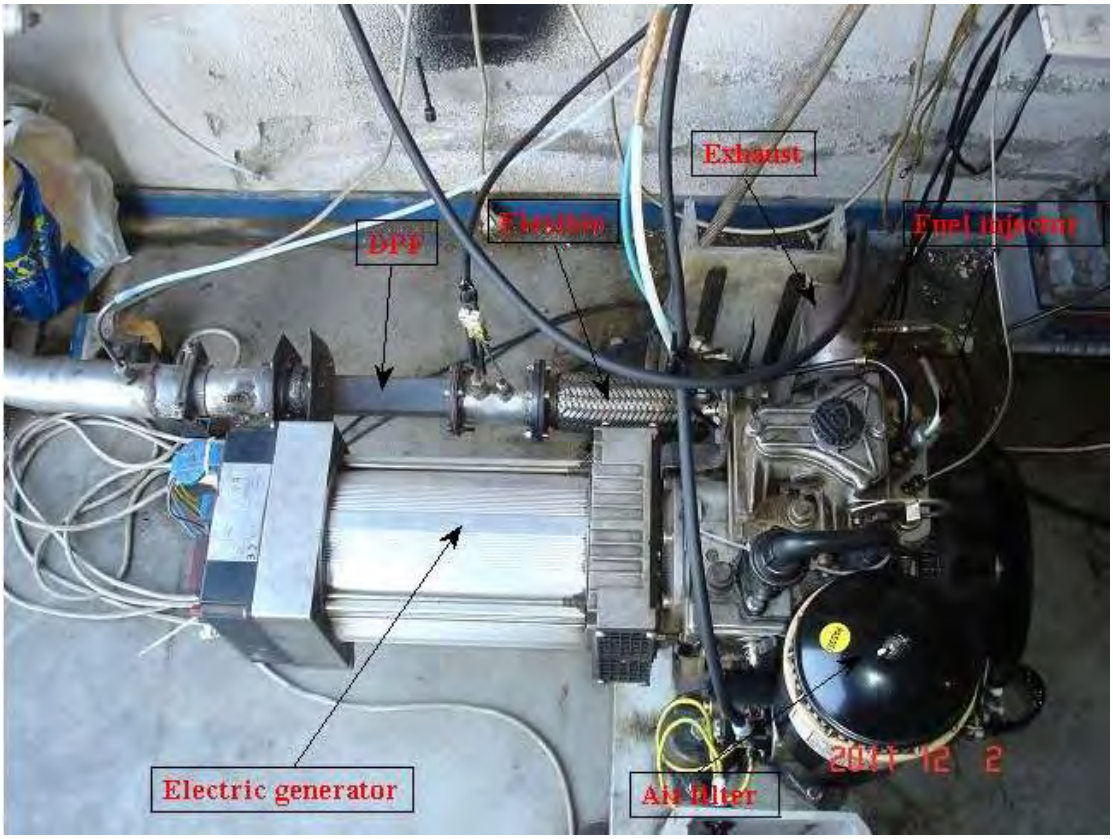

Figure 3.3: The electric generator and various visible engine parts.

Table 3.3: Generator MS 100LG characteristics.

50 Hz – 3000 rpm			60 Hz – 3600 rpm		
Power	**Break power**		**Power**	**Break power**	
6 kVA	8 kW	η = 75%	7.2 kVA	9.6 kW	η = 75%

Figure 3.4: The 4-resistance device with the battery. 2/4 resistances are operating.

3.4.1 Temperature measurement

For all the temperature measurements we used K-type thermocouples of 1 and 2 inches diameter. The thermocouples we placed inside the DPF were 1 inch and the thermocouples for the measurement of the exhaust temperature and the DPF inlet were 2 inches. Their exact position is shown in Figures 3.5, 3.6, 3.7 and their reference tables can be found at Reference 47 [47]. In Figure 3.6 it can be noticed how the thermocouples were mounted inside the DPF.

3.4.2 Air to fuel ratio measurement

The measurement of air to fuel ratio has been made with the use of UEGO (universal exhaust gas oxygen) sensor TL-6312-W1 (Figure 3.8) and UEGO controller TC-6110A (Figure 3.9). UEGO's power supply is shown in Figure 3.10 and its specifications at Table 3.5.

Table 3.4: Measured magnitudes and equipment used for each one of it.

Measured magnitude	Equipment used
Exhaust temperature	Type-K thermocouple
DPF inlet temperature	Type-K thermocouple
DPF center temperature	Type-K thermocouple
DPF periphery temperature	Type-K thermocouple
A/F	UEGO
Cylinder pressure	Piezoelectric sensor
DPF pressure drop	Differential pressure sensor
Crank angle	Opto-interrupter
Fuel consumption	Electric scale

Figure 3.5: Laboratory environment.

Figure 3.6: Thermocouples layout.

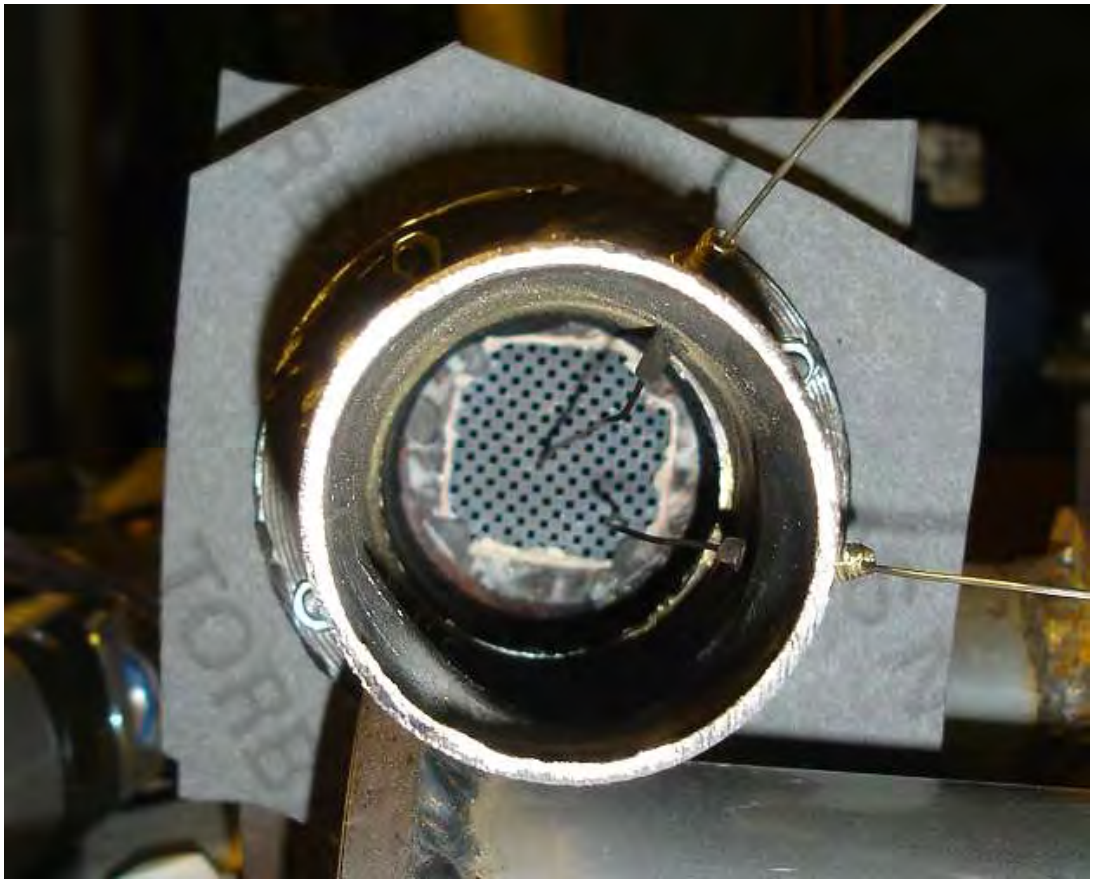

Figure 3.7: Center and periphery thermocouple inside the DPF.

Figure 3.8: Exhaust thermocouple and UEGO.

Figure 3.9: UEGO controller.

Figure 3.10: UEGO's power supply.

Table 3.5: UEGO controller and sensor specifications.

UEGO controller specifications	
Rate voltage	13 V
Operating voltage range	12 V to 28 V
Operating temperature range	-20 ^{o}C to 85 ^{o}C
Storage temperature range	-25 ^{o}C to 85 ^{o}C
UEGO sensor specifications	
Sensor element tip temperature	750 ^{o}C to 950 ^{o}C

3.4.3 In-cylinder pressure measurement

The most important measured magnitude in this thesis was the in-cylinder pressure. This became feasible with the adjustment of a KISTLER piezoelectric sensor in the cylinder head (Figure 3.11, 3.12, 3.13).

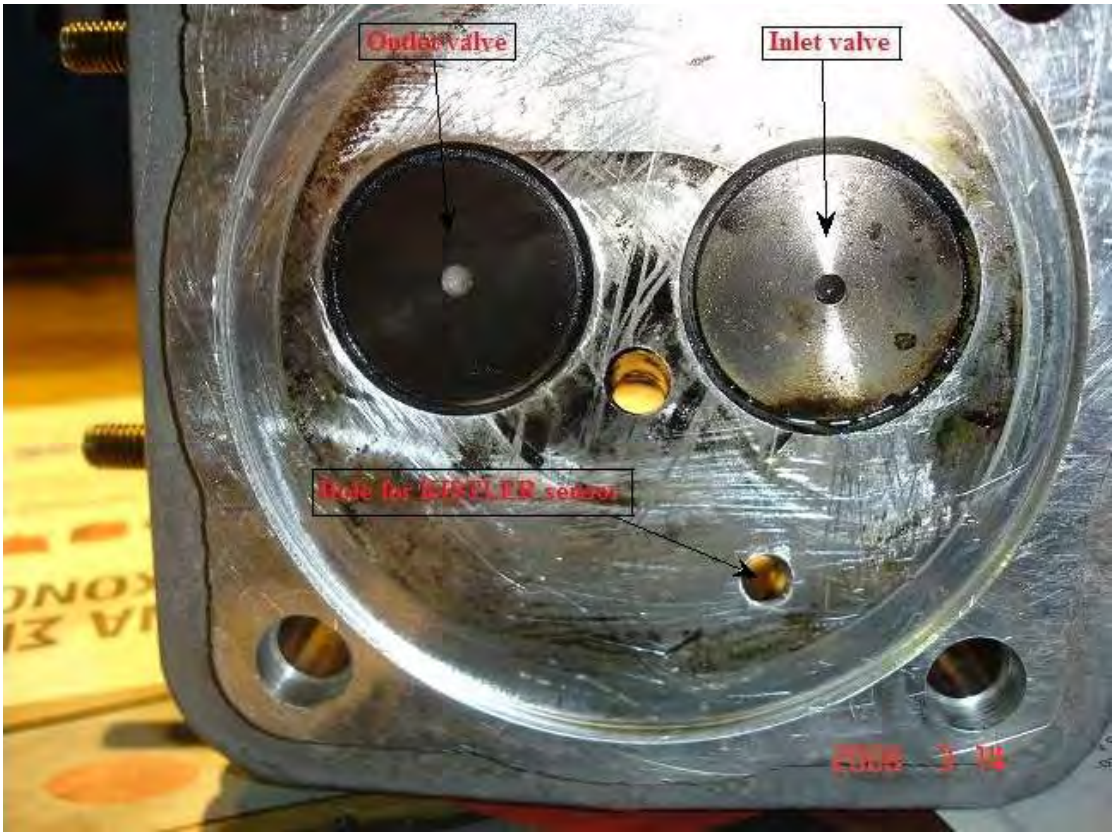

Figure 3.11: Hole for the KISTLER sensor and inlet/outlet valves.

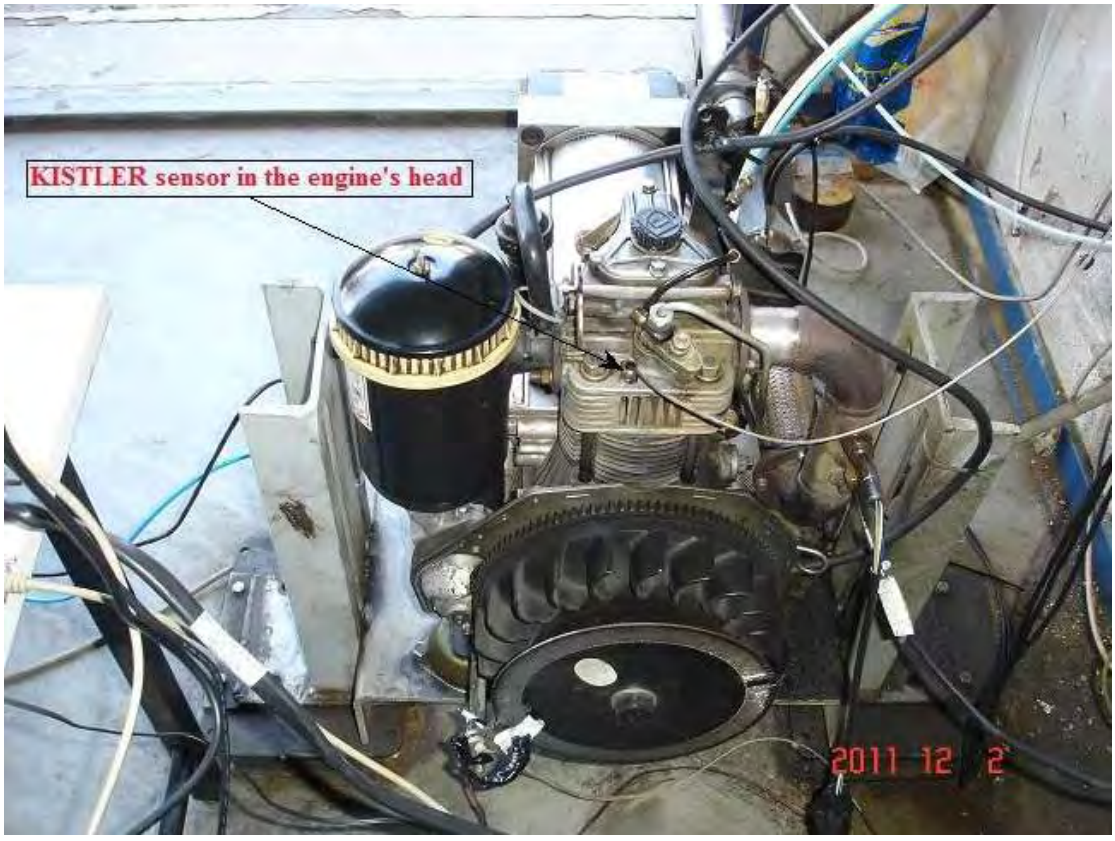

Figure 3.12: KISTLER piezoelectric sensor in the engine's cylinder head.

Our piezoelectric sensor is KISTLER 6052B1 Quartz Pressure Transducer (0-250 bar, 20 cp/bar) [48]. His signal passes through a charge amplifier (KISTLER 5044, 20 bar/V, Figure 3.14) and is connected to our online data acquisition card and the computer.

Figure 3.13: KISTLER 6052B1 (left) mounted over a KISTLER 6525ASP20-50 head (right).

Figure 3.14: KISTLER 5044 charge amplifier.

3.4.4 DPF pressure drop measurement

For the measurement of the DPF pressure drop we used a simple pressure drop sensor (Figure 3.15. 3.16). Its characteristics can be found in Table 3.6.

Figure 3.15: Pressure drop sensor tubes adapted to the exhaust.

Table 3.6: Pressure drop sensor characteristics.

Type	JUMO ADI-55-420/53
Pressure drop range	0 – 500 mbar
Maximum output voltage	10 V
Current range	4 – 20 mA

3.4.5 Crank angle measurement

First, to measure the crank angle we adapt a metal disk with 360 holes to the engines crank. Then a laser in the role of the transmitter is mounted to the disk with its receptor (Figure 3.17). Furthermore, using friction tape we close from the metal disk 4 holes, corresponding to 4 degrees, to determine the initiation degree as Melisourgos

suggests in his thesis for the specific engine [4]. From the crank angle, the engine's cylinder volume can be found from Equation 2.

Figure 3.16: Pressure drop sensor.

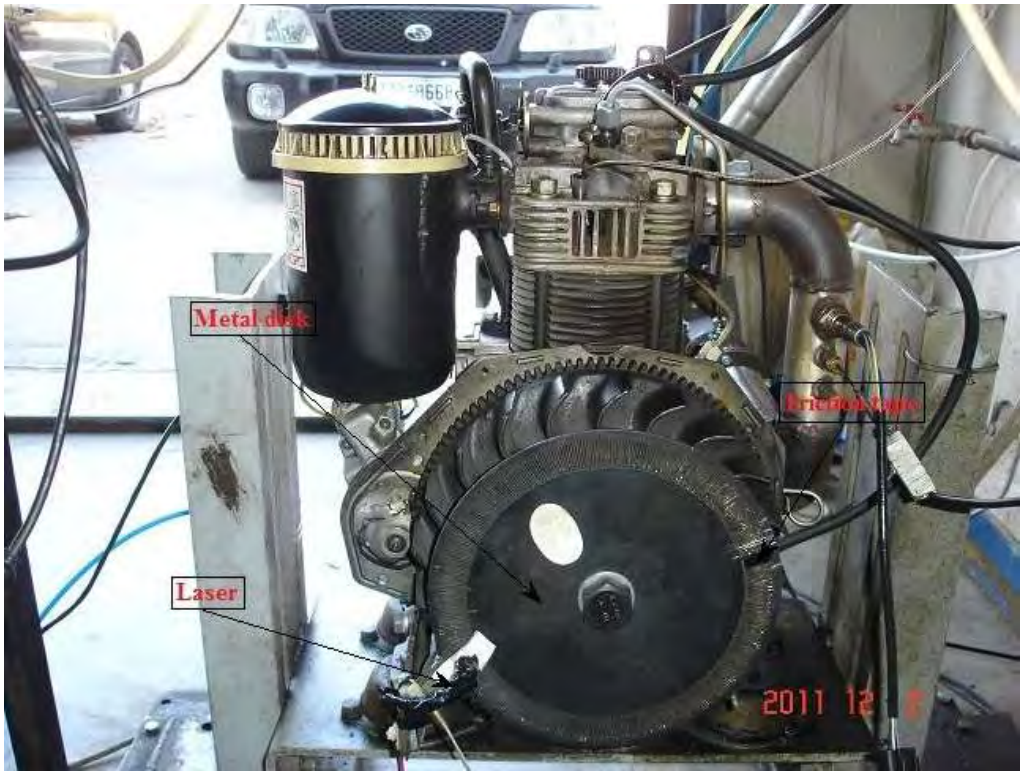

Figure 3.17: Metal disk adapted to the engine's crank and laser.

3.4.6 Fuel consumption measurement

For the measurement of the engine's fuel consumption we plugged an electric scale (model KERN 440-49N, Figure 3.18, [49]) to a computer and programmed LabView to record the scale's indication every 1 second. Thus, with a simple subtraction of 2 values, the fuel consumption rate can be found. The scale specifications are presented in Table 3.7.

Table 3.7: KERN 440-49N specifications.

Readout d	0.1 g
Maximum measuring range	4000 g
Minimum piece weight at counting	200 mg
Weighting plate (WxD)	150x170 (mm^2)

3.5 Data acquisition

3.5.1 Data acquisition cards

Two different data acquisition cards have been used during the experiments.
In order to record the cylinder pressure, a high speed data acquisition card was required. Thus, we used the NI PCI-6259 data acquisition card (up to 1.25 MS/s). Its specifications can be found at Reference 50 [50]. NI PCI-6259 was inserted at control PC 1 (as shown in Figure 3.1 and 3.5). At PC 1 we also connected the laser's opto interrupter to directly correlate pressure and crank angle. Sampling rate for our experiment was 100,000 samples per second.
For the measurement of A/F ratio we used a slower card, compared to the pressure measurement. The card we used was DAQCard-AI-16XE-50 (up to 20 kS/s). its specifications can be found at Reference 51 [51]. Sampling rate was 1 sample per second.

3.5.2 Data acquisition codes

For the measured magnitudes the front panel of the LabView codes used is shown in Figures 3.18 – 3.20.

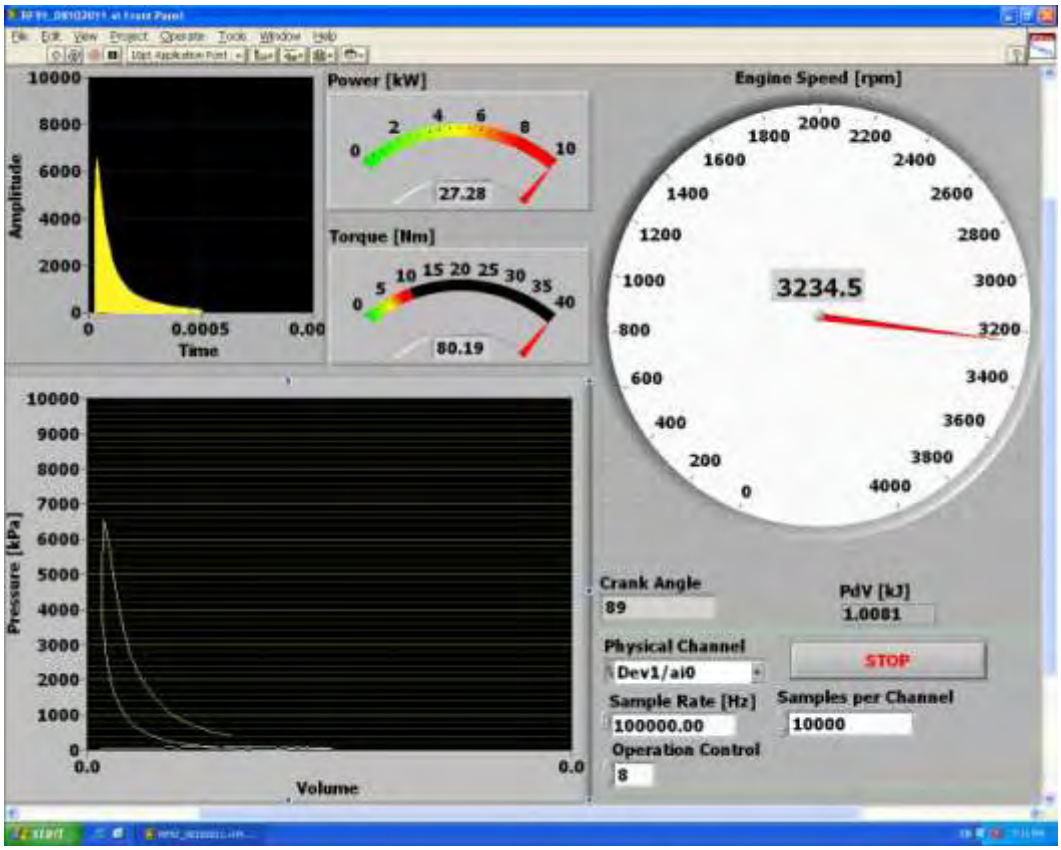

Figure 3.18: Engine speed, pressure and crank angle front panel.

Figure 3.18 illustrates our engine's instant operation at approximately 3200 rpm. The important graphs shown are the Engine Speed and the instant P vs V graph. The Engine Speed graph is important because through it we could set our engine to the desirable rpm value and the P vs V graph is important because we could discover any problems that had to do with the laser. Amplitude vs Time graph is similar to P vs V graph and used only for evaluation as did the Crank Angle indicator. Power, Torque and PdV indicators are not operating properly and are to be removed. The rest indicators have constant values and are correlated with the smooth operation of the specific code, concerning data acquisition.

In Figure 3.19 it is shown the temperatures and fuel consumption LabView code. Down left can be observed how much fuel we have in our scale. By subtracting two consequent values of the fuel mass we have the instant fuel consumption rate, which is shown upper left. Once our fuel mass goes below 500 g, fuel alarm indicator (top right) goes red. Also in the same code we have put the thermocouples' control. It is obvious that the periphery thermocouple is not operating properly, a problem which we experienced in our experiments.

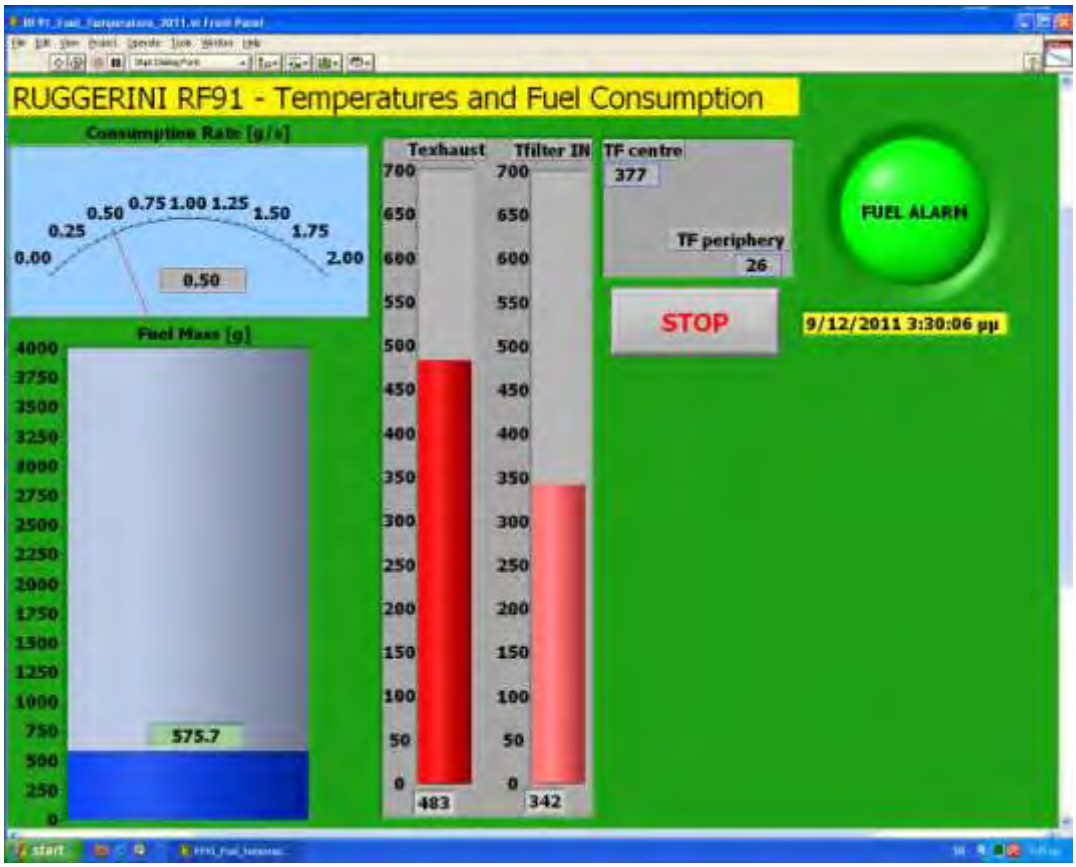

Figure 3.19: Temperatures, fuel mass and consumption rate front panel.

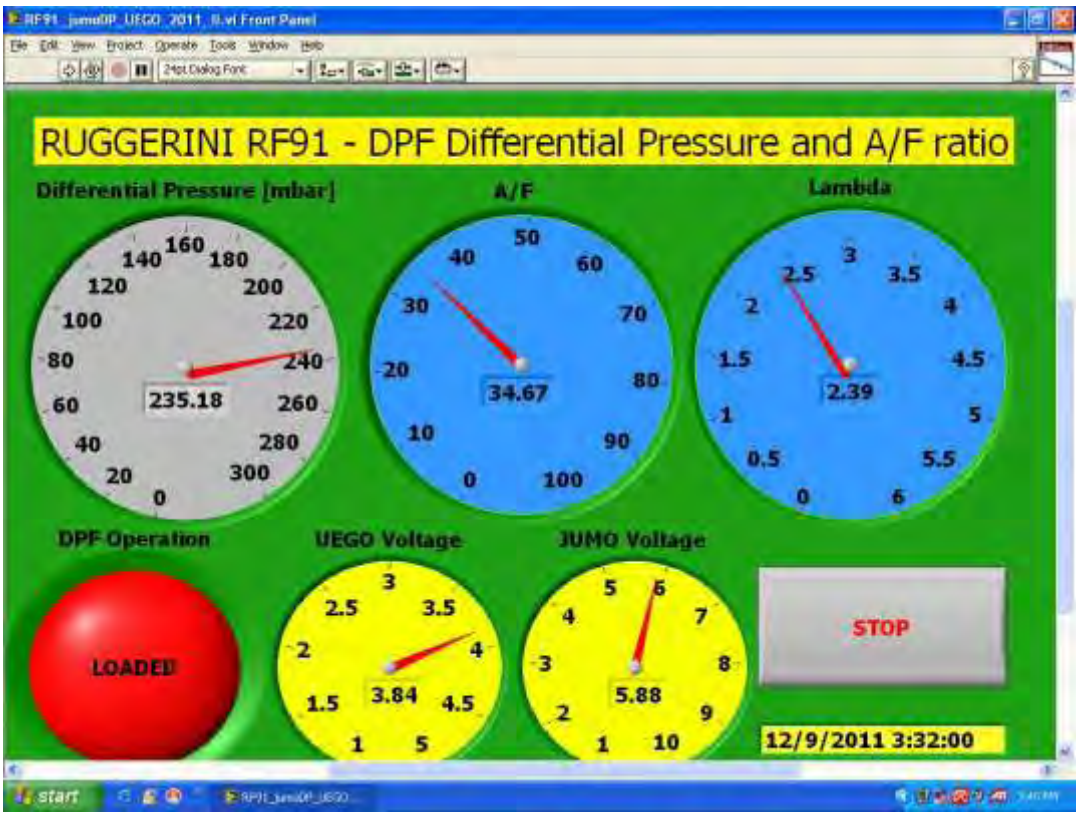

Figure 3.20: DPF differential pressure and A/F ration front panel.

Finally, in Figure 3.20 it is shown the DPF pressure drop and the A/F ratio front panel. Apart from the momentary differential pressure, the A/F and the lambda (λ), it is shown the instantaneous UEGO and JUMO (pressure drop sensor) voltage. We connected them with the LabView code in order to have a consecutive surveillance on the sensors' operation. If the differential pressure is above 200 mbar, an indicator in the down left corner turns red to inform us that the DPF filter is loaded.

3.6 Experimental approach

3.6.1 Equipment preparation

We have begun working on our Ruggerini RF91 engine on May 2011. We had a one and a half month holidays (July – 20th of August) and then continued till September 2011. First, we assured that our existing equipment operated properly and once this happened we calibrated it. The correlation of electric power produced by the generator when one, two and three resistances were operating is shown in Figures 3.21 – 3.23. In one resistance operating the equation describing the electric power is $y = 0.0012x - 2.1$, $R^2=0.98$ where x is the rpm. When two resistances were operating the equation becomes $y = 0.0025x - 4.5$, $R^2=0.99$ and when three resistances were operating we have $y = 0.0031x - 5.2$, $R2=0.99$. The three resistance correlation lacks of data points (only three) and it cannot be taken into serious consideration. More data points are needed. From now one when referring on one/two/three resistances, or 1.5/3/4.5 kW indicated load, one has to run though Figures 3.21 – 3.23 to find the real power produced by the generator.

We also had to adjust a new pressure drop sensor on the DPF. Furthermore, we partly modified old LabView codes (Figure 3.18) and created new ones (Figures 3.19 and 3.20). Hence, when we finished with the above and the initiative preparation experiments on the engine we started our measurements on September – October 2011.

3.6.2 Assessment cycle

Our engine's assessment cycle is shown in Figure 3.24. We performed two measurements series, one started in October 2011 and the other in November 2011.

Before starting the experiments we decided to scatter as many operation points we could in steady state. The time for each point was set to 10 minutes. Every time we started our engine in order to measure, we operated the engine for 20 minutes in 2000 rpm to warm it up (10 minutes without load, 5 minutes with one resistance operating and 5 minutes with two resistances).

Engine's warm up is a very important experimental parameter. Its importance is shown in Figure 3.25. When we start our engine, its various parts are not warmed up, with the outcome the engine needs to produce more work, in order to overcome the frictions and turn the crank. In Figure 3.25 the engine comes to a steady state at about 1000 cycles after it started. If the first cycles are to be included for calculations, the error and standard deviation will rise significantly.

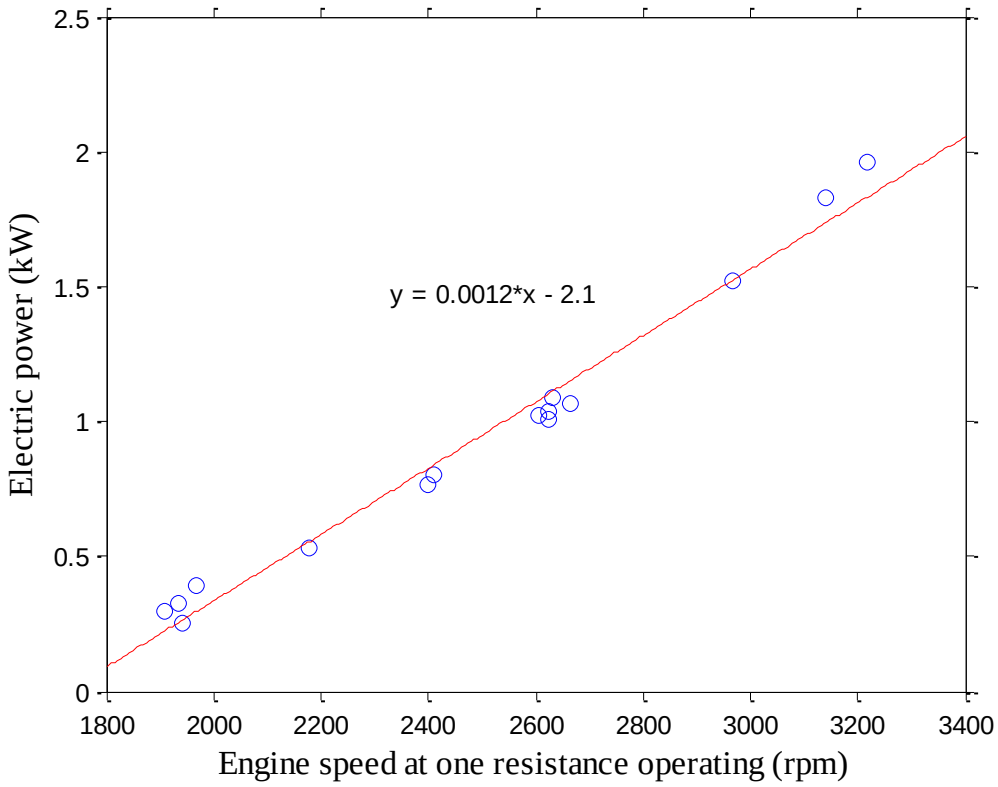

Figure 3.21: Correlation of the electric generator and engine speed when one resistance was operating (indicated load 1.5 kW).

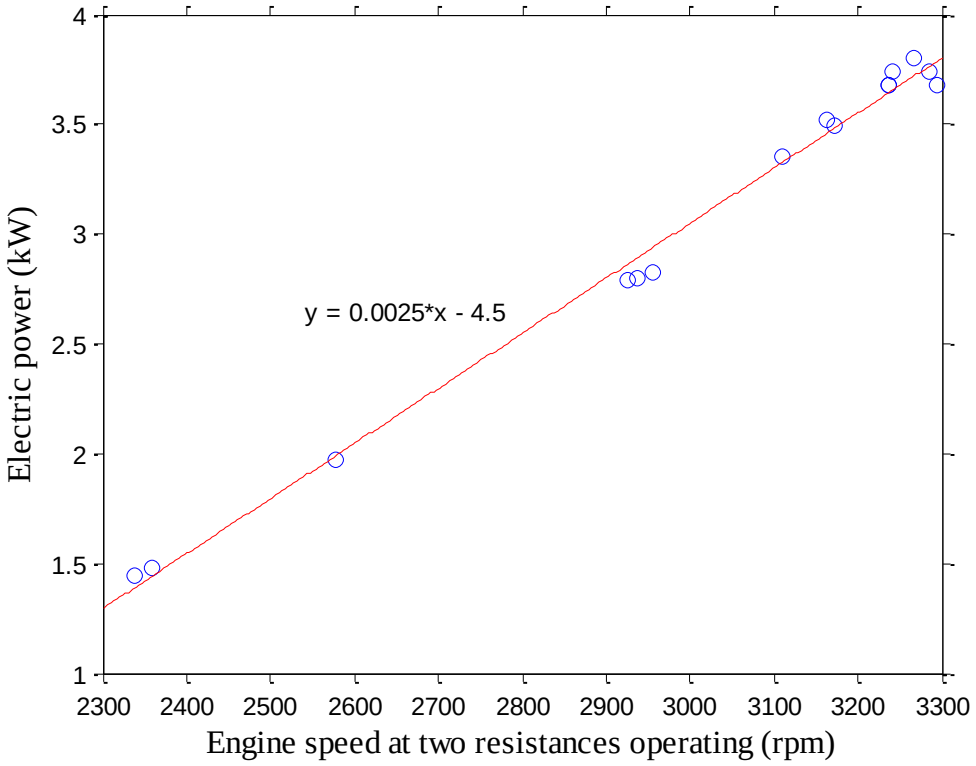

Figure 3.22: Correlation of the electric generator and engine speed when one resistance was operating (indicated load 3 kW).

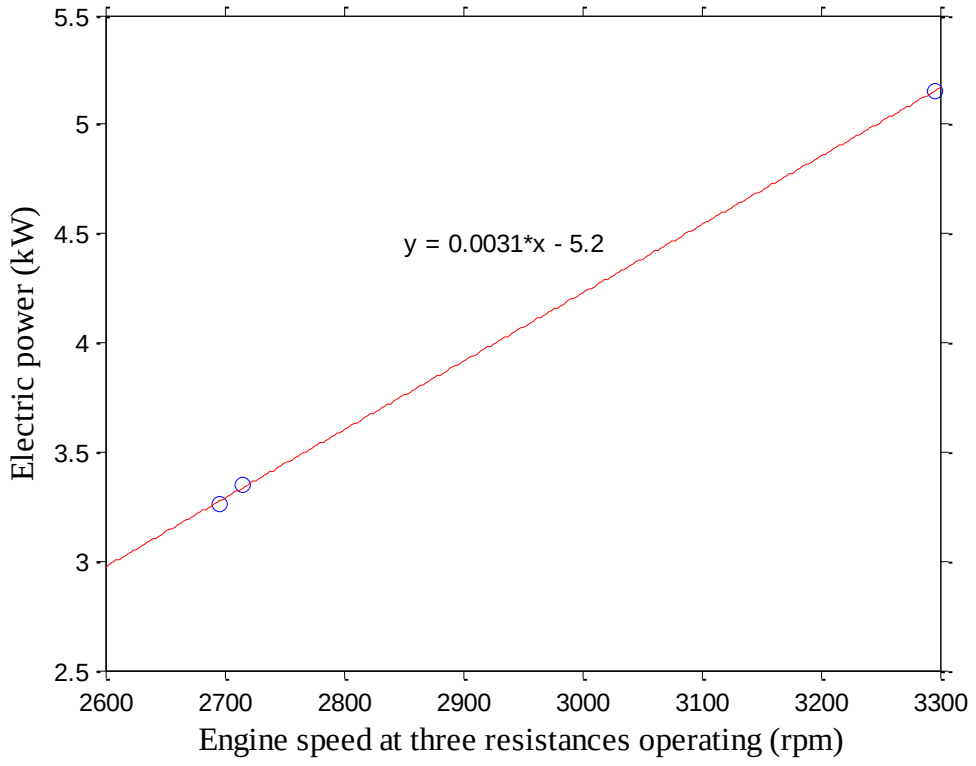

Figure 3.23: Correlation of the electric generator and engine speed when three resistances were operating (indicated load 4.5 kW).

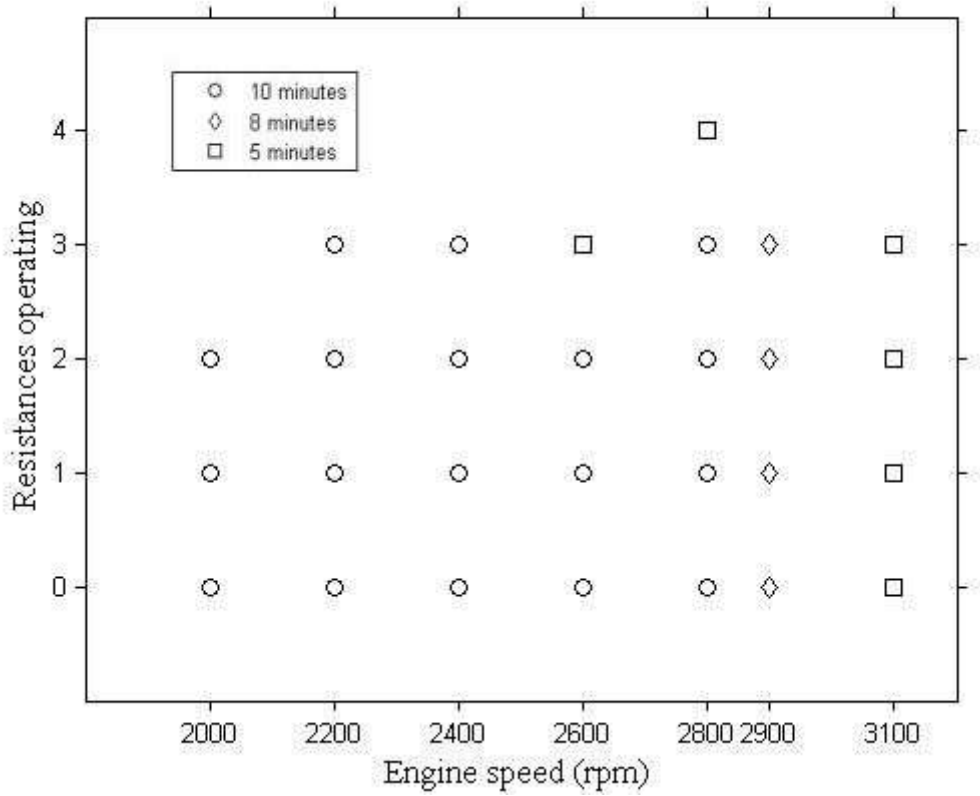

Figure 3.24: Engine's assessment cycle.

In Table 3.8 is shown the real rpm our engine operated in each point plus the indicated cycles through which we made our calculations.

3.7 Troubleshooting

In this section it is discussed the various problems we experienced while performing measurements with the engine.

To begin with, while we had programmed to measure 10 minutes at every operation point shown in Figure 3.24. This did not become possible because we experienced large engine oscillations. Particularly, in 2600 rpm and three resistances, the exhaust oscillations were very high, something which lead us to measure for 5 minutes instead of 10. Moreover, engine and exhaust oscillations took place at 2800 rpm and four resistances and again we only measured for 5 minutes that particular operation point.

Table 3.8: Indicated rpm, load, real rpm and number of calculation cycles.

Indicated rpm	Resistances operating	Real rpm	Calculation cycles
2000	0	2073	Warm up
	1	2035	630
	2	2010	911
2200	0	2212	1049
	1	2179	885
	2	2144	946
	3	2117	1007
2400	0	2389	1214
	1	2355	1158
	2	2315	1136
	3	2284	1127
2600	0	2586	1135
	1	2550	1322
	2	2514	1144
	3	2479	670
2800	0	2836	1413
	1	2790	1325
	2	2754	1200
	3	2716	1285
	4	2675	666
2900	0	2891	1228
	1	2838	1270
	2	2800	1200
	3	2760	479
3100	0	3078	916
	1	3026	933
	2	2990	816
	3	2959	792

What is more, in test experiments, we observed that at 3000 rpm and above the engine oscillate very much. Thus, we decided to measure at 2900 rpm for 8 minutes and at

3100 rpm for 5 minutes instead of 3000 rpm and 3200 rpm. This decision made in order to preserve the engine for further experimentation.

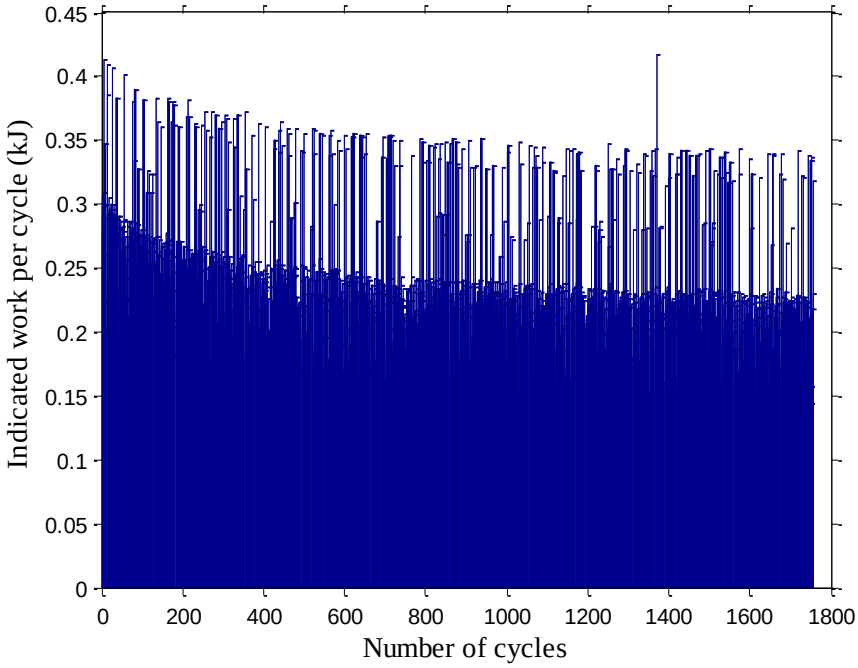

Figure 3.25: Importance of engine's warm up.

During the first series of measurements (October 2011) we experienced a short circuit and the KISTLER's wire has been cut off (Figure 3.26). After we fixed the wire, the short circuit seemed that did not affect the measurements significantly, apart from slightly more noise in the signal.

Figure 3.26: KISTLER's cut off wire due to a short circuit.

Also during the first series of measurements, after 3000 rpm, the DPF has unstuck due to the high exhaust speed developed. We changed the DPF, tested our engine and again the DPF after 3000 rpm has unstuck, thus we decided to analyze the first results and we found significant differences in the engines indicated work per cycle compared to Melisourgos work. In Figure 3.27 is shown the difference between two random graphs of the first and the second series of measurements. The difference is about 0.08 kJ in the two graphs shown.

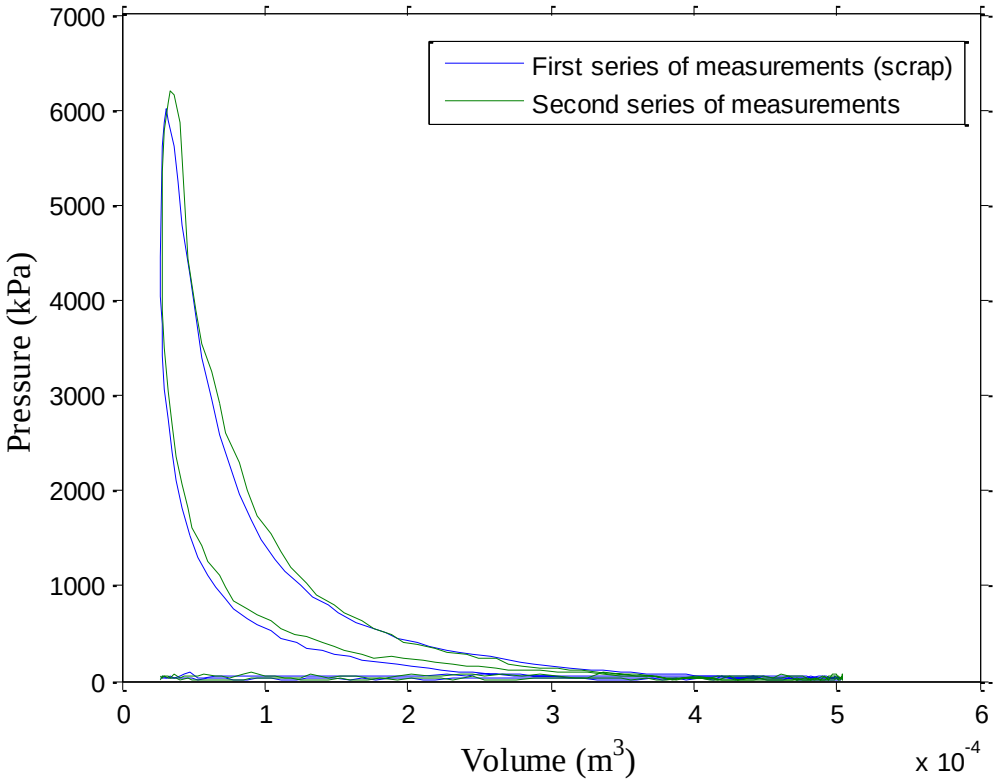

Figure 3.27: The difference in integration between the first and second series of measurements.

The DPF we used during the first series of measurements is a full filter structure with diameter 143.8 mm. In the second series of measurements we changed that with a filter block, 34 mm width, 150 mm length with a square profile.

After the first series of measurements, one of the thermocouples connected to the engine has broken (Figure 3.19, periphery thermocouple). After fixing it, we connected it to the new DPF filter and broken again. We decided to continue without fixing it, because we had to remove the exhaust and the DPF in order to fix it, and this is a time consuming procedure.

Furthermore, before starting with the second series of measurements, we replaced the generator's wires, which were connected to the resistances' device. The wires before replacing them are shown in Figure 3.28.

After we replaced the wires and started the engine again, while it was operating at 2400 rpm and three resistances, the resistances' devise fuse has blown. We changed it with a similar one and it has blown again. Finally, we chose two bigger ampere capacity fuses, replaced them and operated the engine smoothly.

Last, widespread in our experiments, we experienced problems with the laser. Sometimes due to the high oscillation, the laser's wire has loosened from its spot (Figure 3.17). As a result, we received no signal from the crank and we had to delete the empty measurements from the .txt files when we were processing the data.

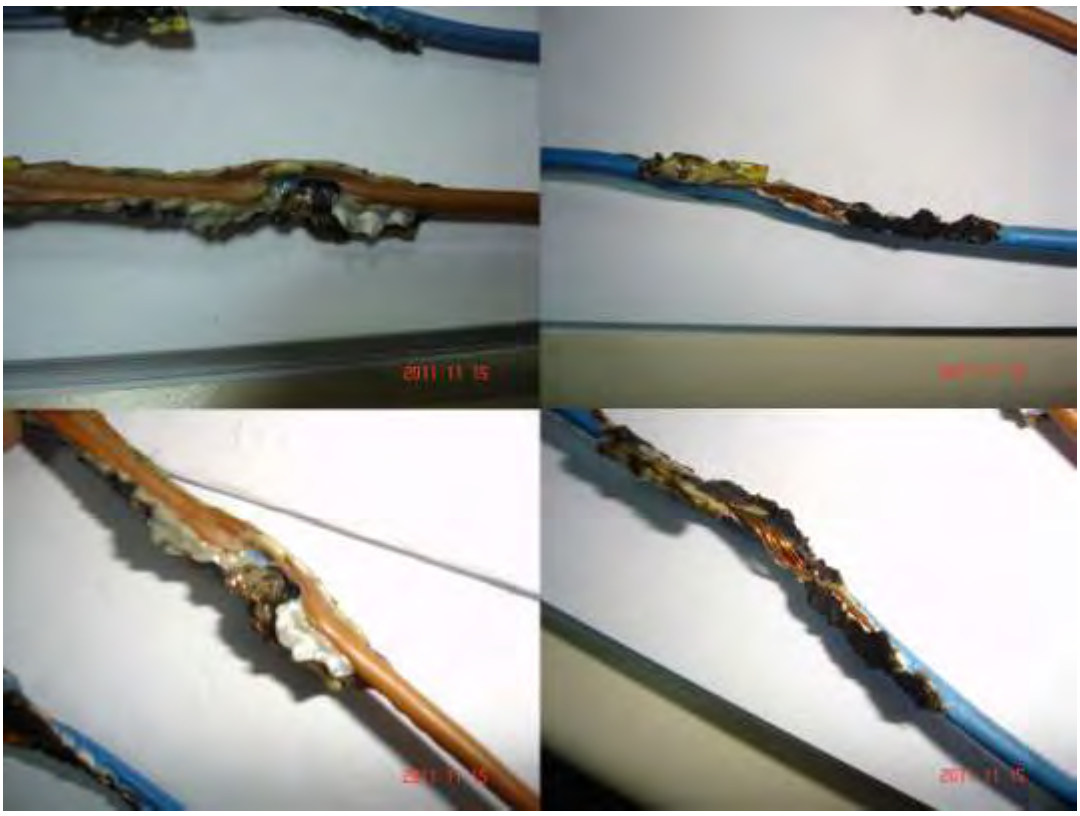

Figure 3.28: Bare generator wires before replacing them.

4 Results and discussion

In this section the results from our experiments will be demonstrated. The graphs that will be represented are P vs CA graphs for all our operation points, COV of max pressure graphs, COV vs CA graphs, mean pressure vs power graphs,

4.1 In cylinder pressure development at steady state operating conditions

All pressure data collected from the assessment cycle of this thesis shown in Figure 3.27 are plotted vs crank angle and shown in Figures 4.1–4.11. The same diagrams are plotted in logarithmic scale in Figures 4.12-4.22. In Figures 4.1–4.7 and 4.12-4.18 for the ensemble average pressure vs crank angle diagrams the rpm is been kept stable and the pressure difference is shown when load is added to the engine. In Figures 4.8–4.11 and 4.19-4.22 we show the same diagrams with the difference that the load added to the engine is been kept stable and the difference of the various rpm operation points at the same load conditions is been shown. While the data we had beginning from crank angle 0^{o}, we manipulated them and for our convenience begin from crank angle 250^{o}. Note also that the data plotted are not continuous but discrete. The line shown has been made from experimental data in each crank angle. We present them through line for our convenience.

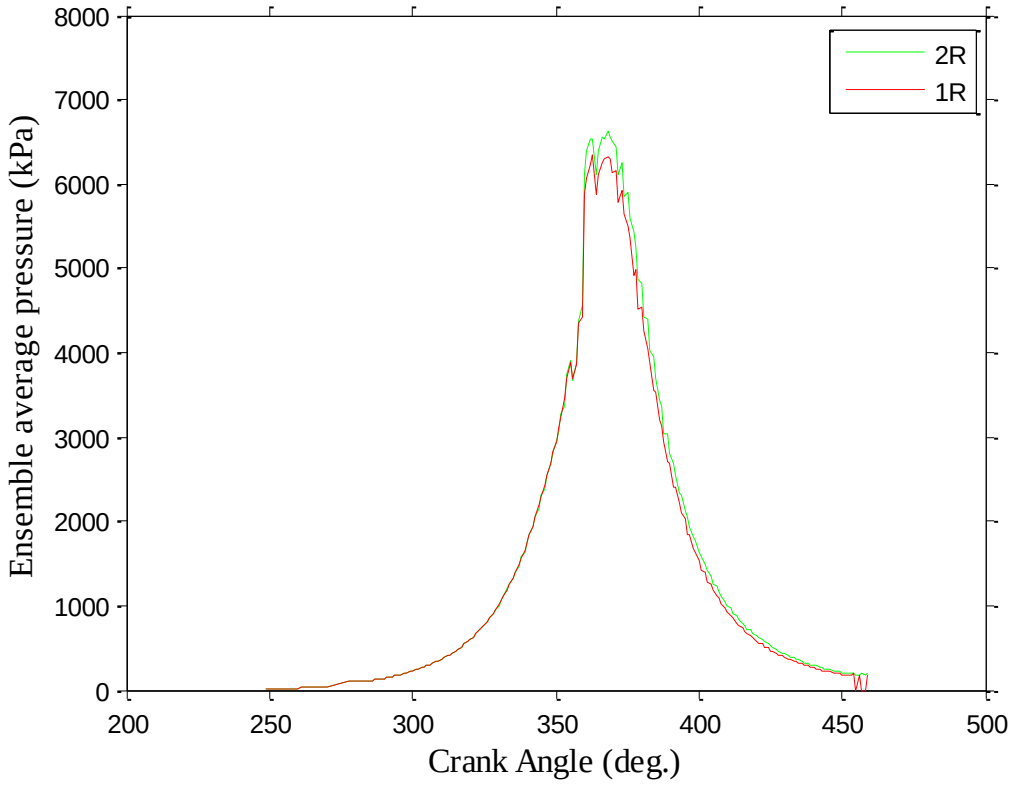

Figure 4.1: Ensemble average pressure vs crank angle at 2000 rpm.

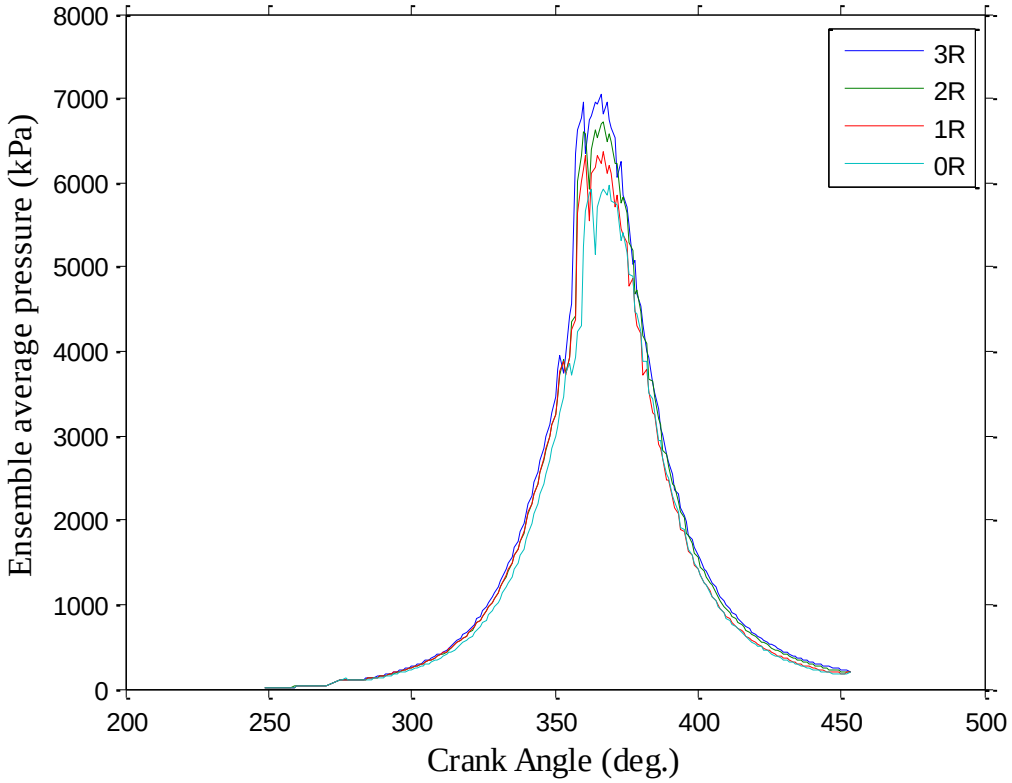

Figure 4.2: Ensemble average pressure vs crank angle at 2200 rpm.

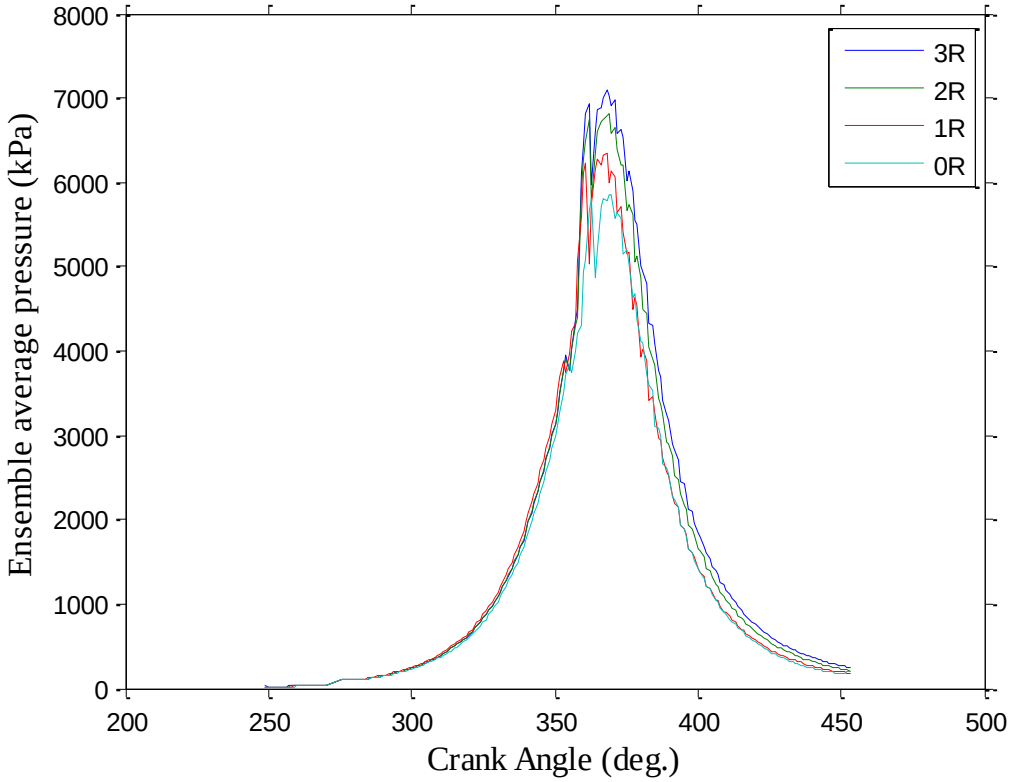

Figure 4.3: Ensemble average pressure vs crank angle at 2400 rpm.

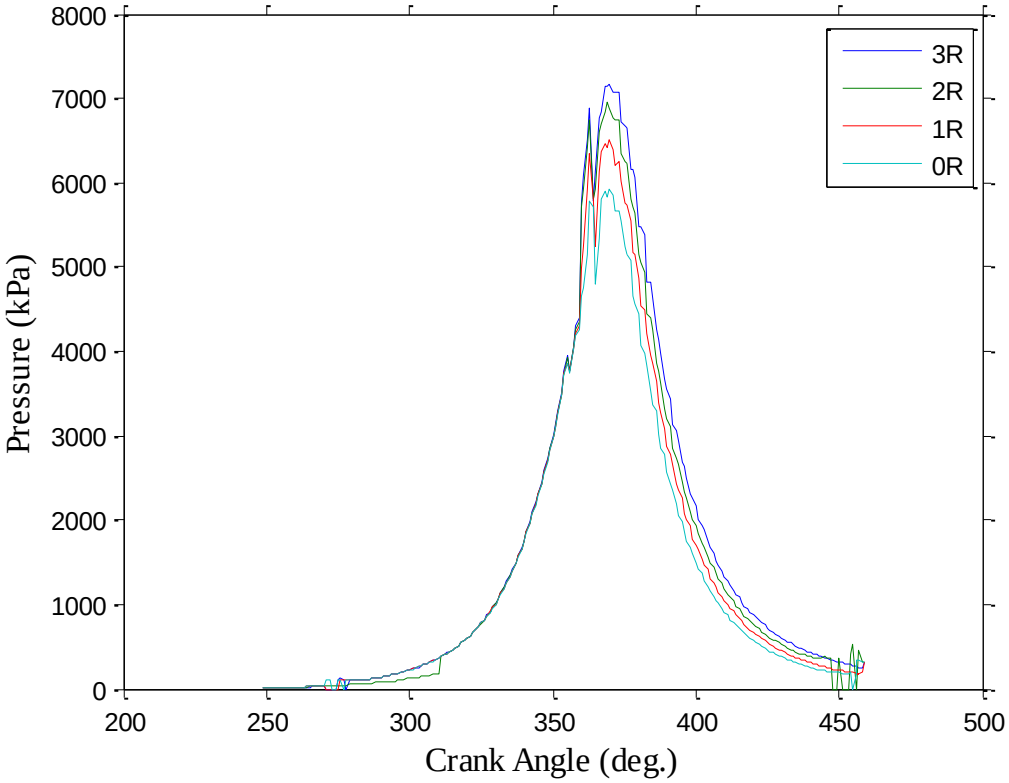

Figure 4.4: Ensemble average pressure vs crank angle at 2600 rpm.

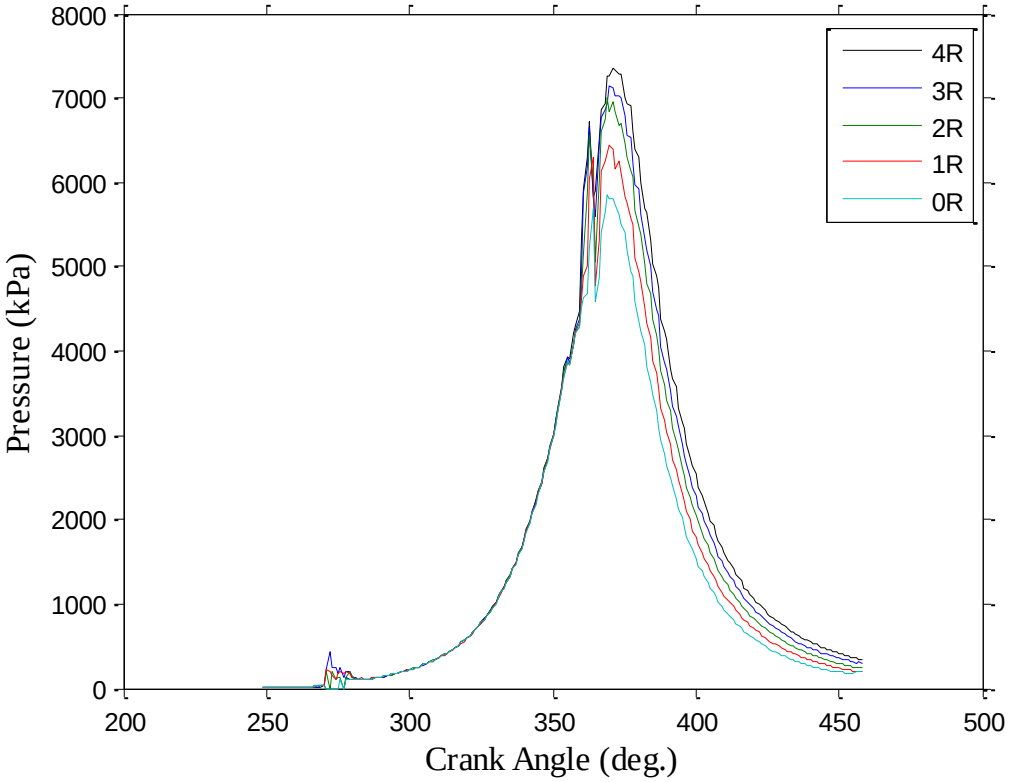

Figure 4.5: Ensemble average pressure vs crank angle at 2800 rpm.

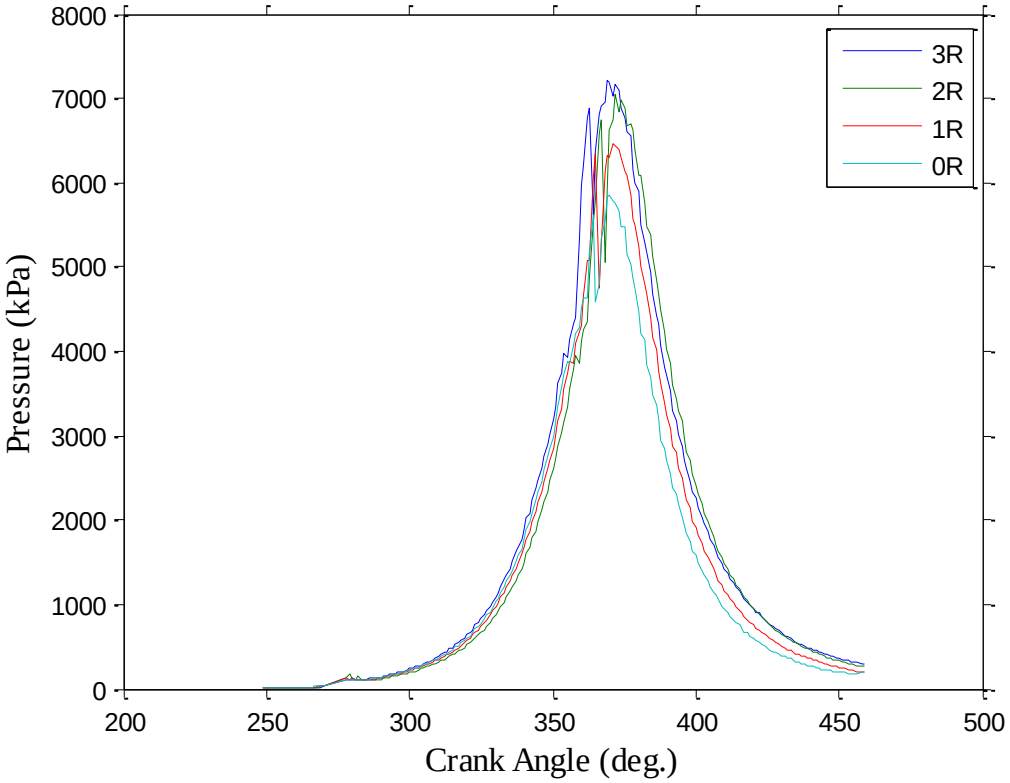

Figure 4.6: Ensemble average pressure vs crank angle at 2900 rpm.

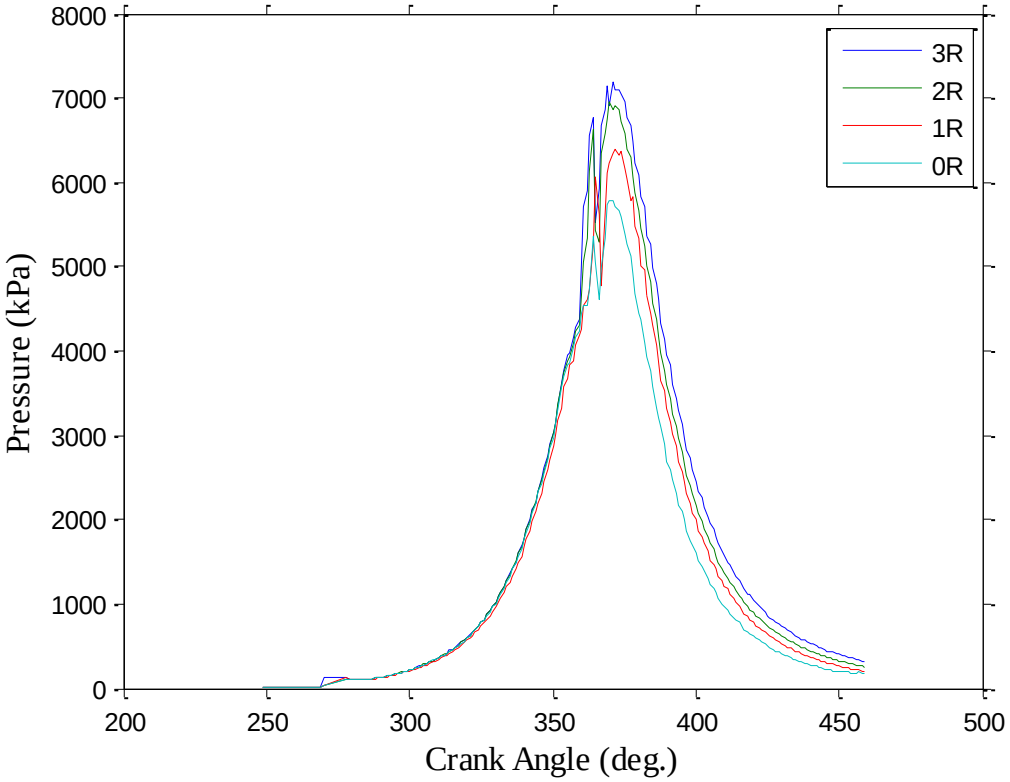

Figure 4.7: Ensemble average pressure vs crank angle at 3100 rpm.

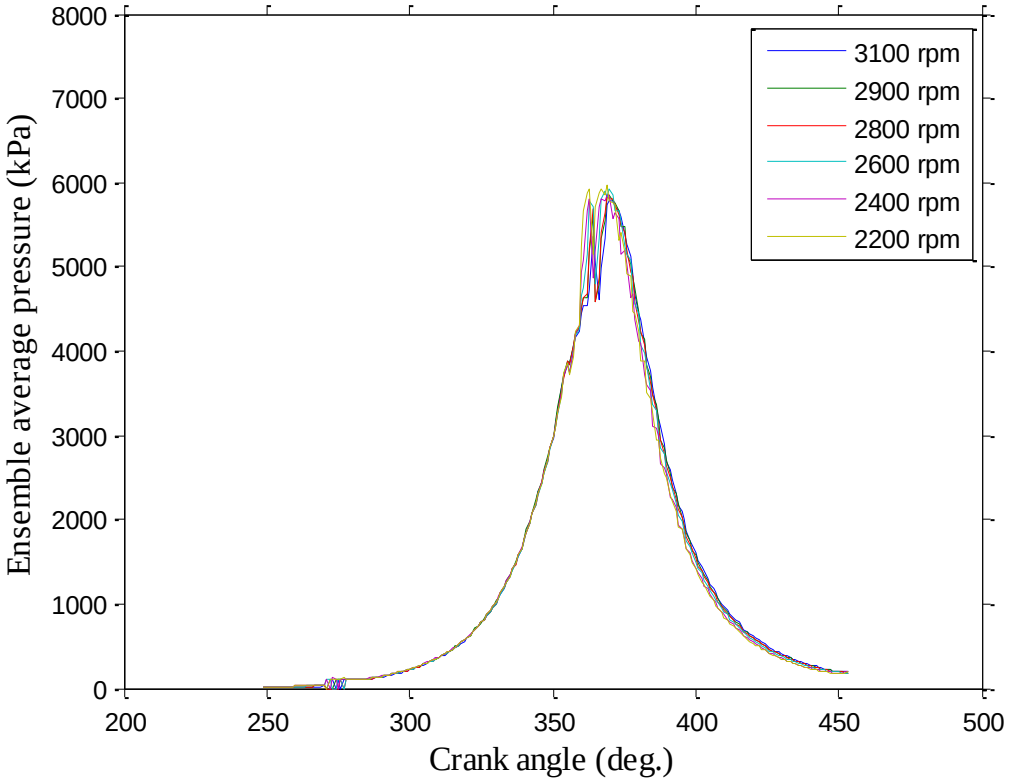

Figure 4.8: Ensemble average pressure vs crank angle at no load.

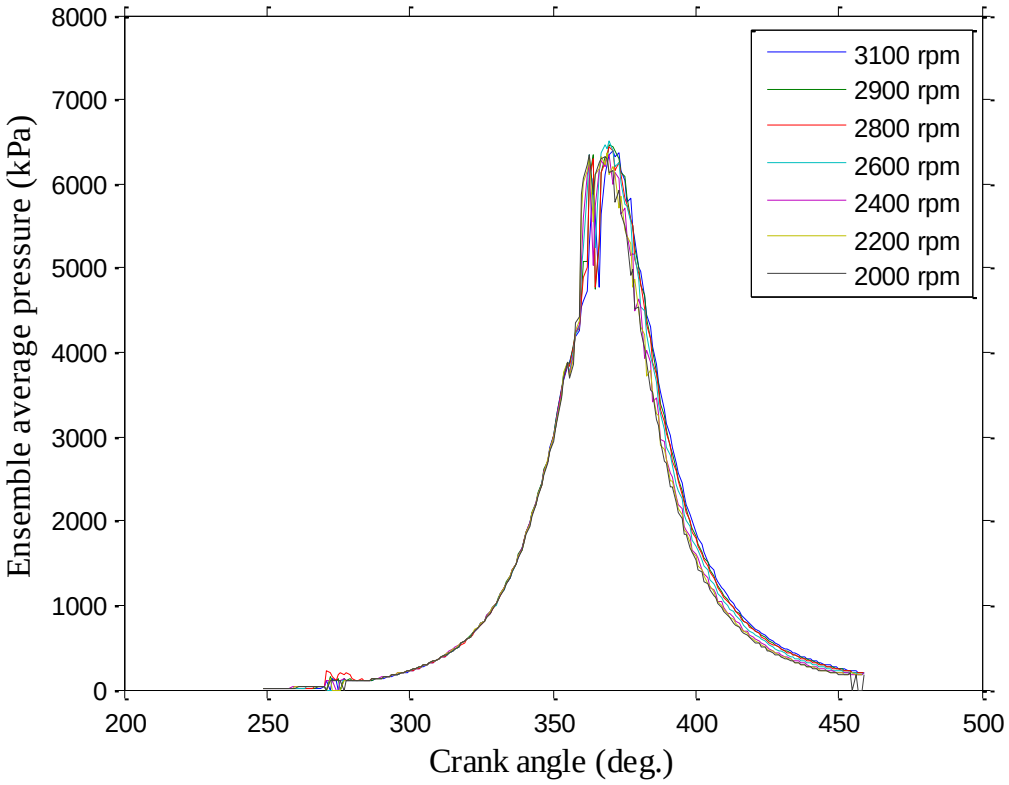

Figure 4.9: Ensemble average pressure vs crank angle at 1R.

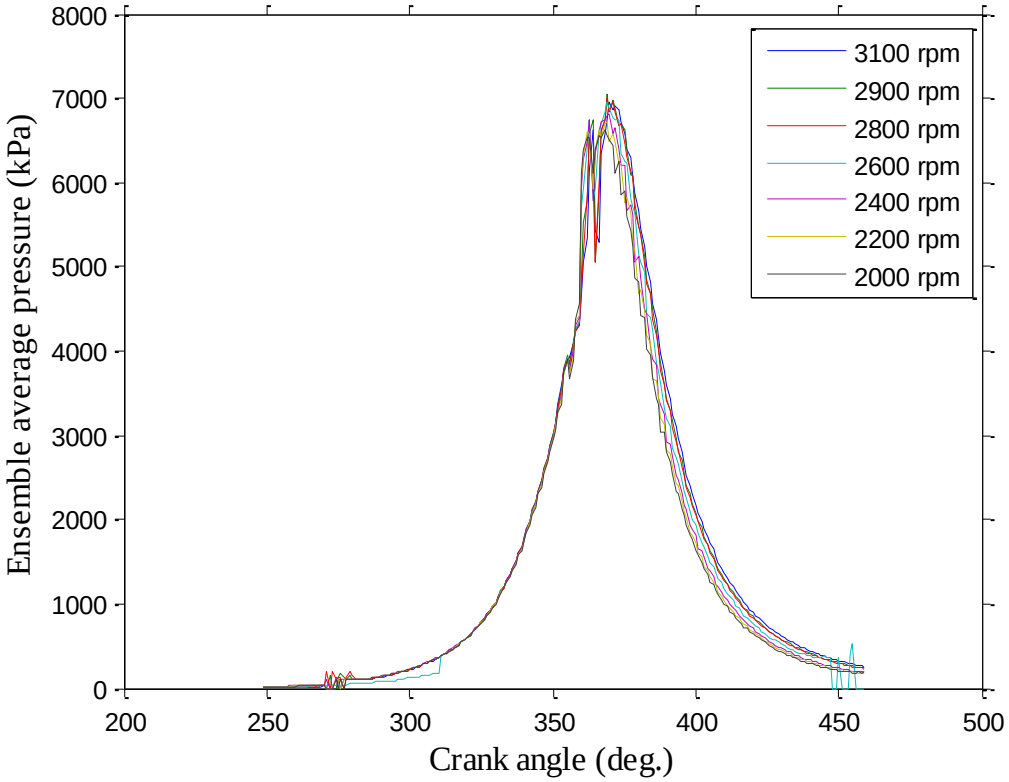

Figure 4.10: Ensemble average pressure vs crank angle at 2R.

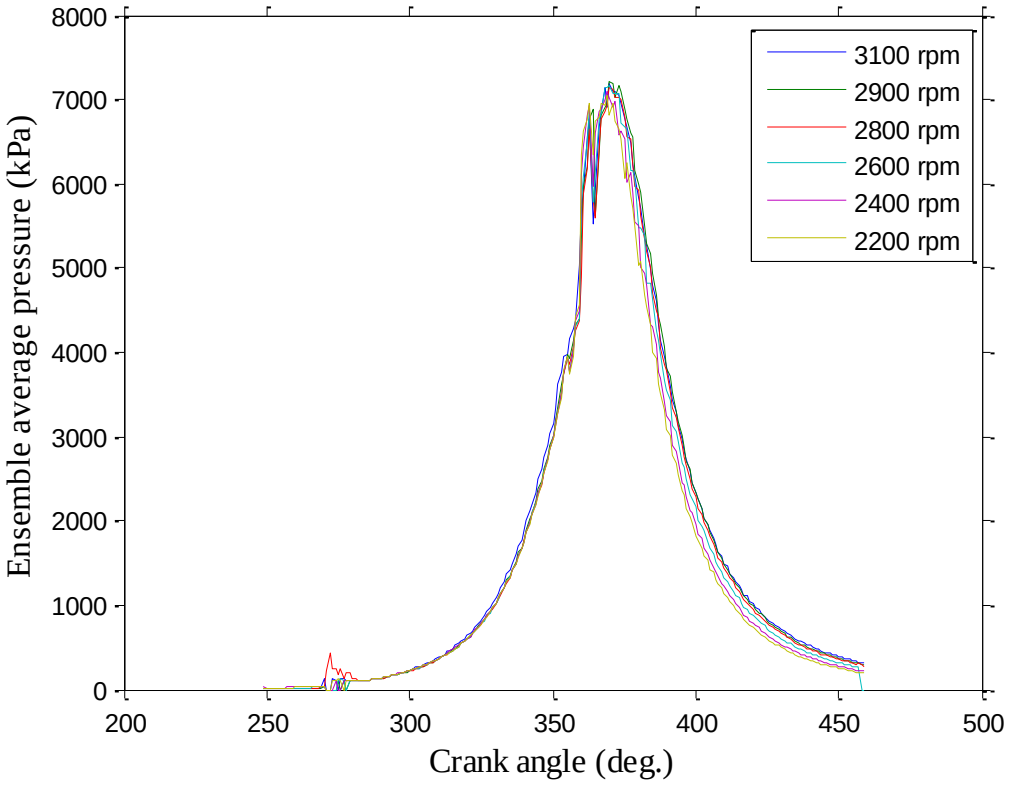

Figure 4.11: Ensemble average pressure vs crank angle at 3R.

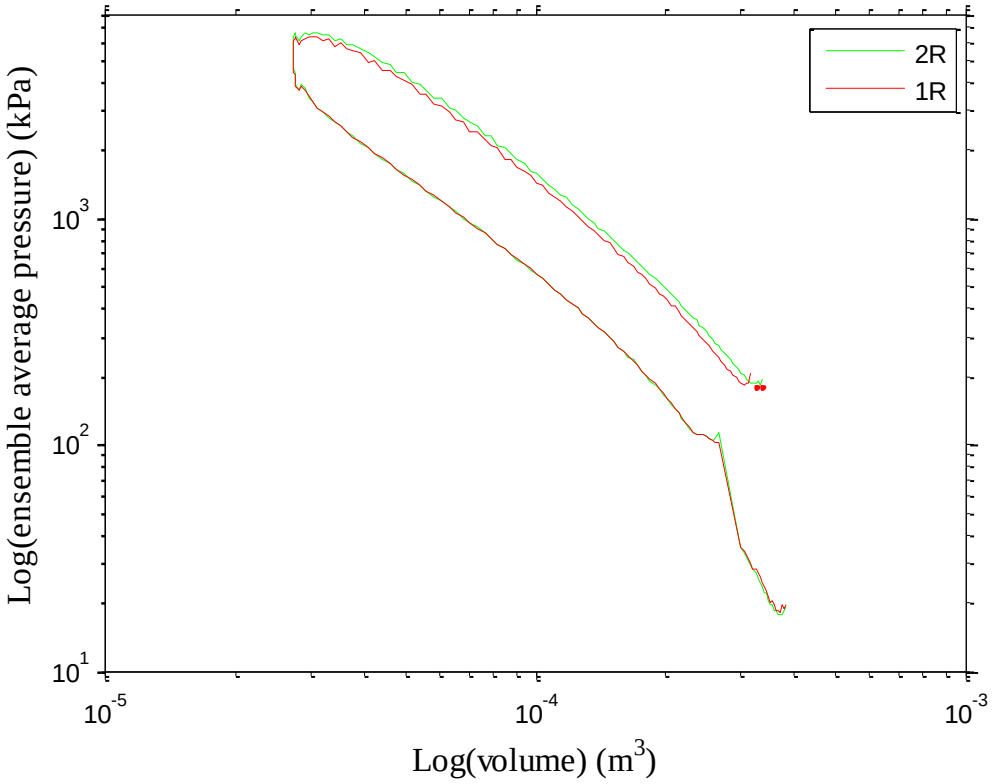

Figure 4.12: Log(ensemble average pressure) vs log(V) at 2000 rpm.

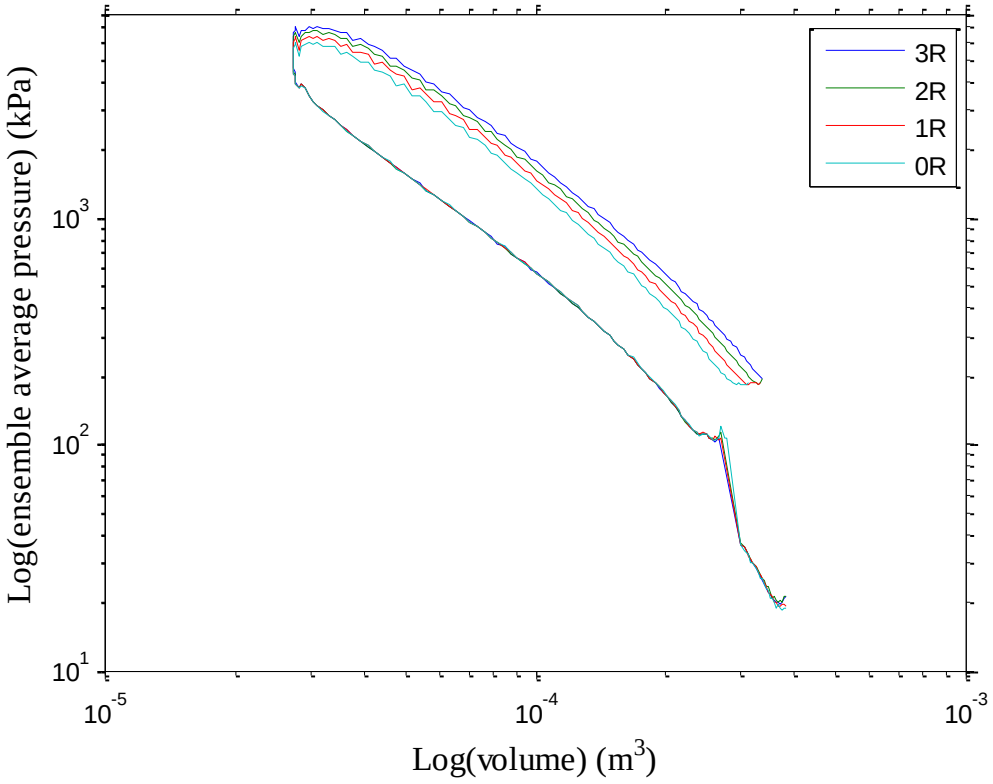

Figure 4.13: Log(ensemble average pressure) vs log(V) at 2200 rpm.

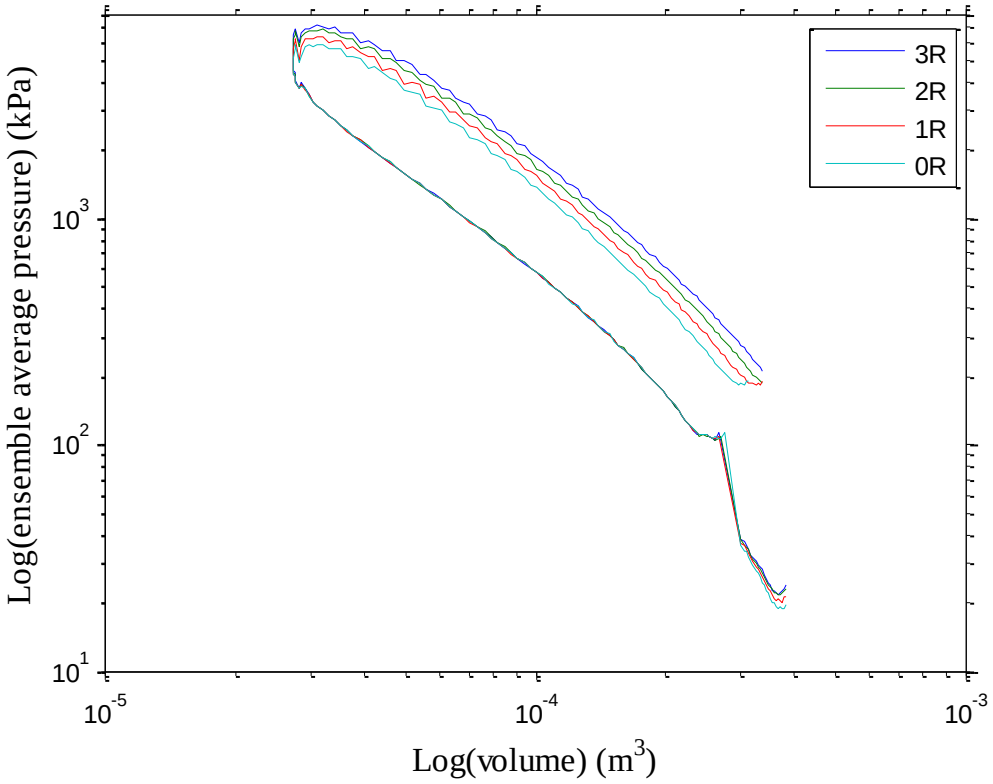

Figure 4.14: Log(ensemble average pressure) vs log(V) at 2400 rpm.

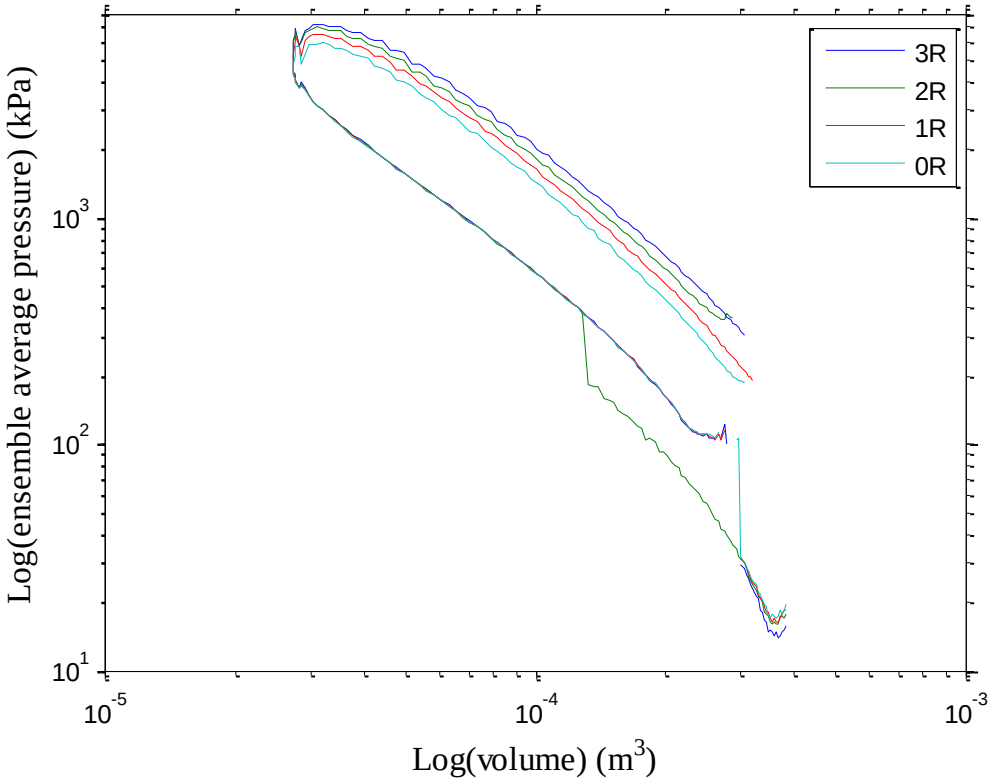

Figure 4.15: Log(ensemble average pressure) vs log(V) at 2600 rpm.

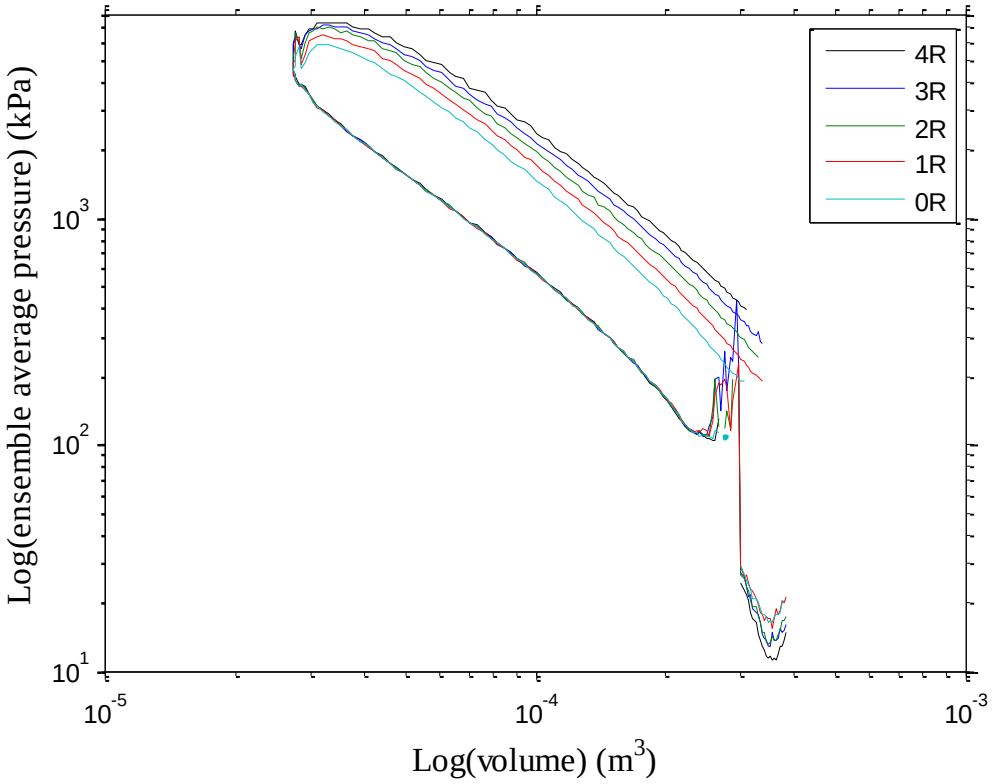

Figure 4.16: Log(ensemble average pressure) vs log(V) at 2800 rpm.

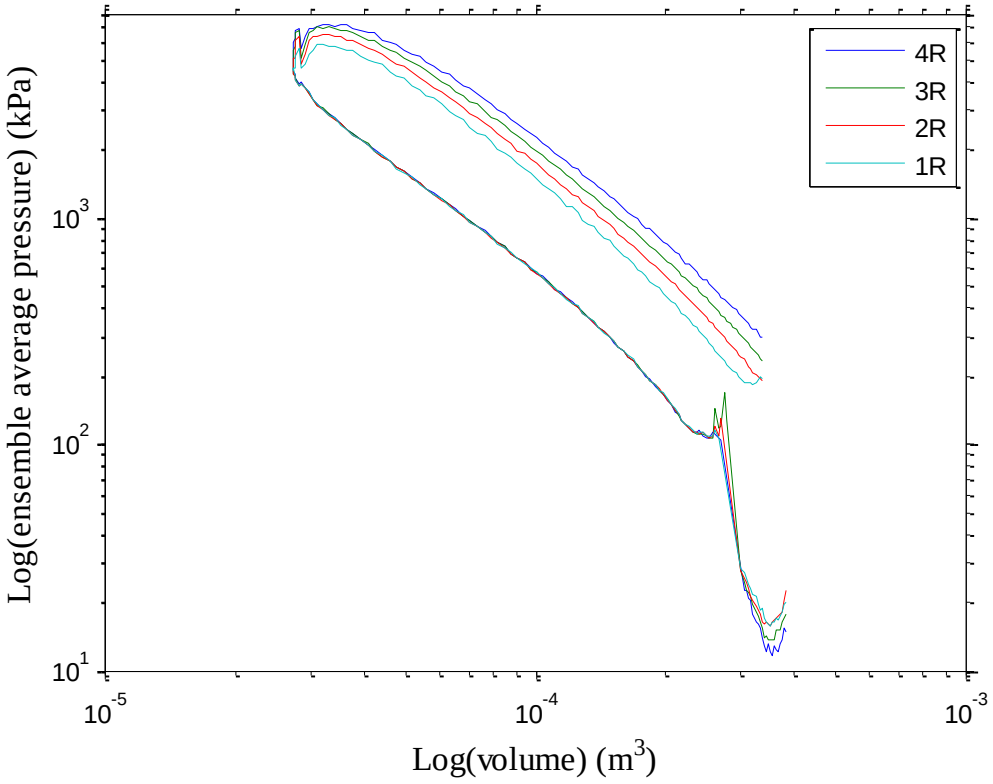

Figure 4.17: Log(ensemble average pressure) vs log(V) at 2900 rpm.

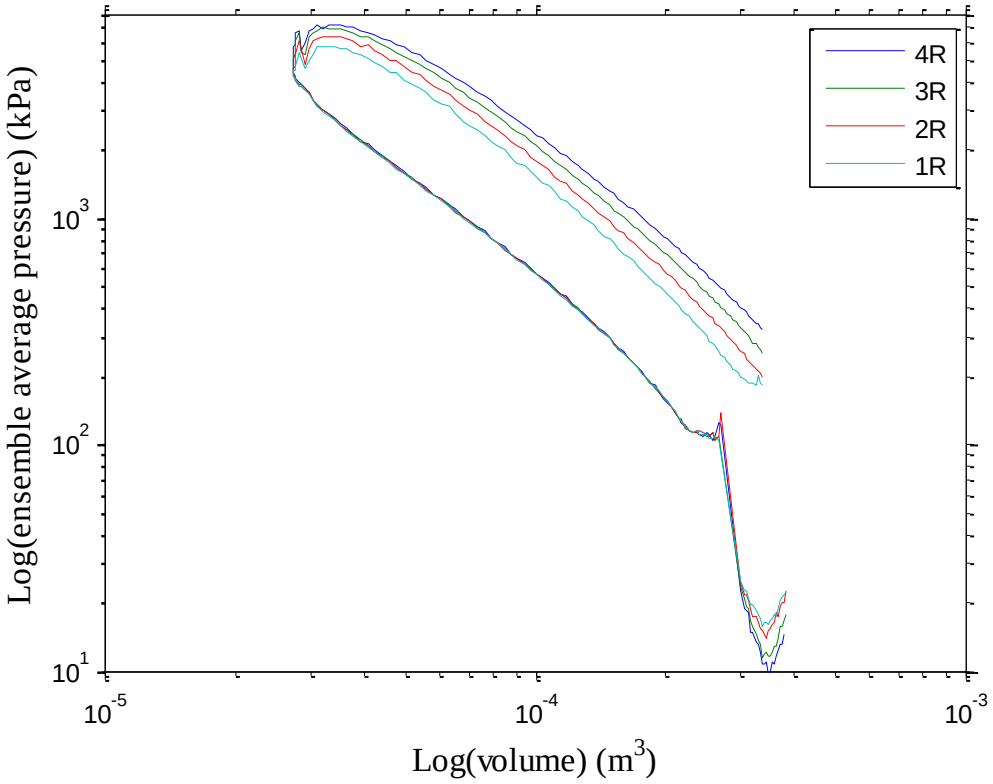

Figure 4.18: Log(ensemble average pressure) vs log(V) at 3100 rpm.

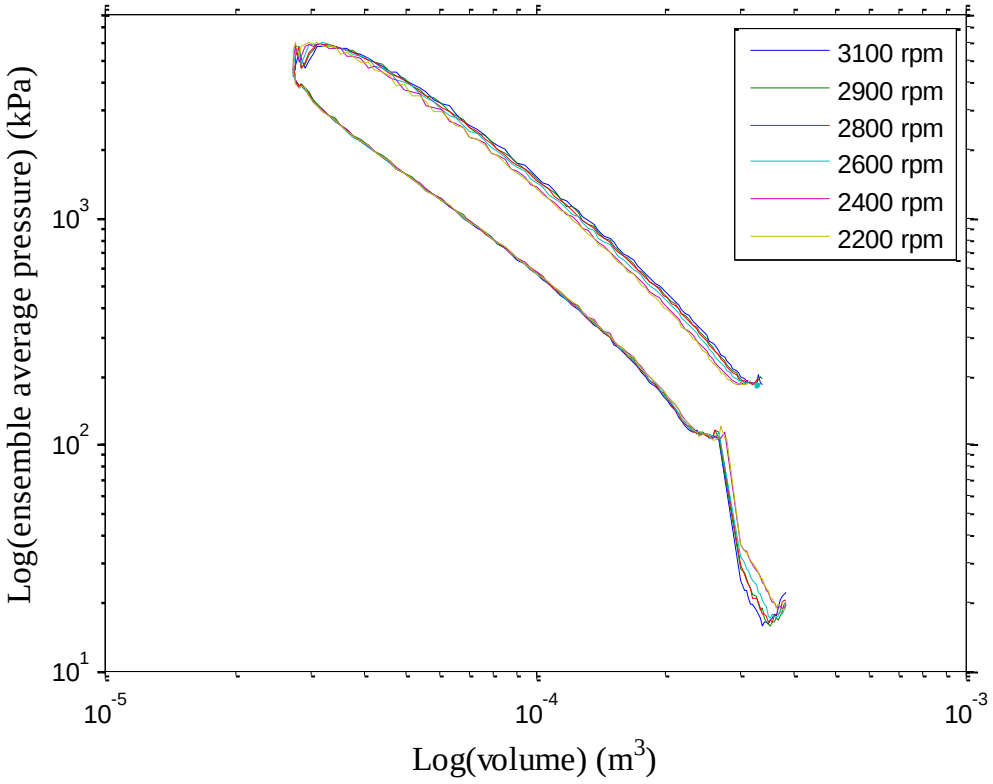

Figure 4.19: Log(ensemble average pressure) vs log(V) at no load.

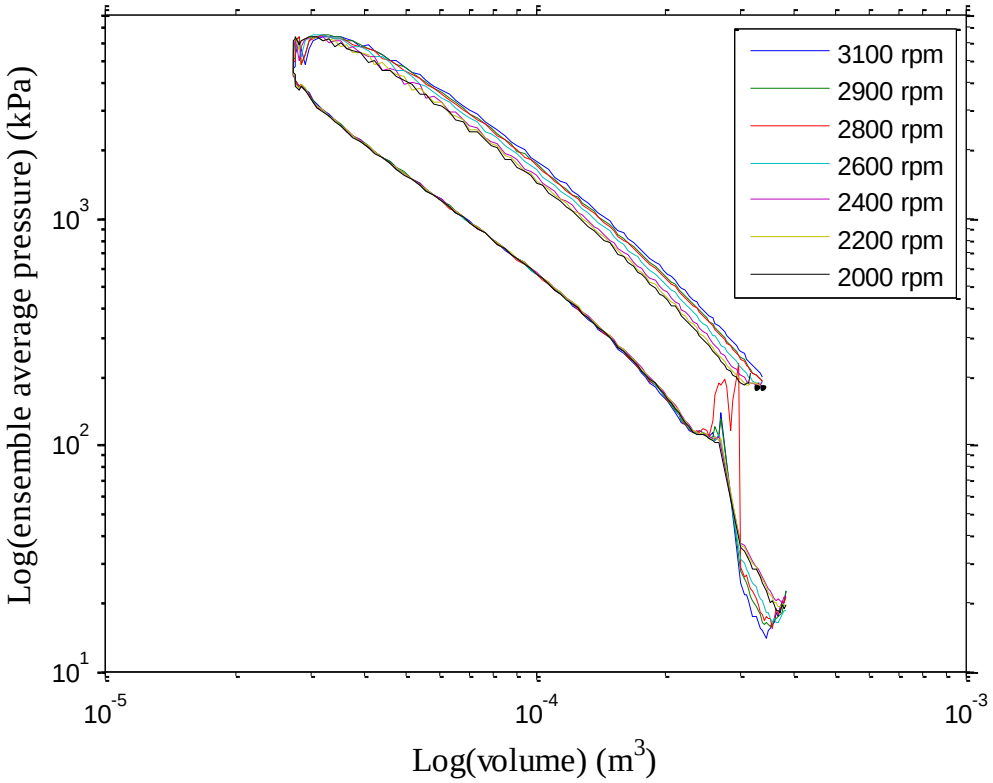

Figure 4.20: Log(ensemble average pressure) vs log(V) at 1R.

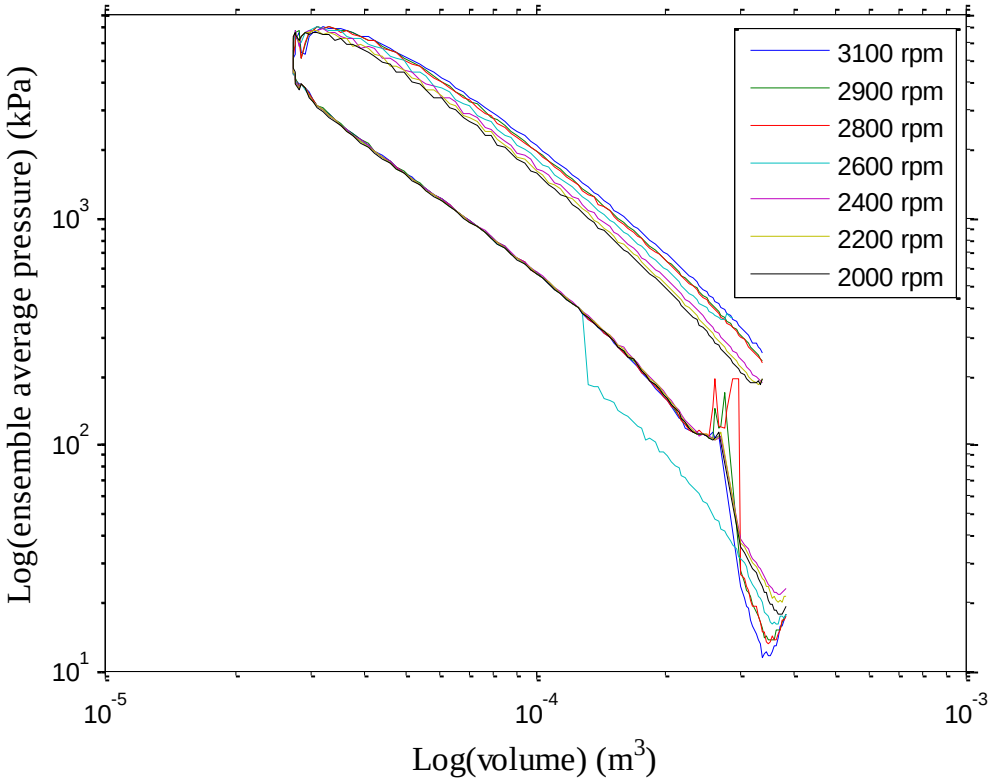

Figure 4.21: Log(ensemble average pressure) vs log(V) at 2R.

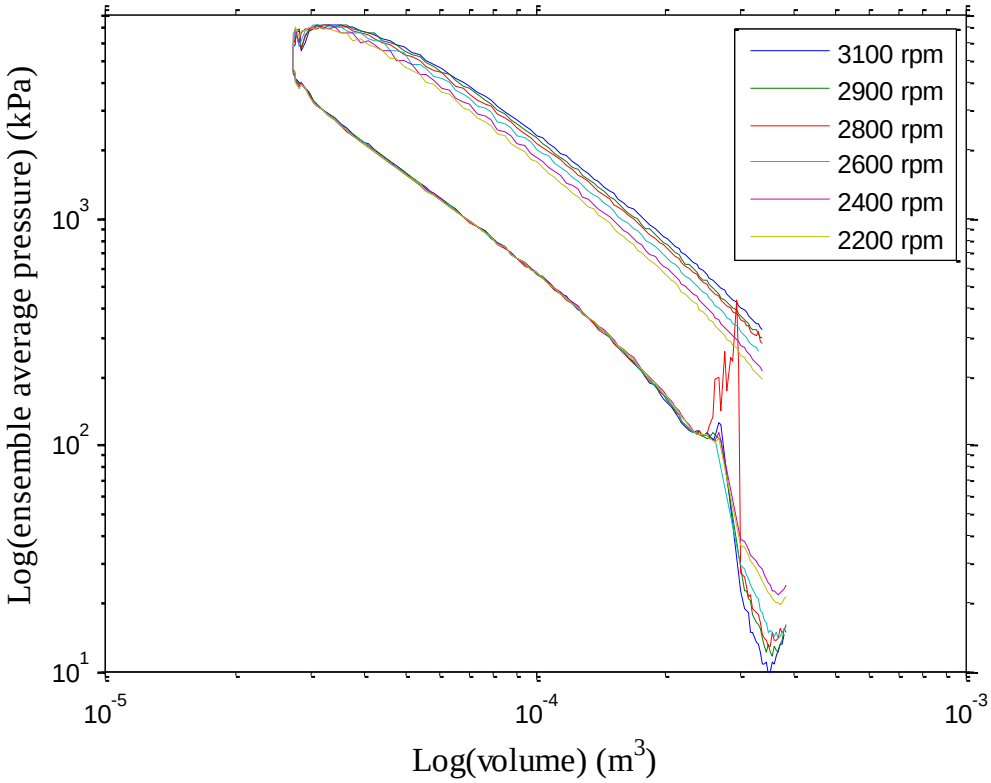

Figure 4.22: Log(ensemble average pressure) vs log(V) at 3R.

Theory [5, 6, 8] denotes that in compression ignition engines, compression begins at about 100^{o} bTDC, then at 20^{o} bTDC the fuel is injected to the cylinder, a 9^{o} delay occurs after the start of injection to the start of the combustion and the peak pressure comes along about 5^{o} after TDC.

All these phenomena are visible throughout our measurements. In the start of compression, pressure begins to rise above atmospheric. The start of injection can be figured out via the abnormality the ensemble average pressure diagram appears. Figure 4.23 illustrates the ensemble average pressure (blue line and dots) of 2000 rpm with 1R operating and a random individual combustion cycle. We zoomed into the start of injection and notice that the ensemble average pressure diagram while it rises, the average pressure drops at the next crank angle and then continues rising.

In the same diagram we have put a random instantaneous combustion cycle to illustrate that in an individual diagram, the injection start cannot be noticed. What can be noticed is the start of combustions which is visible from a sudden change of slope [6] (Figure 4.24).

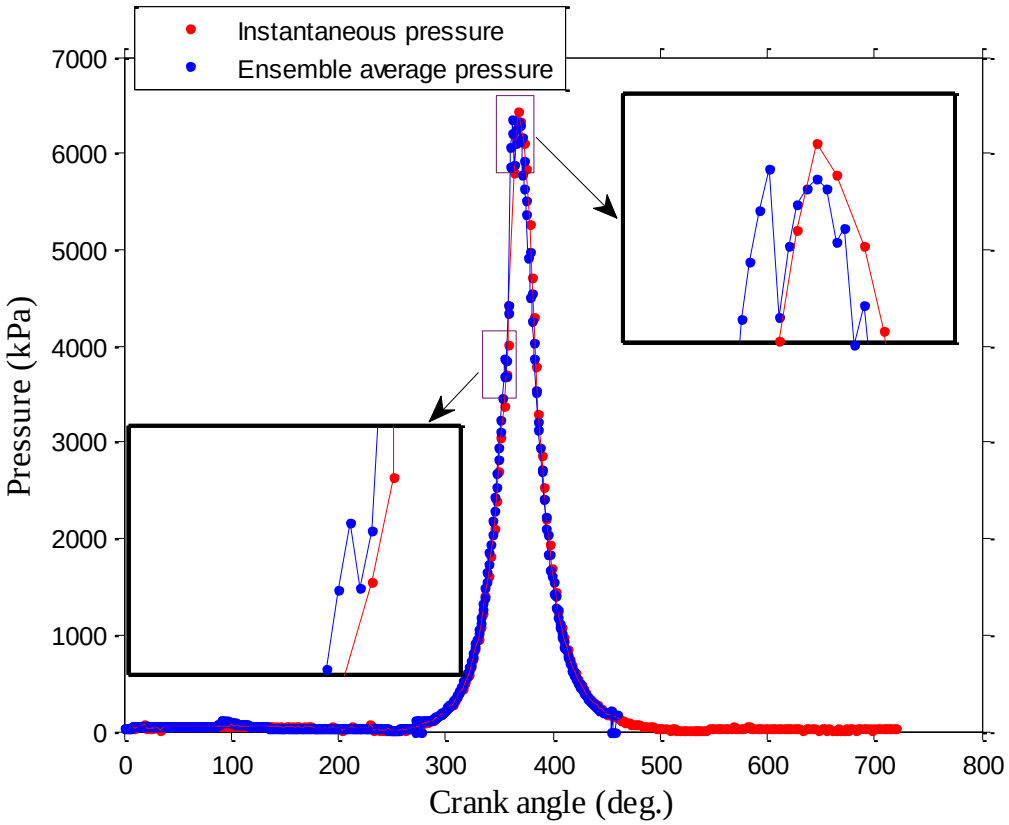

Figure 4.23: Instantaneous and ensemble average pressure vs crank angle. A closer look.

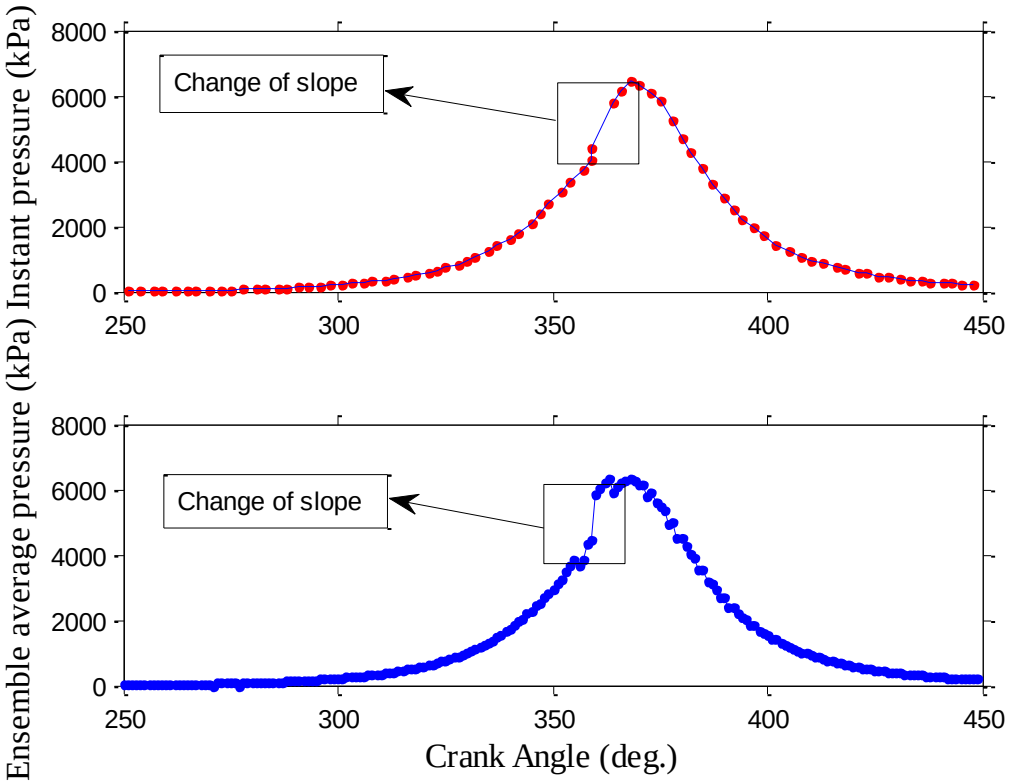

Figure 4.24: Ensemble average pressure and instant pressure vs crank angle.

The strangest result of these pressure diagrams is the sudden drop of ensemble average pressure, while it tries to reach its peak, and rise again (Figure 4.23). Similar behavior is appeared to common rail diesel engines (because of pilot injection), but our engine is not common rail, it is naturally aspired. In gas or petrol engines a similar behavior is not observed [2, 9]. What can be seen from Zervas's diagram is the sudden change of slope that indicates the beginning of combustion.

We tried to attribute the abnormality to statistical phenomena (number of combustion cycles used, excel turbulence) but failed. Probably during the first combustion phase (when pressure falls) fuel residues are been burned and then when pressure rises, combustion is been controlled by the fuel injection rate.

One other reason that may explain the abnormality may have to do with the friction tape attached to the crank disk and the data acquisition code.

To further investigate the abnormality we measured from the diagrams its height and length for each operation point. Height and length can be found in Table 4.1. It is noticed that the length of the abnormality, for engine steady load operations, extends with the rpm in all our occasions. Specifically, for no engine load, length goes from 4 to 6 degrees, at 1R length goes from 5 (2000 rpm) and 4 (2200 rpm) degrees to 7 degrees, at 2R goes from 3 to 6 degrees and at 3R length goes from 4 to 7 (2800 rpm). At 2900 rpm its length is 6 degrees and at 3100 5.

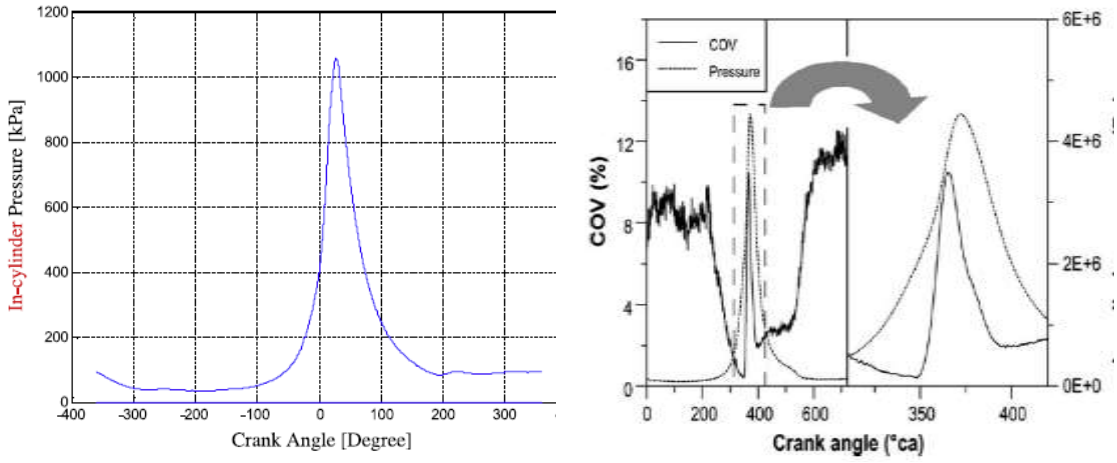

Figure 4.25: Ceviz et al. ensemble average pressure vs crank angle diagram of 100 consecutive cycles [2] (left) and Zervas ensemble average pressure vs crank angle diagram of 200 consecutive cycles [9] (right).

Table 4.1: Abnormality's height and length for all our operation points.

Rpm	Resistances operating	Abnormality's height (kPa)	Abnormality's length (deg.)
2000	1	480	5
	2	430	3
2200	0	775	4
	1	775	4
	2	645	3
	3	615	4
2400	0	940	4
	1	1205	4
	2	950	4
	3	965	6
2600	0	990	5
	1	1110	5
	2	940	6
	3	1075	6
2800	0	1090	5
	1	1515	6
	2	1520	6
	3	1060	7
	4	895	7
2900	0	960	5
	1	1600	6
	2	1680	5
	3	1275	6
3100	0	750	6
	1	1285	7
	2	1325	6
	3	1230	5

More interesting appears to be the abnormality's height. For engine steady load it starts from its minimum value at 2000/2200 rpm, peaks at 2900 rpm (apart from no

load conditions when it peaks to 2800 rpm) and then drops at 3100 rpm. For our series of measurements it cannot be correlated with any other factor and needs further investigation.

That purpose tries to accomplish Figures 4.26-4.32. The red line represents the average maximum pressure at each crank angle, the box represents the 25 and 75 % confidence interval and the blue lines the 1 and 99 % confidence interval. The red cross represents a totally out of confidence interval value. At 2000, 2200 and 2400 rpm, 4 degrees is the value with the lowest mean maximum pressure at each combustion cycle, at 2600, 2800 and 2900 rpm, 5 degrees has the lowest average maximum pressure and at 3100 rpm, we find minimum pressure at 6 degrees. This may have a correlation with the abnormality's length growth with rpm. If we gather all the crank angle values of maximum pressure, then the distribution that best describes them is normal distribution, with sample average 9 degrees and standard deviation 3 degrees (not shown). This data fit became with the Rockwell's Arena program.

Apart from the pressure abnormality, our ensemble average pressure vs crank angle diagrams do not appear something else unusual. Maximum pressure rises with rpm and load added to the engine as expected in all operation points. The pressure lines start from almost the same point, and after combustion they follow a different path. Pressure lines of higher rpm and load are broader than the ones of lower rpm and load.

4.2 COV analysis

Another way to examine our engine's operation is to perform a COV analysis for its various operation points. Equation 10 stands for imep, but we can expand the equation for any measurable quantity. Figure 4.33 illustrates the average pressure with its std vs indicated load for all operation points. Without load all rpm have the same average maximum pressure. The slight differences exist due to the different level our engine was operating. The more our engine operates the less frictions it will develop thus less power and pressure will be needed to overcome the friction.

Operation at 2600 rpm produces more mean maximum pressure at 1R, more than 2800, 3100 rpm and almost equal with 2900 rpm. At 3 kW indicated load 2600, 2800, 2900 and 3100 rpm have very little difference in mean maximum

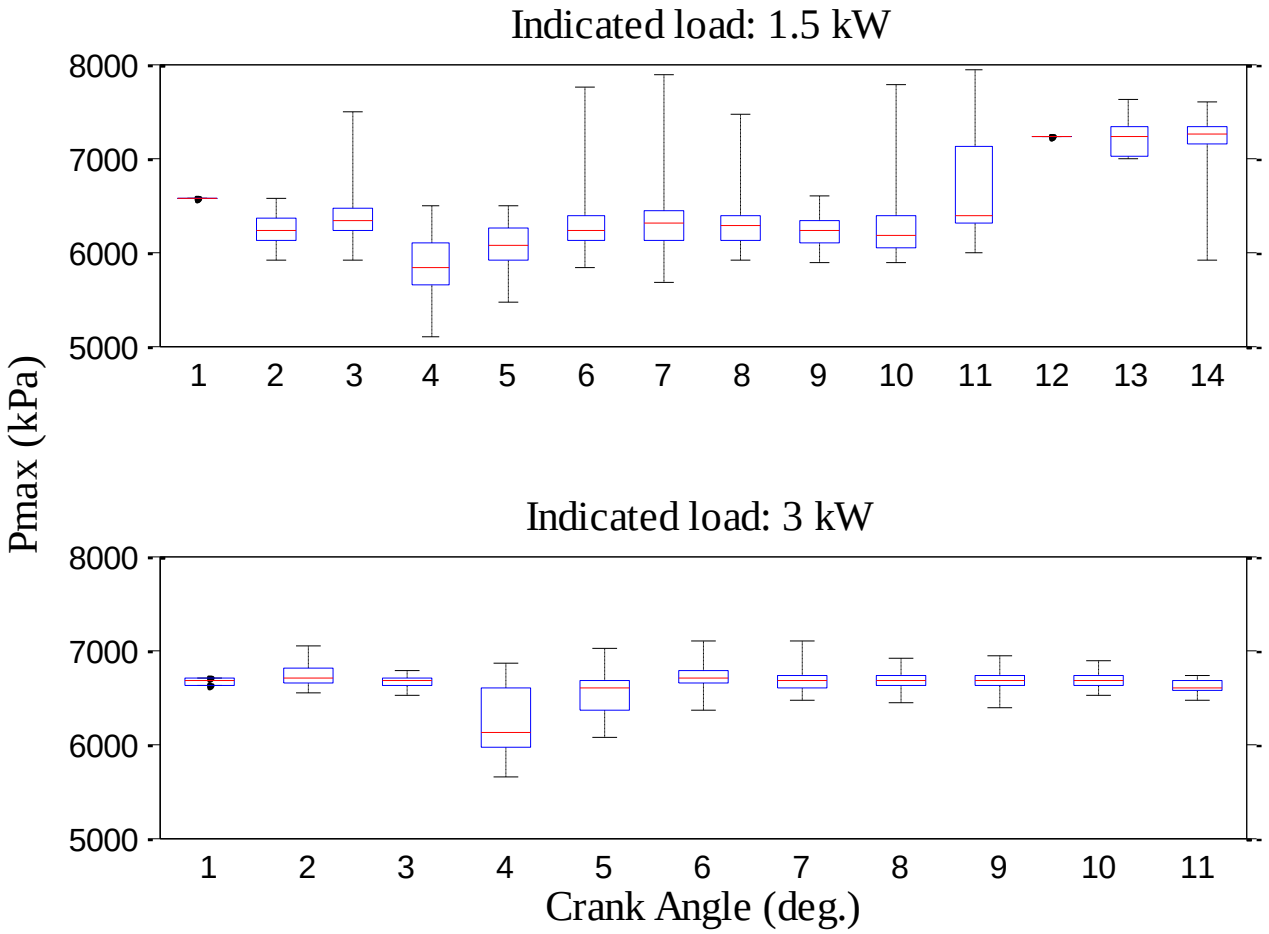

Figure 4.26: Box-and-whisker diagram of maximum pressure vs crank angle at 2000 rpm.

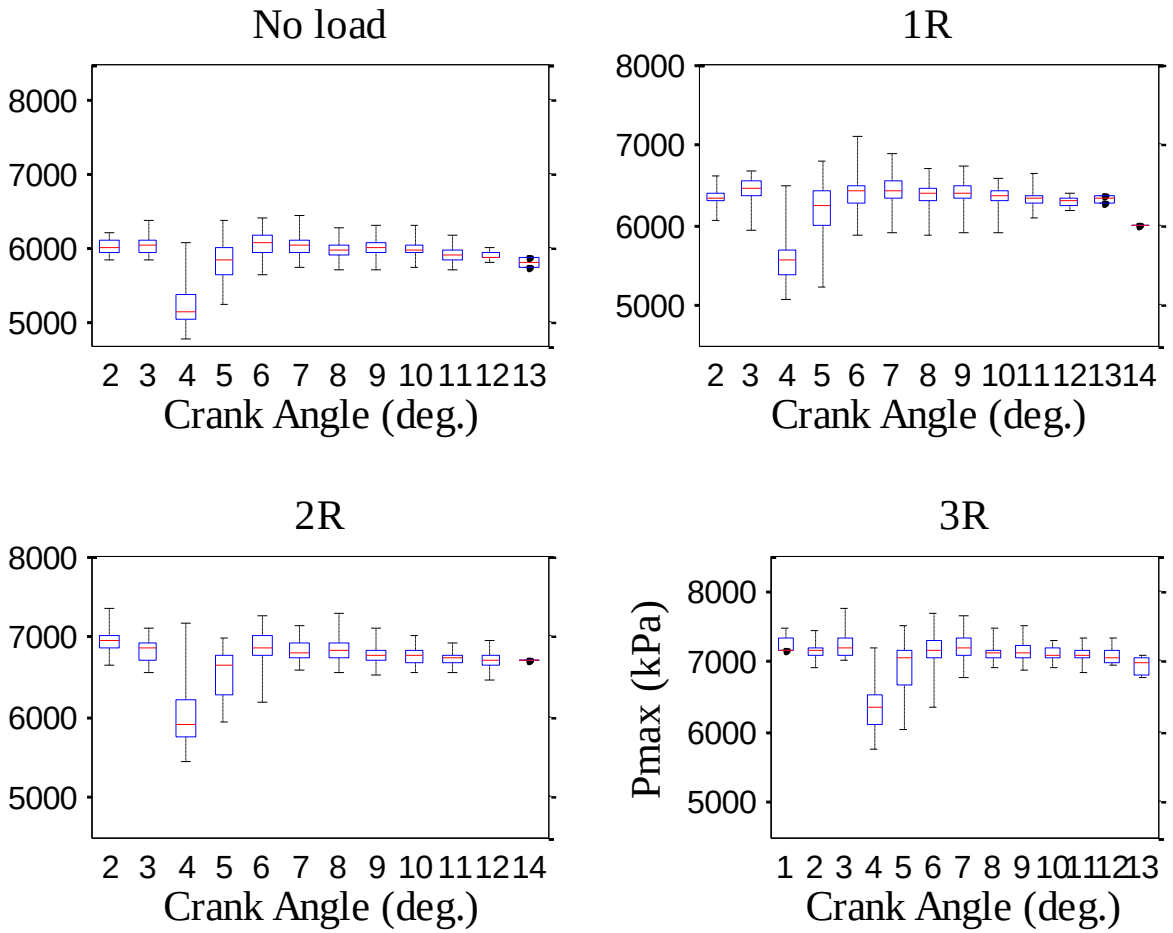

Figure 4.27: Box-and-whisker diagram of maximum pressure vs crank angle at 2200 rpm.

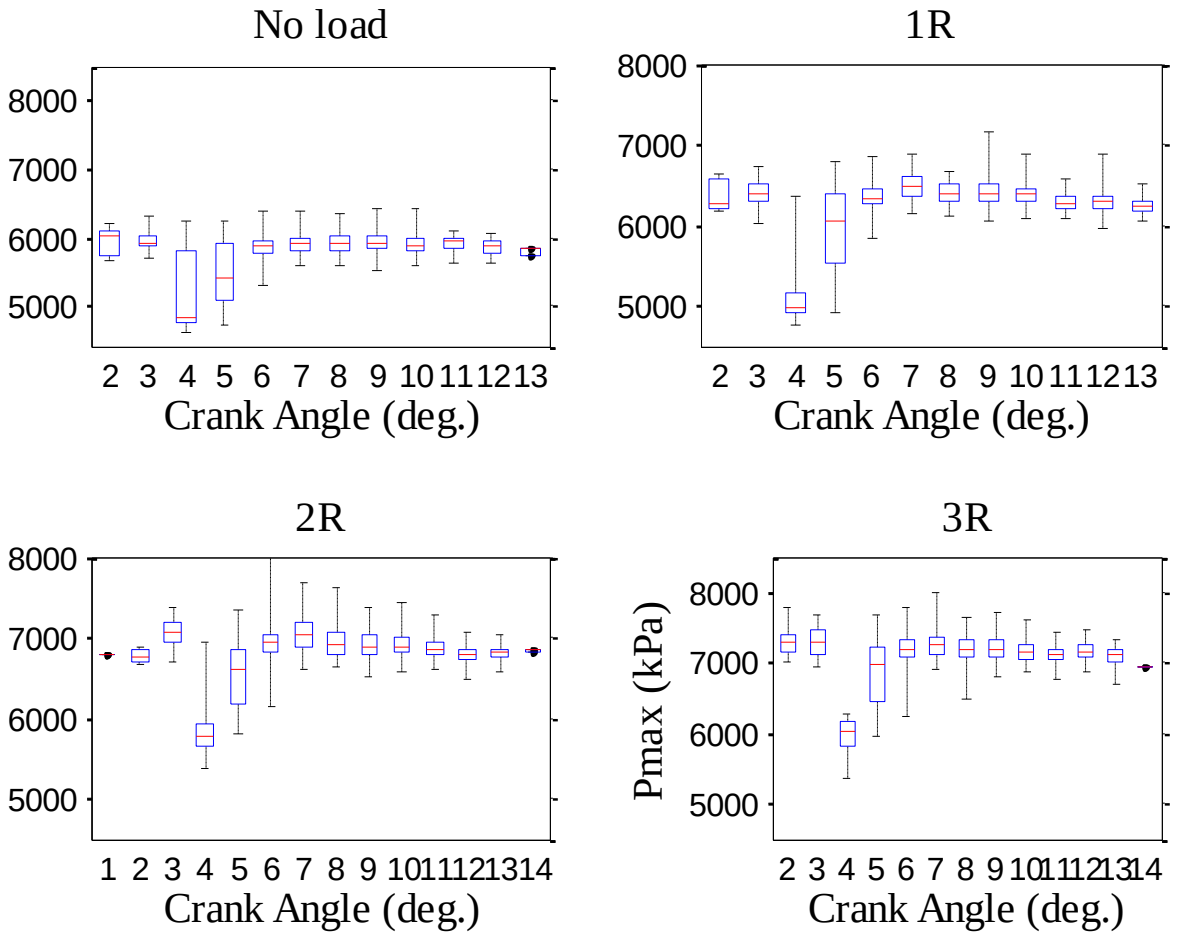

Figure 4.28: Box-and-whisker diagram of maximum pressure vs crank angle at 2400 rpm.

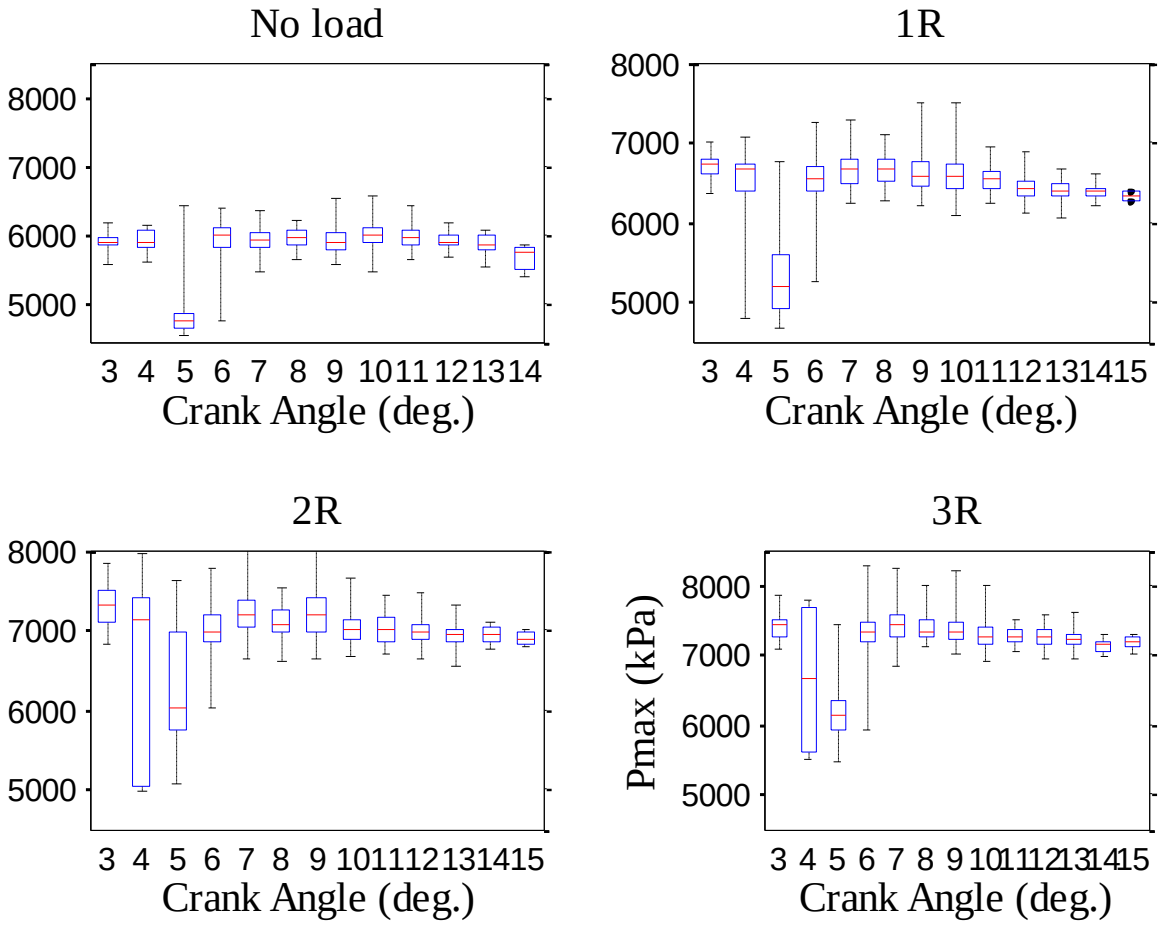

Figure 4.29: Box-and-whisker diagram of maximum pressure vs crank angle at 2600 rpm.

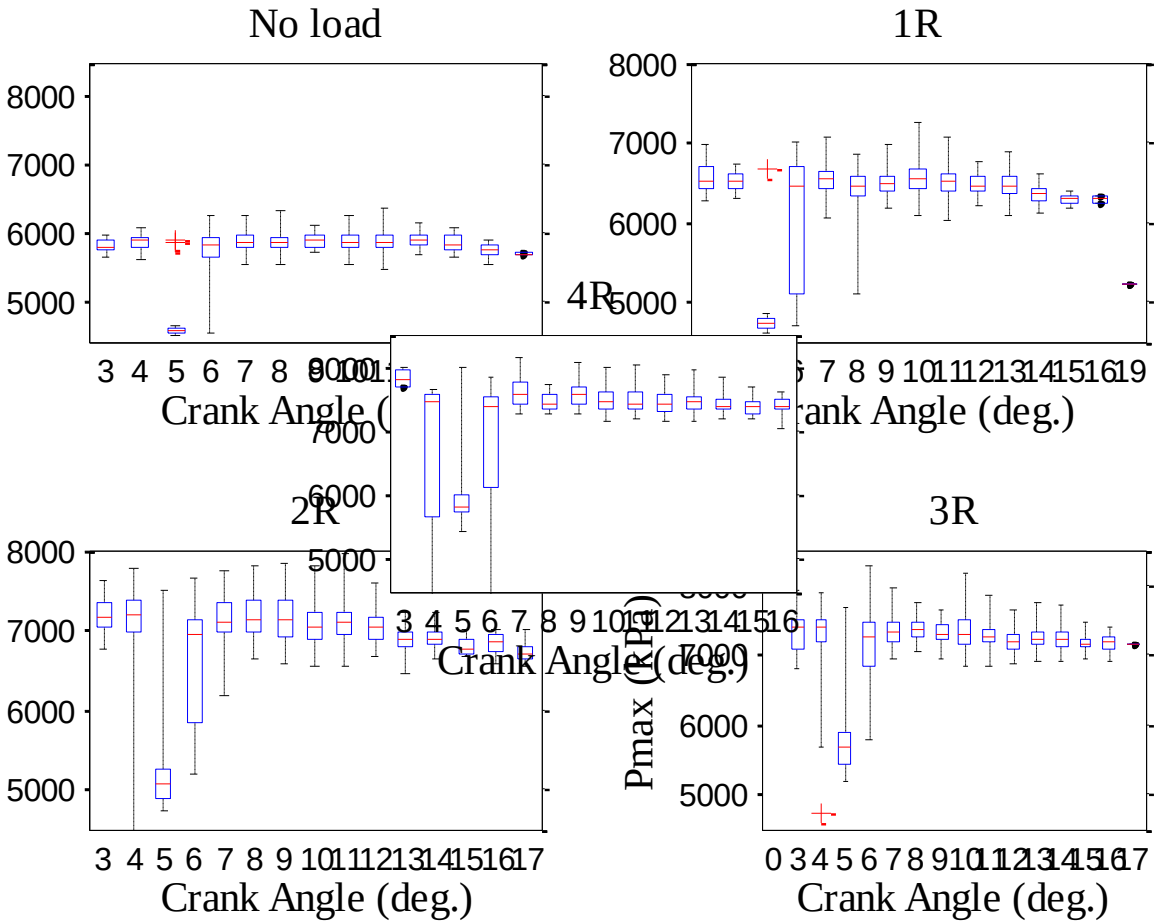

Figure 4.30: Box-and-whisker diagram of maximum pressure vs crank angle at 2800 rpm.

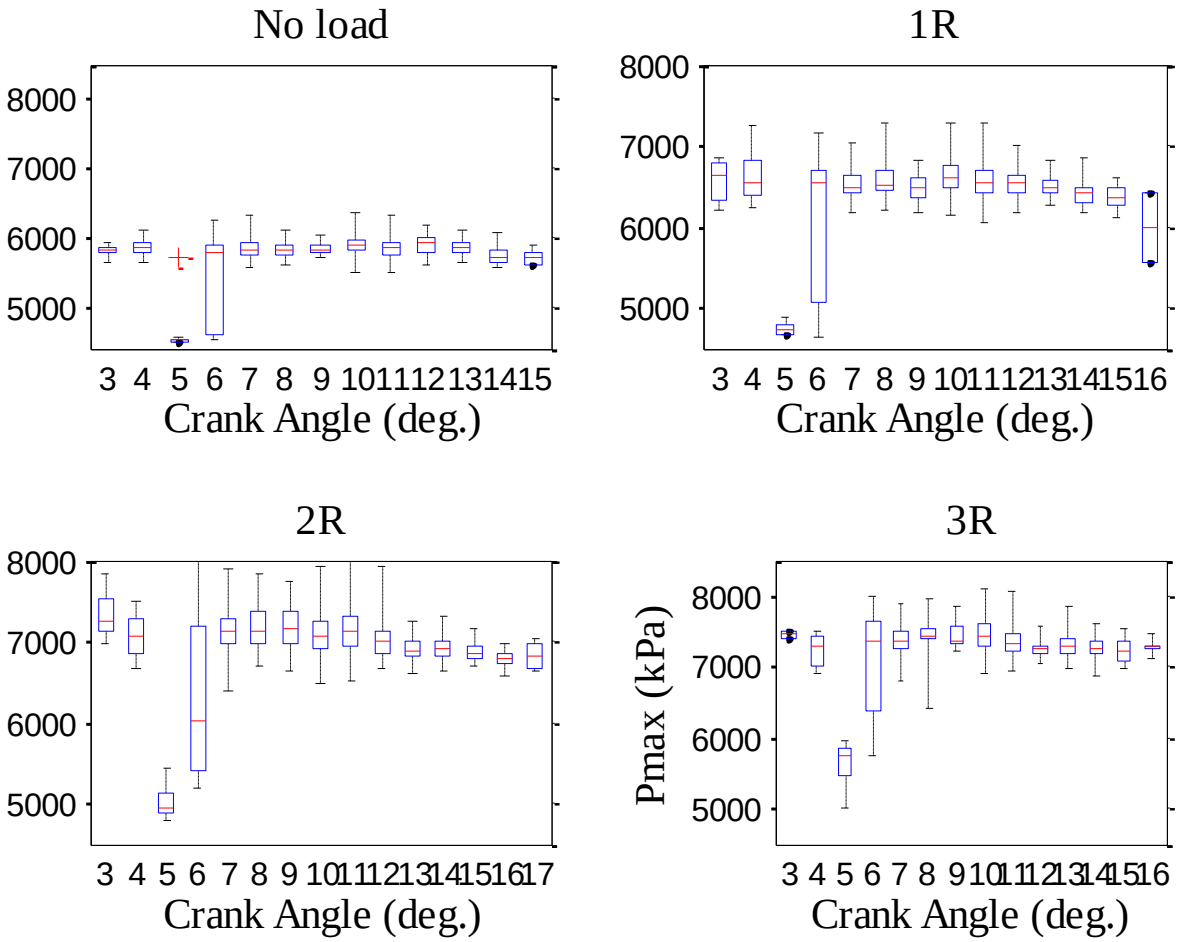

Figure 4.31: Box-and-whisker diagram of maximum pressure vs crank angle at 2900 rpm.

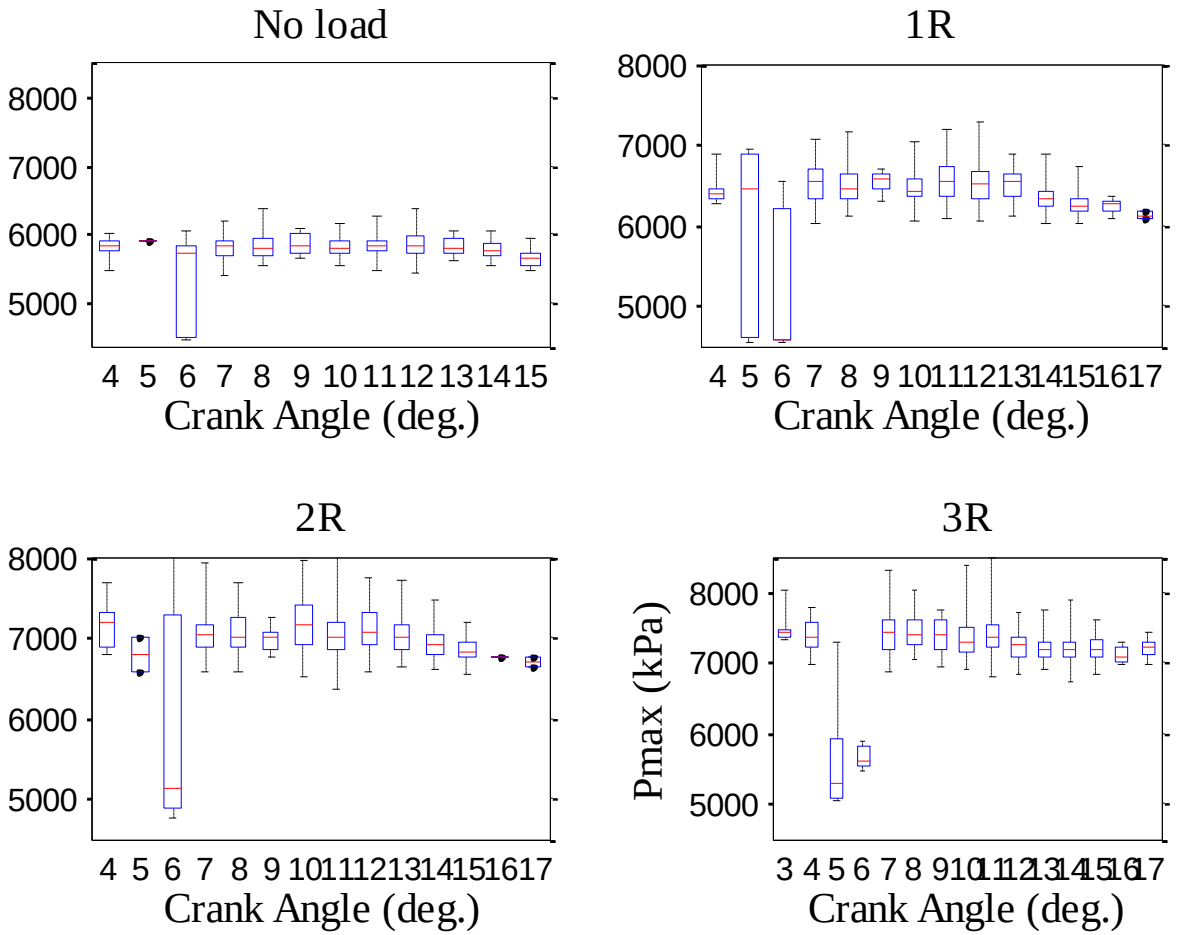

Figure 4.32: Box-and-whisker diagram of maximum pressure vs crank angle at 3100 rpm.

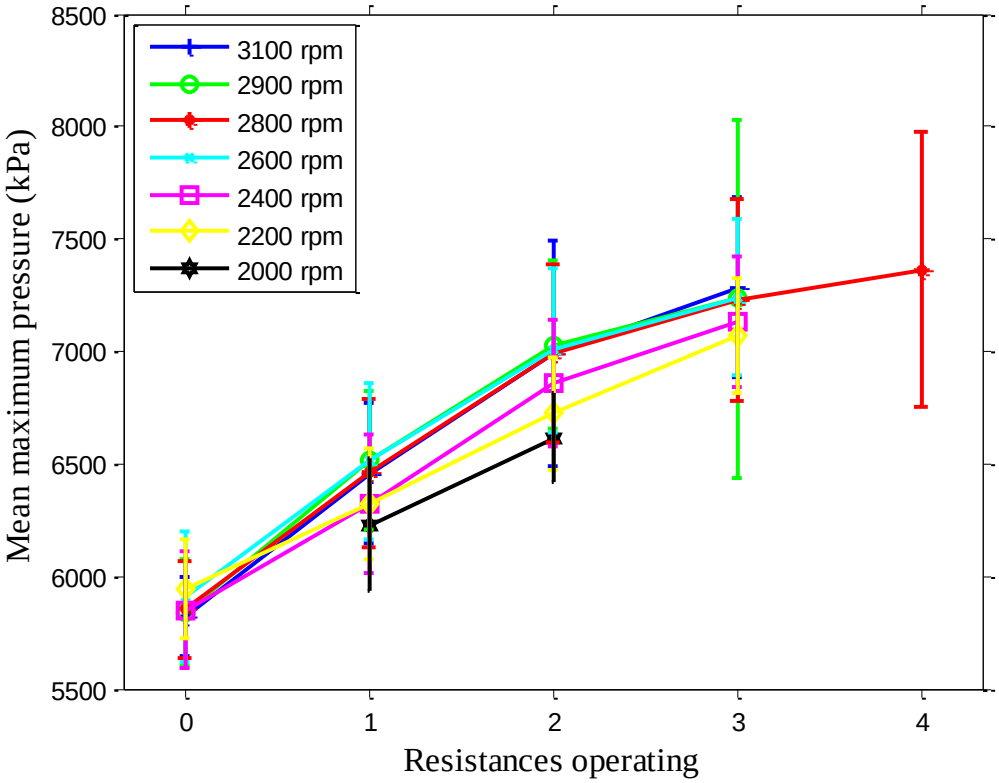

Figure 4.33: Mean maximum pressure vs resistances operating.

pressure, with 2800 and 3100 rpm have almost identical average pressure. Finally, at 3R 3100 rpm has the largest value with 2600 rpm have again identical value with 2800 and 2900.

In Figure 4.34 we plotted the COV of maximum pressure vs indicated load. It is noticeable that operation in low-medium rpm (2200, 2400, 2600 rpm) has the least fluctuation. Operation in medium-high rpm (2800, 2900, 3100 rpm) has larger fluctuation in COV. That fact may be attributed to the engine oscillations which were growing as we moved into higher rpm and load. COV of maximum pressure does not follow a specific trend.

Figure 4.35 illustrates an overall COV vs crank angle diagram at 2000 rpm and 1.5 kW indicated load. From 0 degrees to about 260, we notice no change in cylinder's pressure. This is the exhaust and intake phase of the combustion cycle.

On the other hand, COV line varies a lot. It goes up to 40%, then falls to 10%, up again to 60% etc. This is something that observed in the rest COV vs crank angle diagrams (not shown). The explanation for his particular behavior is that the piezoelectric transducer operates when inside the cylinder we have the pressure

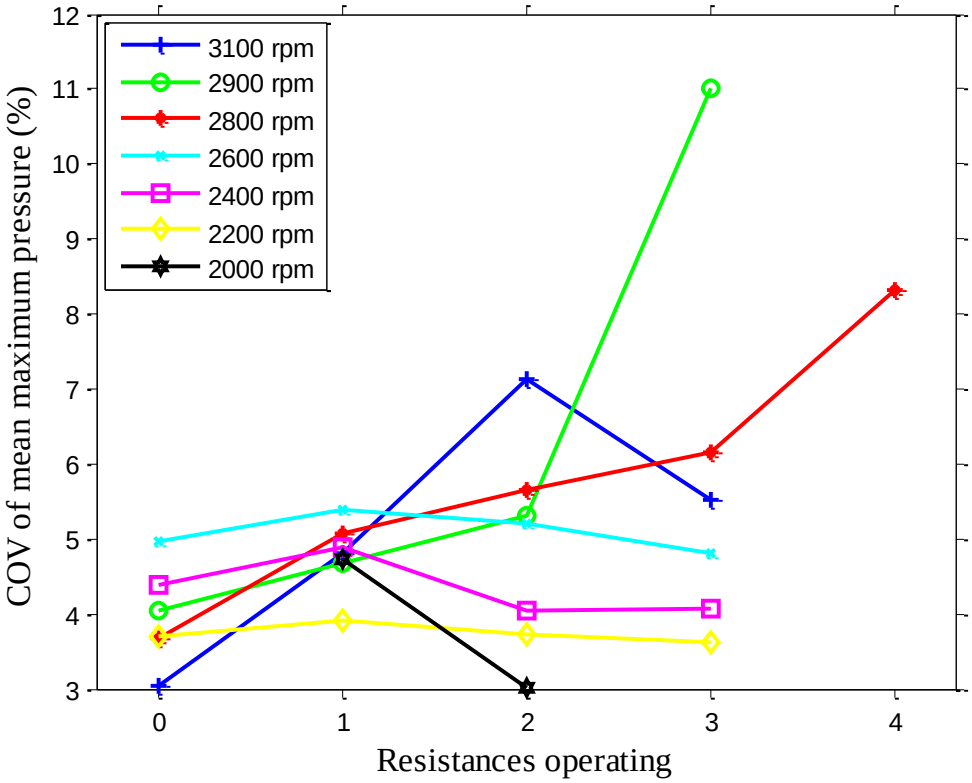

Figure 4.34: COV of maximum pressure vs resistances operating.

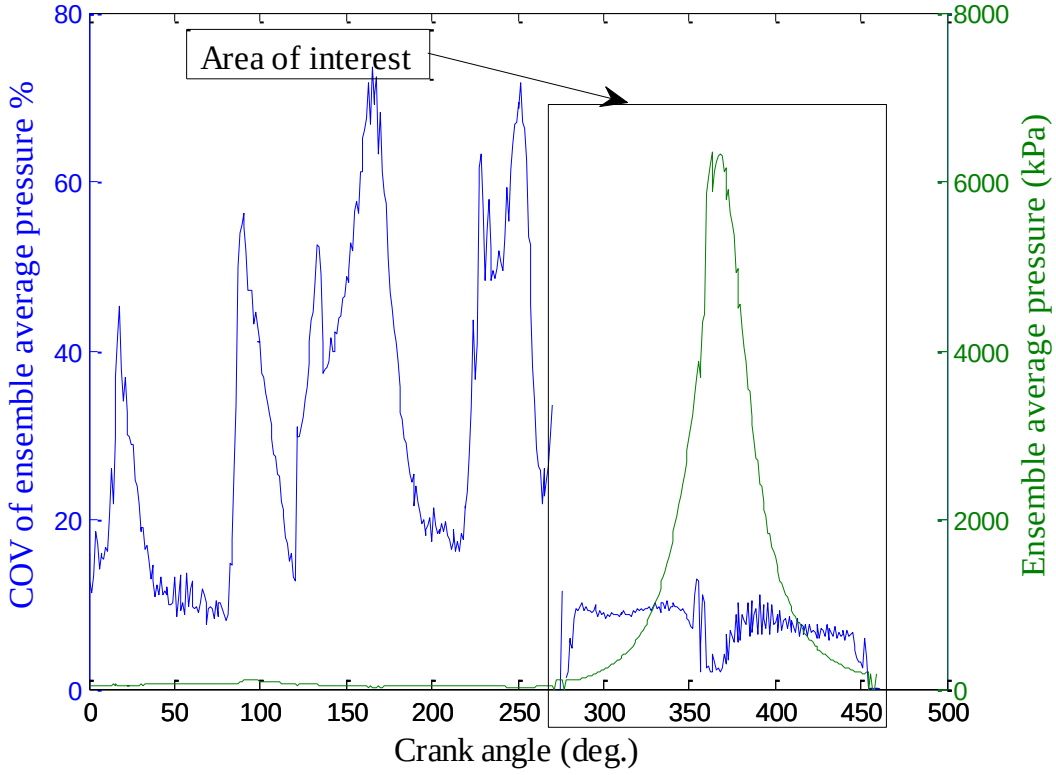

Figure 4.35: COV of ensemble average pressure vs crank angle, 2000 rpm, 1R, our area of interest.

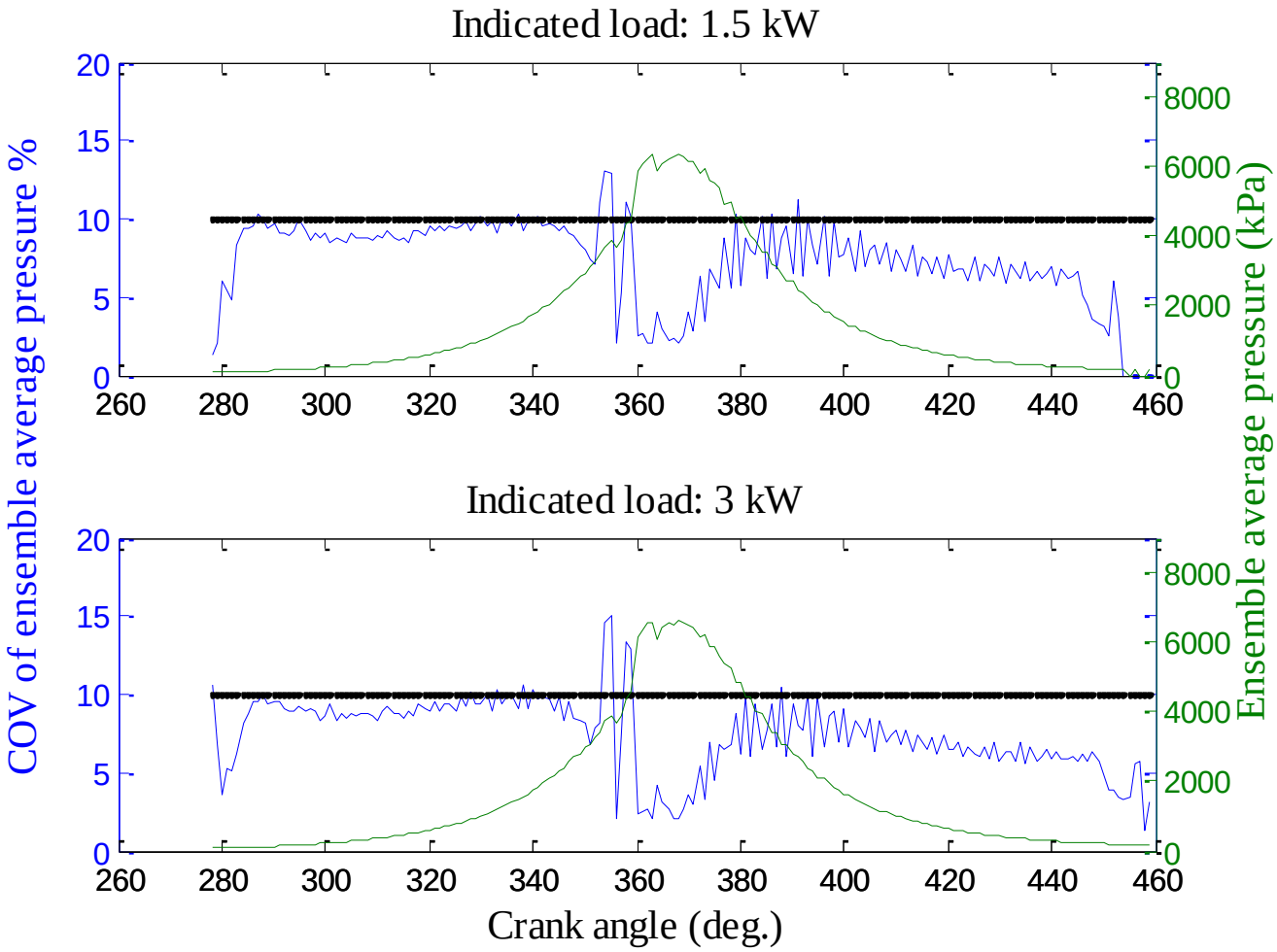

Figure 4.36: COV of ensemble average pressure vs crank angle at 2000 rpm.

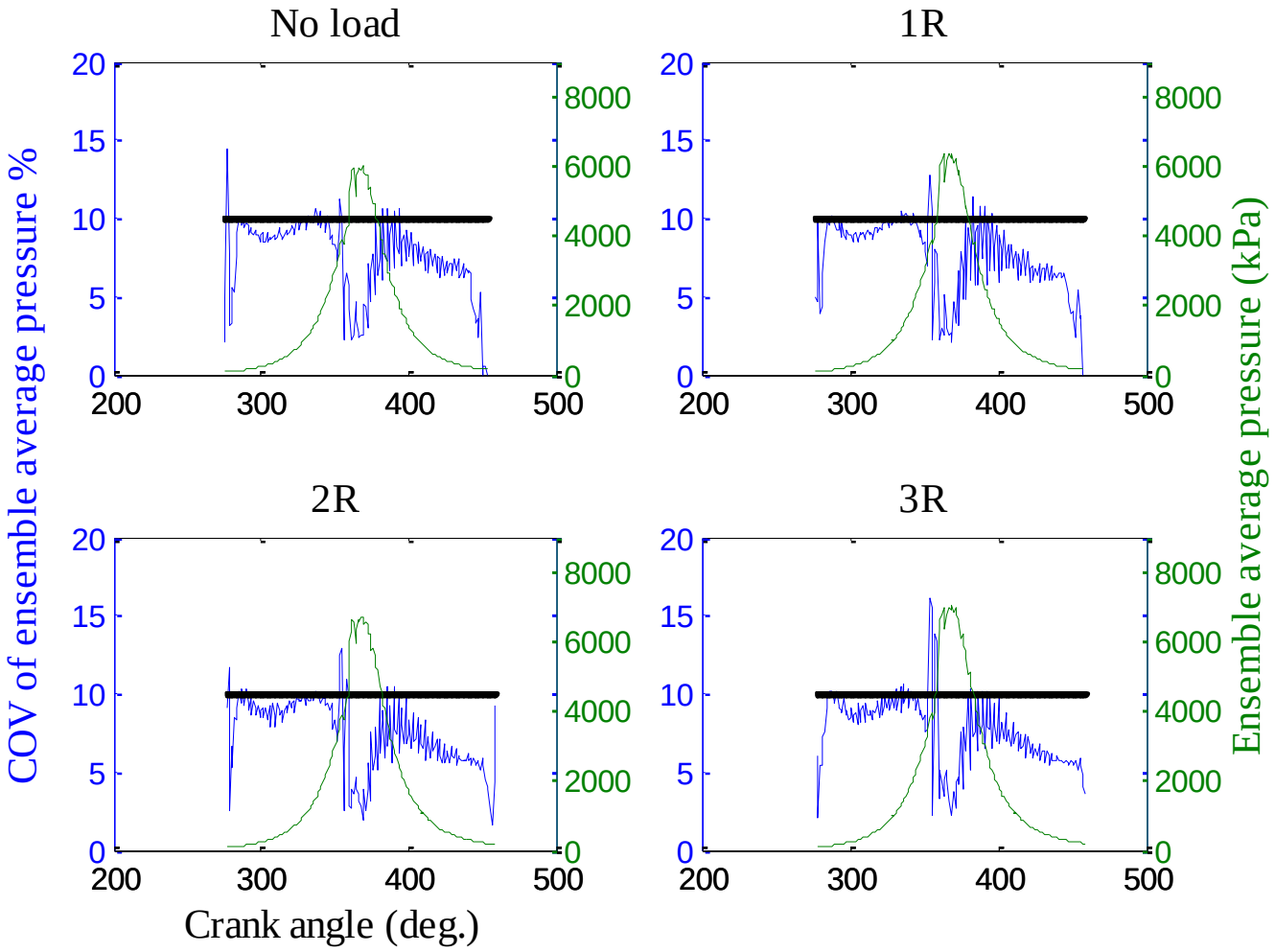

Figure 4.37: COV of ensemble average pressure vs crank angle at 2200 rpm.

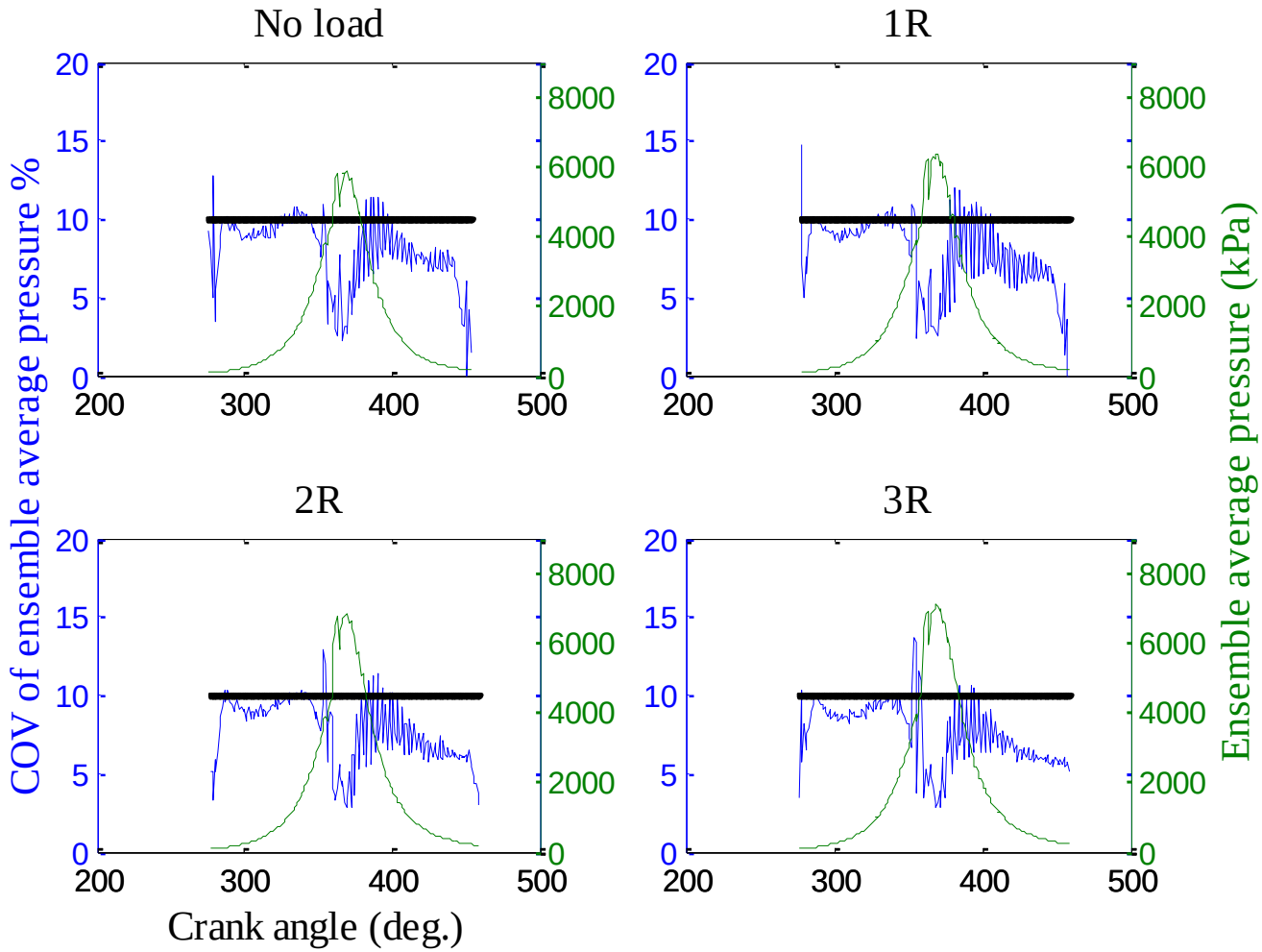

Figure 4.38: COV of ensemble average pressure vs crank angle at 2400 rpm.

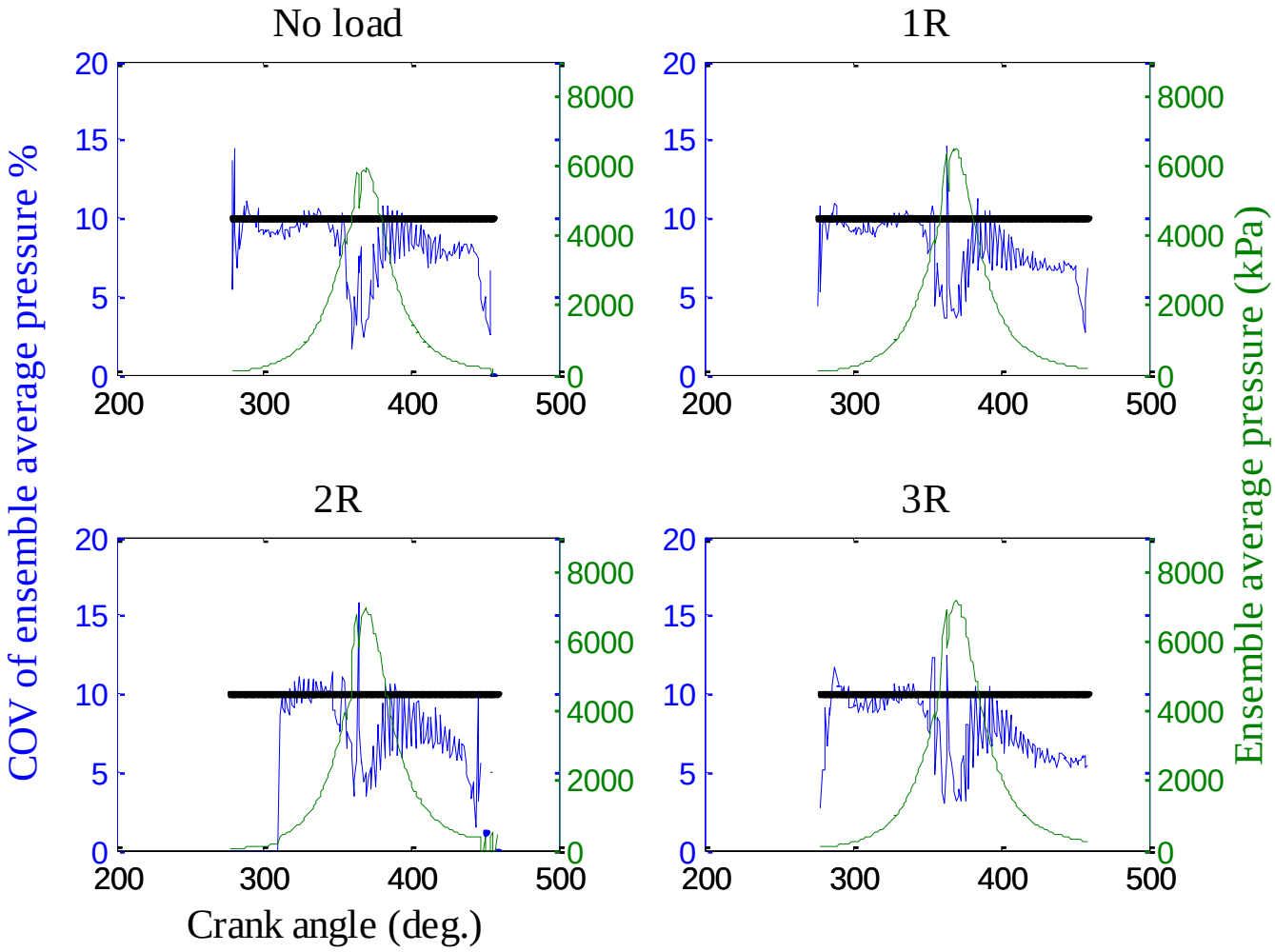

Figure 4.39: COV of ensemble average pressure vs crank angle at 2600 rpm.

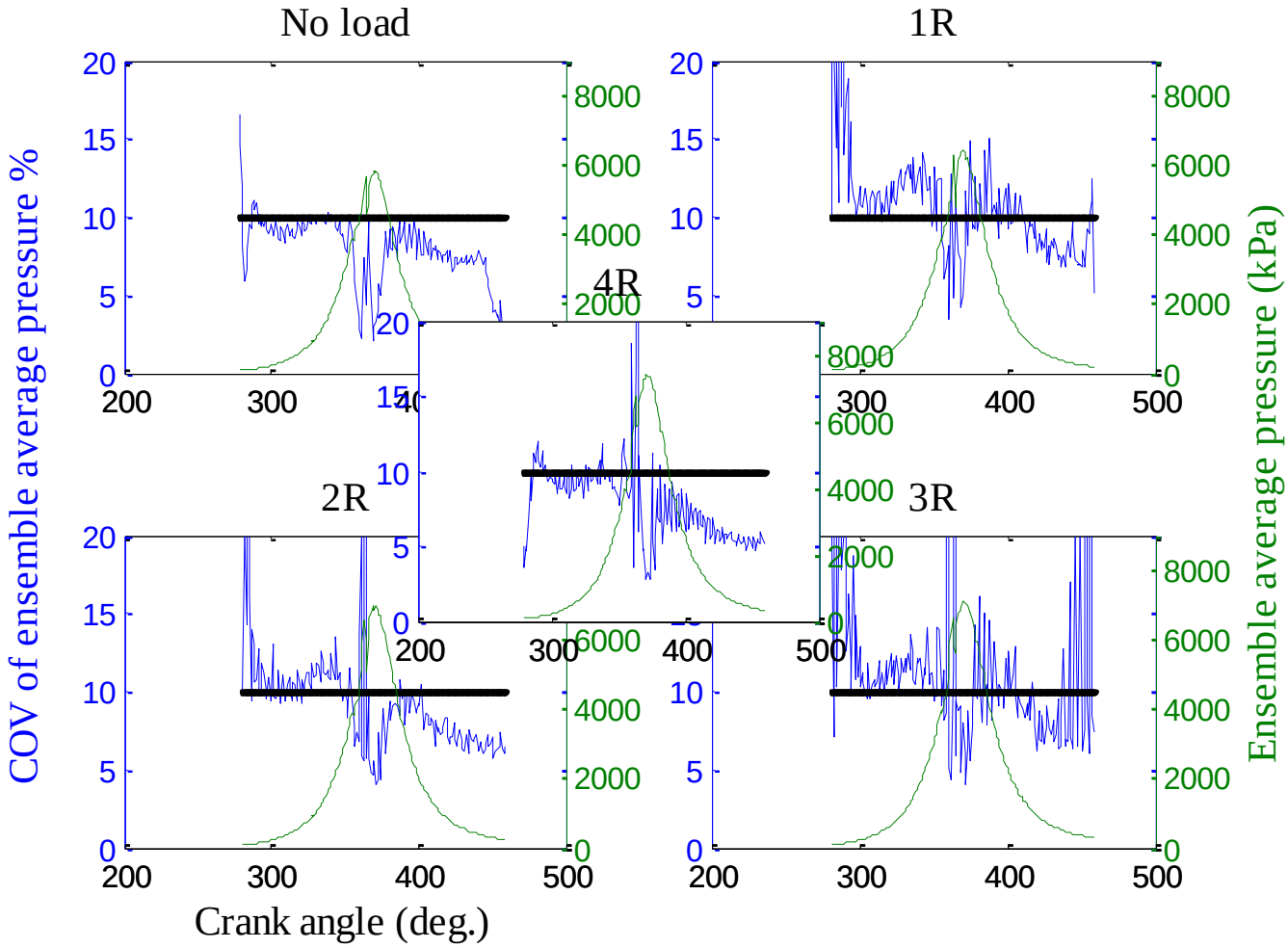

Figure 4.40: COV of ensemble average pressure vs crank angle at 2800 rpm.

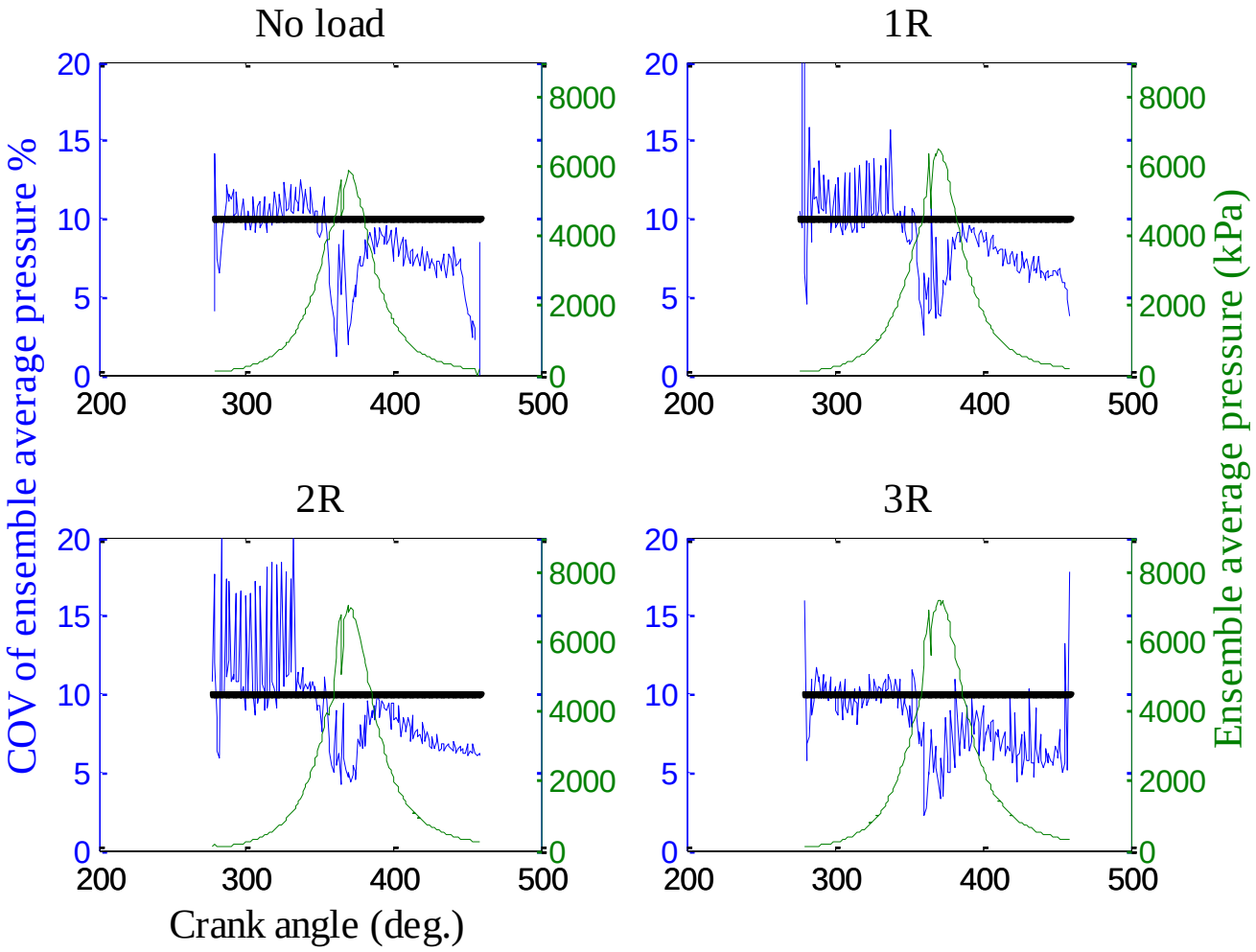

Figure 4.41: COV of ensemble average pressure vs crank angle at 2900 rpm.

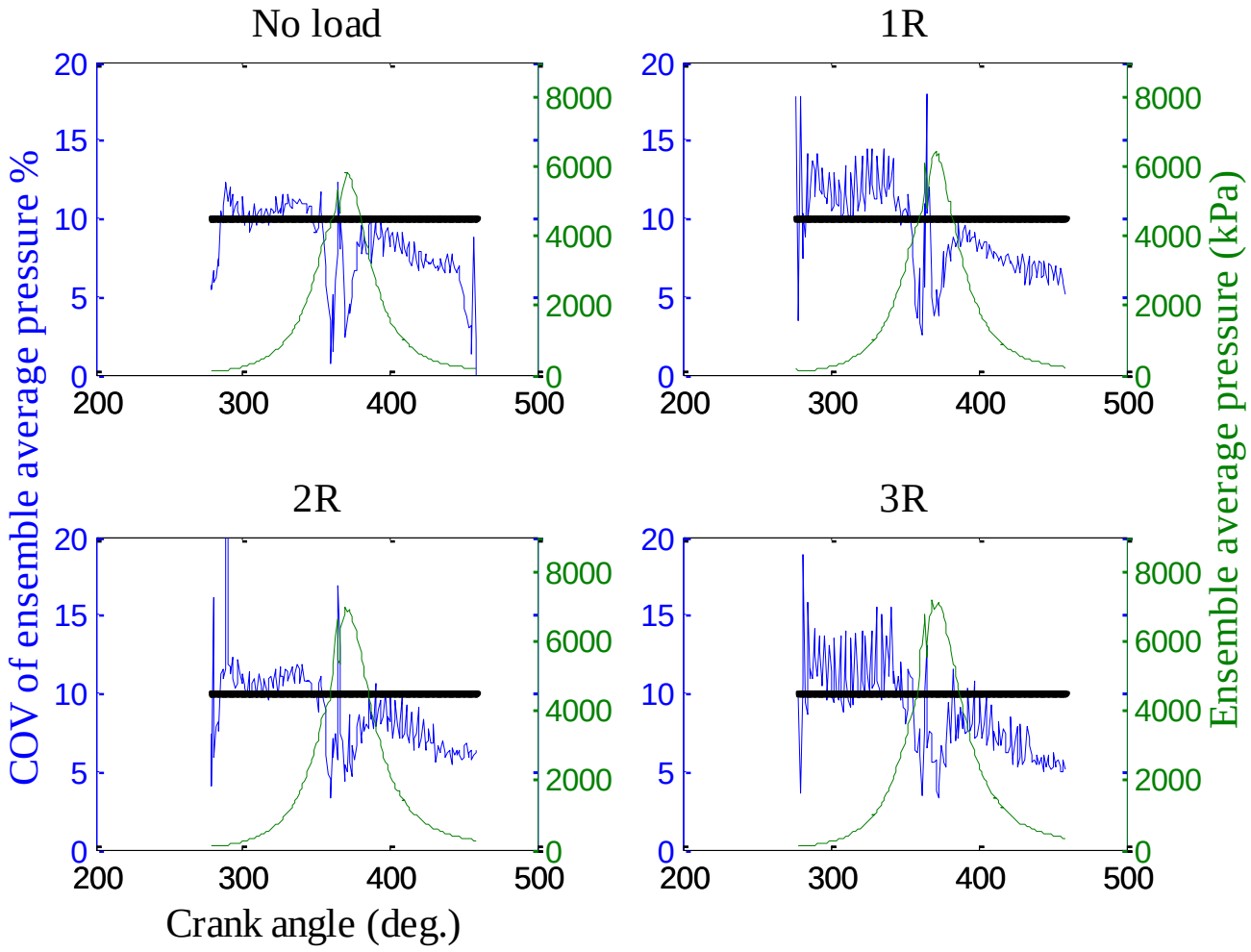

Figure 4.42: COV of ensemble average pressure vs crank angle at 3100 rpm.

changing. Thus, during the intake and the exhaust phase, no pressure change occurs. As a result, the piezoelectric sensor has no input variable, to give us voltage and translate it to pressure. So, we assume that the COV line from 0 degrees to 260 is noise from our sensor. Our area of interest, the compression and power phase of the combustion cycle, is shown in Figure 4.35. Figures 4.36 – 4.42 present the pressure and COV vs crank angle diagrams of all our operation points.

According to theory [6], if an engine operates smoothly, COV in each crank angle is below 10%. In Figures 4.36 – 4.42 the black line represents that 10% limit of good performance. In our measurements for 2000, 2200, 2400 and 2600 rpm COV has a normal behavior and is mostly below the 10% line apart from some random parts in each operation point and the compression phase in 2600 rpm with 2R. In 2800 rpm, COV appears to have the worst behavior. This is caused probably by the laser problems that took place during the 2800 rpm measurements. 2900 and 3100 rpm COV exceeds the 10% limit during the compression phase.

Furthermore, in all our operation points COV raises instantly when the fuel is injected into the cylinder (20^o bTDC) and drops below the level it was before the injection. Moreover, when the pressure abnormality reaches its lowest value, COV appears a local maximum point. This behavior occurs because when COV is calculated from Equation 10, mean pressure at each crank angle is in the denominator. Thus, pressure drops and COV rises locally.

Finally, after pressure reaches its peak, COV oscillates and fades to the end of the power phase of the combustion cycle.

4.3 Engine's indicated power

From our measurements we had pressure and crank angle data to process. The crank angle data we can turn them into volume data from Equation 1 or Equation 2 and obtain the graph shown in Figure 2.2. Then, we created a MatLab code to manipulate the vast amount of data we had. Thus, from the *PdV* integration, we could find the cylinder's indicated work in kJ and turn it into power from Equation 4 and Equation 5. In Figure 4.1 is shown an overall graph of the mean indicated cylinder's power for all our operation points.

Obviously, our cylinder should produce the maximum power at maximum load at maximum rpm, which happens. At 3R load and at 3100 rpm, our engine produces the

maximum indicated power for this series of measurements, 11.23 kW. We also expect the indicated power to rise proportionally as we load the engine and keeping the rpm stable, which also happens.

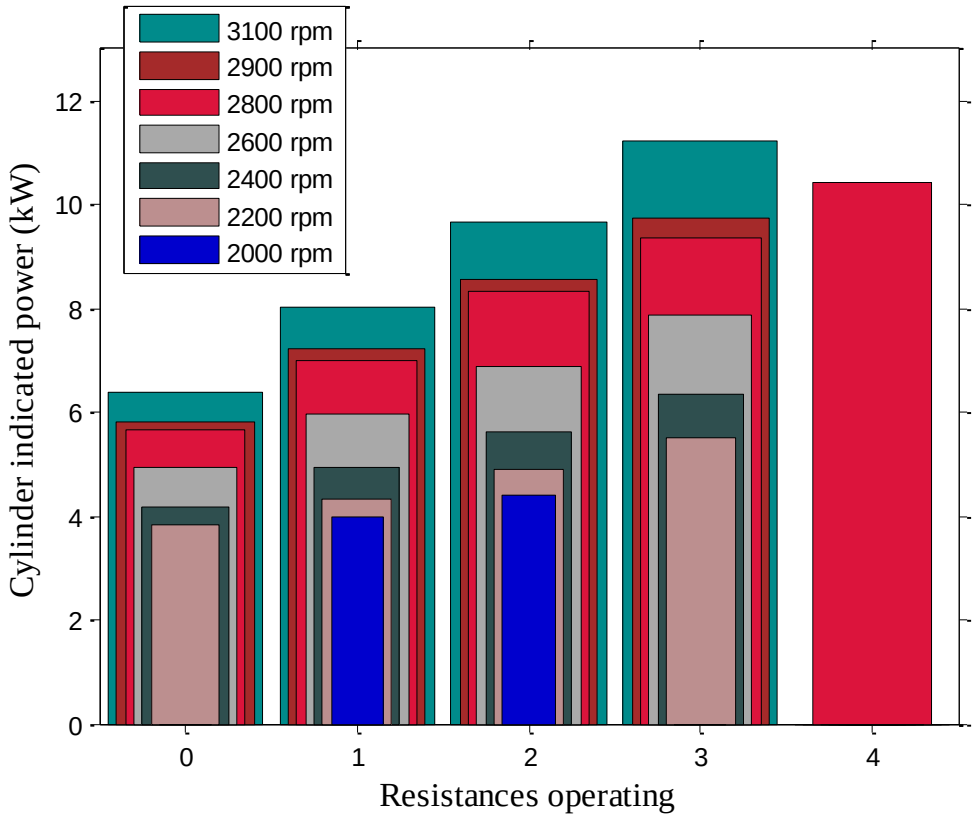

Figure 4.43: Overall cylinder's indicated power vs operating resistances.

Another way to exploit this graph is to compare similar power operating conditions with various engine characteristics such as brake specific fuel consumption (bsfc) and emission inventories, and among these conditions choose e.g. the less hazardous for the environment.

Last to mention, when integrating to find the indicated work per cycle, one would expect little differences when our engine operated without load, which is something that happens in our measurements (not shown). When it comes to compare the indicated power, we notice similar proportional indicated power rise instead. That is explained from Equation 4, where the indicated work per cycle is multiplied by the rpm at each operation point, thus the indicated power rises with rpm.

4.4 Energy Balance

From the theory governing engine energy balance discussed in chapter 2.3.1 one can easily create pie charts consisted of the brake work, the exhaust loss, the heat loss and friction loss of our engine.

Brake work is calculated from the difference of indicated power and friction power ($P_b = P_i - P_f$), whereas indicated and friction power are calculated from equation 5 (for friction power we assumed that fmep used was the 10% of the rpm real [6] and used equation 5).

Exhaust losses were calculated from the equation shown below [52]

$$Q_{exh} = \frac{1.02 \cdot \left(\dot{m}_a + \dot{m}_f \right) \cdot \left(T_{exh} - 25 \right)}{1000} \tag{14}$$

Finally heat losses were calculated from the difference of fuel energy ($\dot{m}_f Q_{LHV}$) and the brake work plus friction power plus exhaust losses.

The results are shown in Figures 4.44 – 4.15 for selected steady state operation points. In addition, Table 4.2 summarizes the thermal (P_b / Q_f) and indicated (P_i / Q_f) efficiency for these operation points.

For the operation points of concern, brake work ranges between 32 and 35 %, friction power between 16 and 26 %, heat losses between 15 and 30 % and exhaust losses between 18 and 26 %.

Brake work appears to have the lowest variation in our operation points (2000 – 2600 rpm and 1-3 resistances) and its percentage comes to accordance with theory and other energy balance experimental studies [5, 6, 32-34, 53-57].

The exhaust temperature in these rpm ranges between 161 and 231 ^{o}C and rises with rpm and engine load. This results in greater exhaust losses with both rpm and engine load.

Friction losses are in analogy with rpm. That is why they increase slightly with rpm and steady load and they drop with steady rpm and variable load. During our experiments we have set the engine in the indicated rpm without load and simply added load, without changing the rpm value. This way rpm decreased so as friction losses.

Finally heat losses appeared not to be disturbed with rpm rising, but dropping with steady rpm and adjustable load.

Indicated efficiency (Table 4.2) remains steady with rpm and adjustable load but it is droping by changing the load. Thermal efficiency has an almost steady value (~0.33).

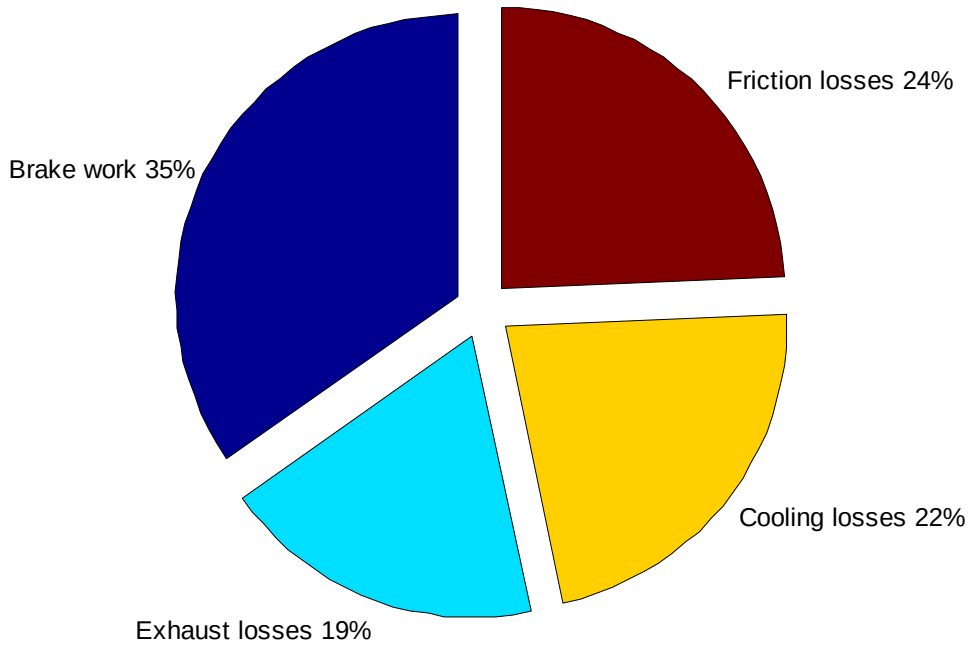

Figure 4.44: Distribution of the fuel energy – 2000 rpm 1R.

Table 4.2: Indicated and thermal efficiency for selected operation points.

Operation point	Indicated efficiency	Thermal efficiency
2000 rpm – 1R	0.59	0.35
2200 rpm – 1R	0.59	0.33
2200 rpm – 2R	0.55	0.35
2200 rpm – 3R	0.48	0.32
2400 rpm – 1R	0.60	0.33
2400 rpm – 2R	0.55	0.34
2400 rpm – 3R	0.51	0.34
2600 rpm – 1R	0.59	0.33

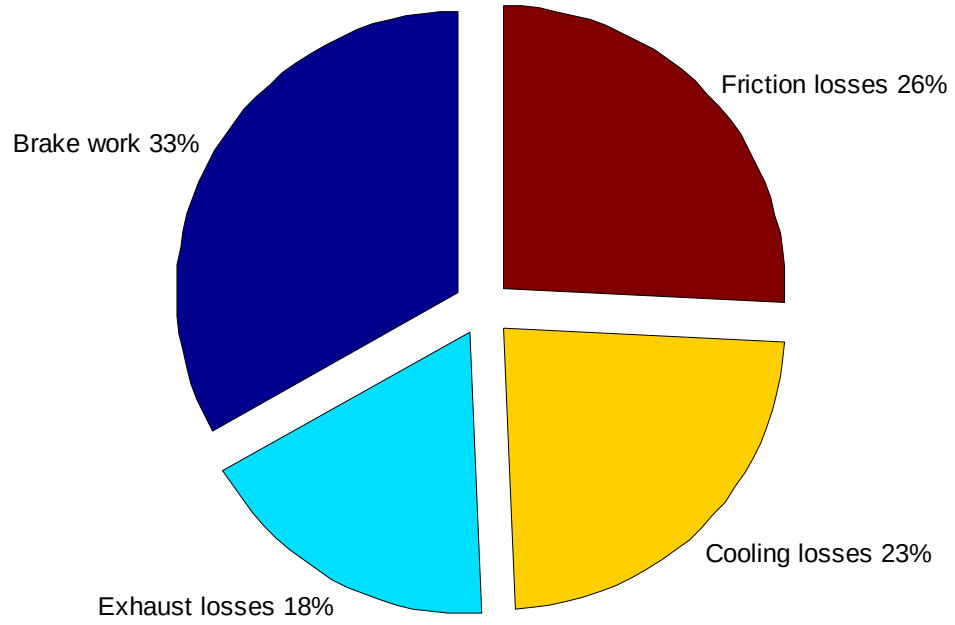

Figure 4.45: Distribution of the fuel energy – 2200 rpm 1R.

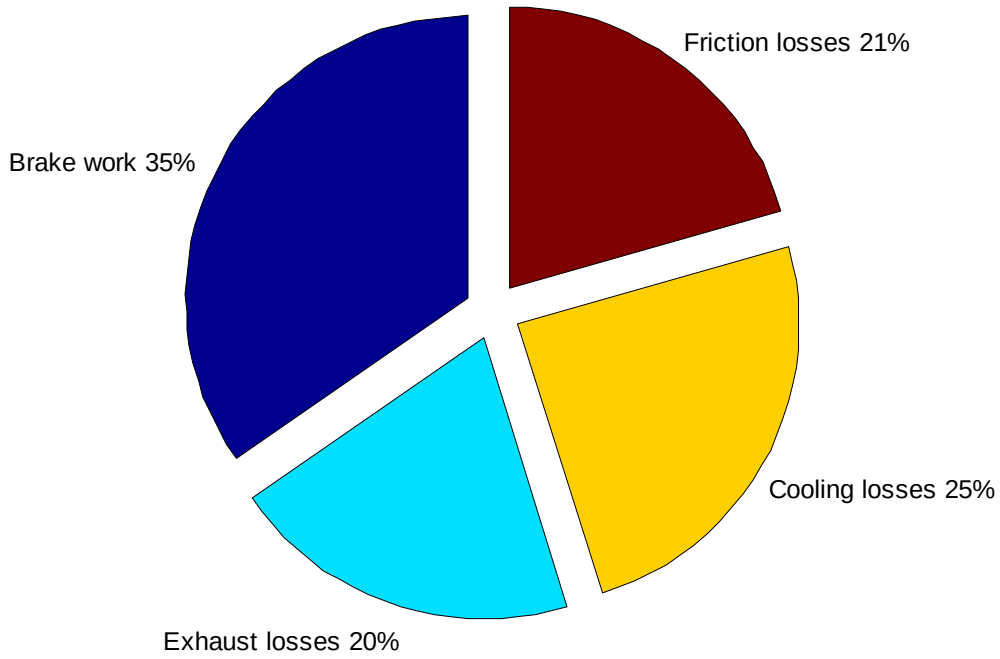

Figure 4.46: Distribution of the fuel energy – 2200 rpm 2R.

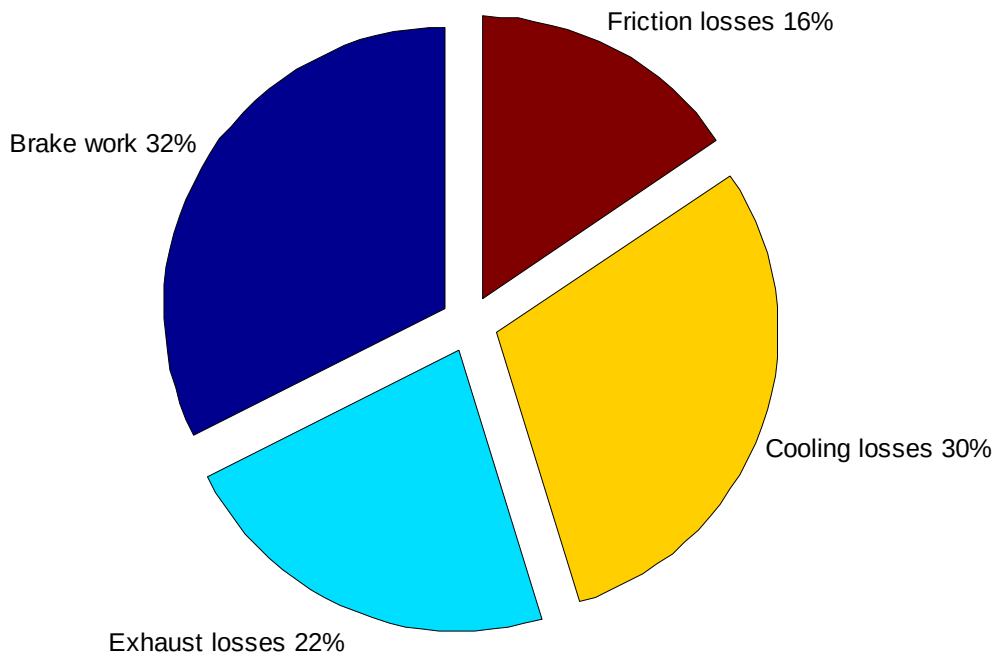

Figure 4.47: Distribution of the fuel energy – 2200 rpm 3R.

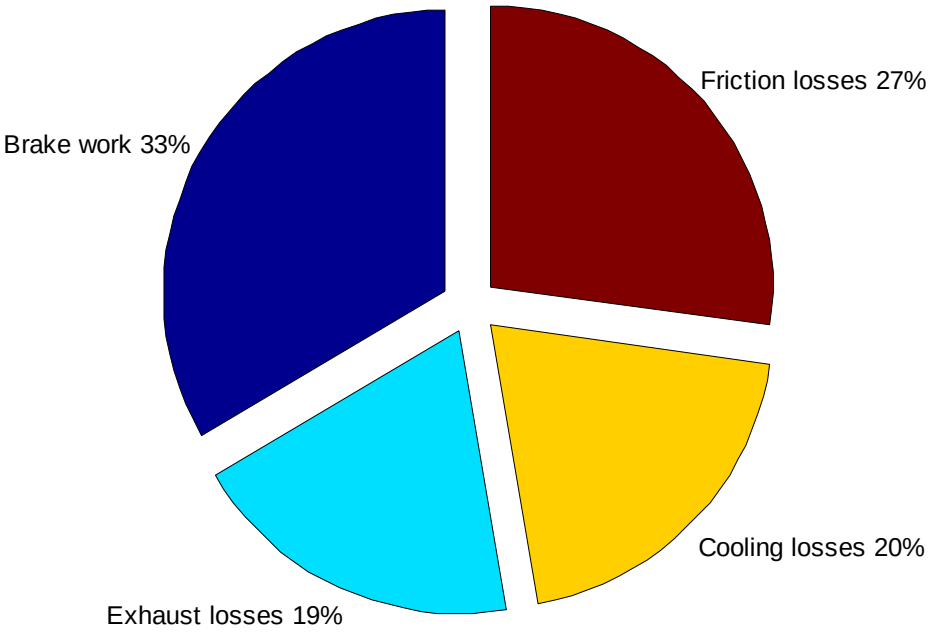

Figure 4.48: Distribution of the fuel energy – 2400 rpm 1R.

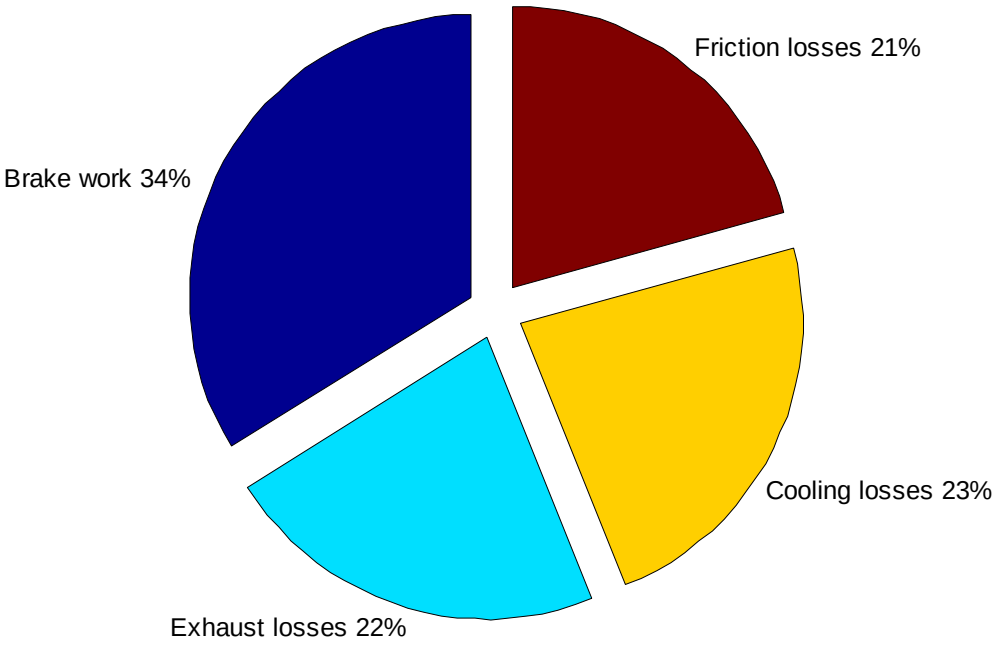

Figure 4.49: Distribution of the fuel energy – 2400 rpm 2R.

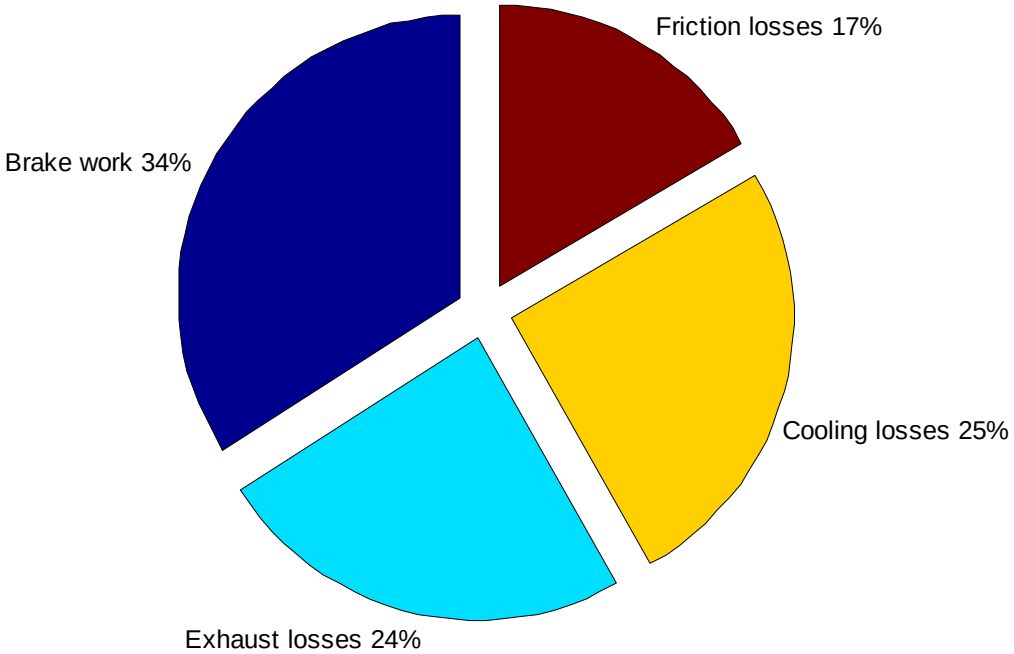

Figure 4.50: Distribution of the fuel energy – 2400 rpm 3R.

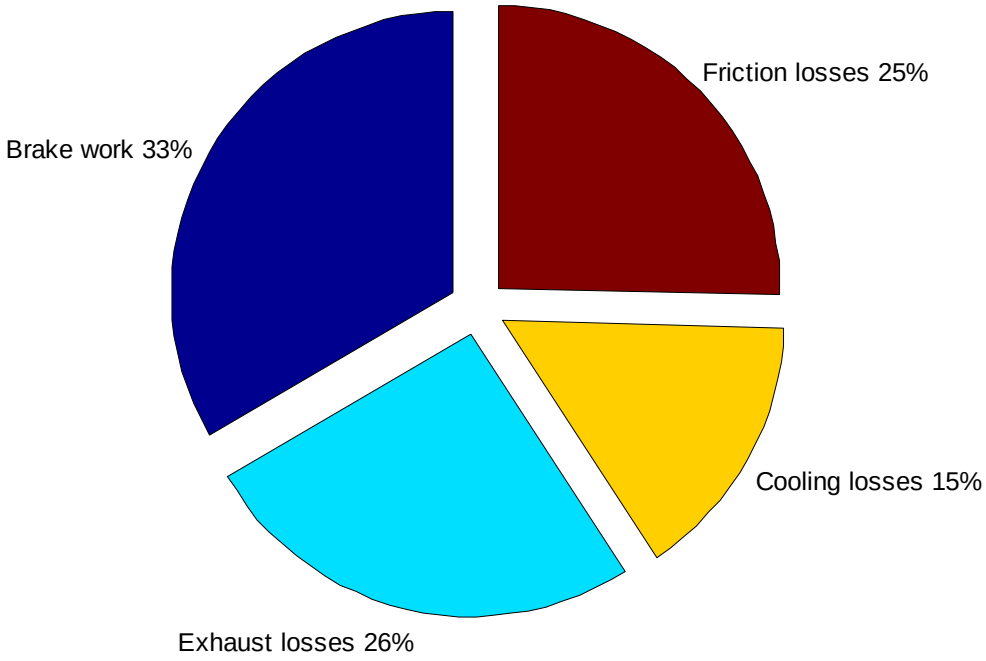

Figure 4.51: Distribution of the fuel energy – 2600 rpm 1R.

5 Conclusions and future work

5.1 Conclusions

Engine bench tests of the single cylinder diesel engine Ruggerini RF91 were conducted in the Laboratory of Thermodynamics and Thermal Engine, Department of Mechanical Engineers, University of Thessaly during September – December 2011. Our goal was to test the in-cylinder pressure development of our engine and its behavior by examining the COV_{imep} in steady state conditions.

The engine was tested in 2000, 2200, 2400, 2600, 2800, 2900 and 3100 rpm with the indicated load varying from 0 to 4 resistances (0 to 6 kW with 1.5 kW intervals). That depended to the engine's performance curves shown in APPENDIX A. Analytically our operating cycle is shown in Figure 3.21.

Concerning pressure and indicated power development, engine showed a normal behavior with pressure and indicated power rising with rpm and indicated load in all cases. When the ensemble average pressure in each crank angle was examined, two certain abnormalities appeared. The first abnormality takes place in cylinder's fuel

injection, about 20^o bTDC, and was attributed to the turbulent phenomena taking place. The second and more interesting abnormality takes place when pressure tries to reach its peak, about 5^o bTDC.

We measured the abnormality's length and height and found out that its length rises with rpm. Height has an almost similar behavior, with the height reaching its maximum value in 2800 or 2900 rpm and then falling again. Various assumptions have been made for its cause, with the most possible being the friction tape attached to the crank angle metal disk.

As for COV, we observed that in 2000, 2200, 2400 and 2600 rpm it mainly stays below its critical value 10%, in 2900 and 3100 rpm COV is slightly above 10% during the compression phase of our combustion cycle and in 2800 rpm operation, COV has the worst behavior because of laser problems that occurred during our measurements.

It is proposed for future tests to prefer the operation in 2600 rpm, where the COV does not exceed its critical value, the variation in maximum pressure is stable in its various operation points and the mean maximum pressure reaches the 2800, 2900 and 3100 values.

Also, 2800 rpm pressure experiments need to be repeated in order to have absolute correct results.

Our engine energy balance study is according to theory with the brake work varying from 32 and 35 %, friction power between 16 and 26 %, heat losses between 15 and 30 % and exhaust losses between 18 and 26 %.

5.2 Future work

To further investigate our engine, an exergy balance should be performed, in order to totally clarify the engine's exergy apparatus and the role of frictions. The data obtained for this thesis can be used.

In addition, due to the current global trend of alternative fuel use, our series of measurements need to be done with biodiesel and compare the results with other measurements.

Furthermore, it is of paramount importance to investigate how the abnormality indicated in this thesis behaves, apart from the change of load and rpm. For this reason a new LabView code needs to be developed so the sudden pressure drop not to be revealed in a similar analysis.

Last, new data acquisition codes must be developed to have clear pressure results from 0 to 720 degrees and not manipulate the obtained ones to investigate the combustion process.

References

1. Han, S.B., *Cycle-to-Cycle Variations Under Cylinder-Pressure-Based Combustion Analysis in Spark Ignition Engines.* KSME International Journal, 2000. **14**(10): p. 1151-1158.
2. Ceviz, M.A., et al., *Determination of cycle number for real in-cylinder pressure cycle analysis in internal combustion engines.* Energy, 2011. **36**: p. 2465-2472.
3. Zeibekis, S., *Mapping of Ruggerini RF91 engine and measurement of the charecteristics of particulate filter loading-regeneration equipped on engine*, in *Department of Mechanical Engineering*. 2003, University of Thessaly: Volos.
4. Melissourgos, G., *Code development for a P-V diagram from a single cylinder diesel engine*, in *Department of Mechanical Engineering*. 2010, University of Thessaly: Volos.
5. Mollenhauer, K. and H. Tschoeke, *Handbook of Diesel Engines*. 2010, Berlin Heidelberg: Springer-Verlag.
6. Heywood, J.B., *Internal Combustion Engine Fundamentals*. 1988, New York: McGraw-Hill.
7. *Diesel Engine*. 2011; Available from: http://www.britannica.com/EBchecked/topic/162716/diesel-engine.
8. Pulkrabek, W.W., *Engineering Fundamentals of the Internal Combustion Engine*. 2004: Prentice Hall.
9. Zervas, E., *Correlations between cycle-to-cycle variations and combustion parameters of a spark ignition engine.* Applied Thermal Engineering, 2004. **24**: p. 2073–2081.
10. Galloni, E., *Analyses about parameters that affect cyclic variation in a spark ignition engine.* Applied Thermal Engineering, 2008. **29**: p. 1131–1137.
11. Maurya, R.K. and A.K. Agarwal, *Experimental investigation on the effect of intake air temperature and air–fuel ratio on cycle-to-cycle variations of HCCI combustion and performance parameters.* Applied Energy, 2010. **88**: p. 1153–1163.
12. Ceviz, M.A., et al., *Determination of cycle number for real in-cylinder pressure cycle analysis in internal combustion engines.* Energy, 2011. **36**: p. 2465-2472.
13. Kouremenos, D.A., C.D. Rakopoulos, and K.G. Kotsos., *A Stochastic-experimental investigation of the cyclic pressure variation in a DI single-cylinder diesel engine* International Journal of Energy Research, 1992. **16**(865): p. 877.
14. Rakopoulos, D.C., et al., *Experimental-stochastic investigation of the combustion cyclic variability in HSDI diesel engine using ethanol–diesel fuel blends.* Fuel 2008. **87**: p. 1478–1491.
15. Özkan, M., *Comparative Study of the Effect of Biodiesel and Diesel Fuel on a Compression Ignition Engine's Performance, Emissions, and Its Cycle by Cycle Variations.* Energy & Fuels, 2007. **21**: p. 3627–3636.
16. Barboza, A.B.V., N.Y. Sharma, and C.V. Sudhir, *Cyclic Combustion Studies of a CI Engine Operating on Jatropha B20 Fuel*, in *International Conference on Mechanical and Electrical Technology*. 2010.

17. Han, S.B., *Investigation of Cyclic Variations of IMEP Under Idling Operation in Spark Ignition Engines.* KSME International Journal, 2001. **15**(1): p. 81-87.
18. Cosadia, I., et al., *Cyclic variations of the swirling flow in a Diesel transparent engine.* Experiments in Fluids, 2006. **41**: p. 115-134.
19. Po, L., S. Tielong, and O. Yasufumi, *Experimental Analysis and Control-Oriented Modeling for Cyclic Variation of Cylinder Pressure in IC Engines*, in *26th Chinese Control Conference*. 2007: Zhangjiajie, Hunan, China.
20. Galloni, E., *Analyses about parameters that affect cyclic variation in a spark ignition engine.* Applied Thermal Engineering, 2009. **29**: p. 1131–1137.
21. Mittal, M. and H.J. Schock, *A Study of Cycle-to-Cycle Variations and the Influence of Charge Motion Control on In-Cylinder Flow in an IC Engine.* Journal of Fluids Engineering, 2010. **132**(5): p. 051107 (8 pages).
22. Wang, J., et al., *Study of cycle-by-cycle variations of a spark ignition engine fueled with natural gas–hydrogen blends.* International journal o f hydrogen energy, 2008. **33**: p. 4876–4883.
23. Ma, F., et al., *Effects of hydrogen addition on cycle-by-cycle variations in a lean burn natural gas spark-ignition engine.* International journal o f hydrogen energy, 2008. **33**: p. 823-831.
24. Zheng, J., et al., *Effect of Compression Ratio on Cycle-by-Cycle Variations in a Natural Gas Direct Injection Engine.* Energy Fuels, 2009. **23**: p. 5357–5366.
25. Sen, A.K., J. Zheng, and Z. Huang, *Dynamics of cycle-to-cycle variations in a natural gas direct-injection spark-ignition engine.* Applied Energy, 2011. **88**: p. 2324–2334.
26. Tang, D., et al., *Investigation on the combustion cyclic variability in a non-road diesel engine fuelled with diesel/bio-diesel blends* in *International Conference on Electric Information and Control Engineering* 2011. p. 2286 - 2289
27. Ciniviz, M., *Performance and energy balance of a low heat rejection diesel engine operated with diesel fuel and ethanol blend.* Transactions of the Canadian Society for Mechanical Engineering, 2010. **34**(1): p. 93-104.
28. Sayin, C., et al., *Energy and exergy analyses of a gasoline engine.* International Journal of Energy Research, 2010. **31**: p. 259-273.
29. Sekmen, P. and Z. Yılbaşı, *Application of energy and exergy analyses to a CI engine using biodiesel fuel.* Mathematical and Computational Applications, 2011. **16**(4): p. 797-808.
30. Wallace, S.J., *Diesel engine energy balance study operating on diesel and biodiesel fuels*, in *Russ College of Engineering and Technology*. 2007, Ohio University: Ohio.
31. Canakci, M. and M. Hosoz, *Energy and Exergy Analyses of a Diesel Engine Fuelled with Various Biodiesels.* Energy Sources, Part B: Economics, Planning, and Policy, 2006. **1**(4): p. 379-394.
32. Bourhis, G. and P. Leduc, *Energy and Exergy Balances for Modern Diesel and Gasoline Engines.* Oil & Gas Science and Technology, 2010. **65**(1): p. 39-46.
33. Ajav, E.A., B. Singh, and T.K. Bhattacharya, *Thermal balance of a single cylinder diesel engine operating on alternative fuels.* Energy Conversion & Management, 2000. **41**: p. 1533-1541.
34. Taymaz, I., *An experimental study of energy balance in low heat rejection diesel engine.* Energy, 2003. **31**: p. 364-371.

35. Moran, M.J. and H.N. Shapiro, *Fundamentals of Engineering Thermodnamics*. 2007, West Sussex: John Wiley & Sons Ltd.
36. Rakopoulos, C.D. and E.G. Giakoumis, *Second-law analyses applied to internal combustion engines operation.* Progress in Energy and Combustion Science, 2006. **32**(1): p. 2-47.
37. Rakopoulos, C.D. and D.C. Kyritsis, *Comparative second-law analysis of internal combustion enginge operation for methane, methanol, and dodecane fuels.* Energy, 2001. **26**(7): p. 705-722.
38. Van Gerpen, J.H. and H.N. Shapiro, *Second-law analysis of diesel engine combustion.* Journal of Engineering for Gas Turbines and Power, 1990. **112**(1): p. 129-137.
39. RuggeriniSparePartsCatalogue. Available from: http://www.condustrial.com.co/Admin/Fichas/Ficha171.pdf.
40. LombardiniGroup. Available from: http://www.lombardinigroup.it/en_US/homepage.
41. ElinOil. Available from: http://www.elin.gr/en.html.
42. Jaaskelainen, H. *Biodiesel Standards & Properties*. 2007; Available from: www.dieselnet.com.
43. Knothe, G., *"Designer" Biodiesel: Optimizing Fatty Ester Composition to Improve Fuel Properties.* Energy & Fuels, 2008. **22**: p. 1358–1364.
44. Tziourtzioumis, D., et al., *Experimental investigation of the effect of a B70 biodiesel blend on a common-rail passenger car diesel engine.* Proceedings of the Institution of Mechanical Engineers, Part D: Journal of Automobile Engineering, 2009. **223**(5): p. 695-701.
45. NSM. *Use and maintenance manual*. Available from: http://www.condustrial.com.co/despieces/5_OTROS_EQUIPOS_CONSORCIO/NSM_MS100.pdf.
46. HSaOy. *Data for generator MS 100LG*. Available from: http://www.hsaoy.com/generaattorit/nsm/ms100.html.
47. Omega. *Revised Type-K Thermocouple Reference Tables*. Available from: http://www.omega.com/temperature/z/pdf/z204-206.pdf.
48. Kistler. *High-Temperature Pressure Sensor for combustion engine measurement, Type 6052B*. Available from: http://www.kistler.com/mediaaccess/000-016e-02.02.pdf.
49. KERN. *440 Precision balance*. 2009; Available from: http://www.kern-sohn.com/en/shop/catalogue-9.html.
50. NationalInstruments. *NI PCI-6259*. 2011; Available from: http://sine.ni.com/nips/cds/view/p/lang/en/nid/14128.
51. NationalInstruments. *Specifications for the DAQCard-AI-16XE-50*. 2011; Available from: http://digital.ni.com/manuals.nsf/websearch/6B4038404C0BD9218625665E00642111.
52. Moran, M.J. and H.N. Shapiro, *Fundamentals of Engineering Thermodynamics*. 2003, New York: John Wiley & Sons, Inc.
53. Canakci, M. and M. Hosoz, *Energy and Exergy Analyses of a Diesel Engine Fuelled with Various Biodiesels.* Energy Sources, 2006. **1**: p. 379–394.
54. Wallace, S.J., *Diesel engine energy balance study operating ondiesel and biodiesel fuels*, in *Russ College of Engineering and Technology of Ohio University*. 2007: Ohio.

55. Ciniviz, M., *Performance and energy balance of a low heat rejection diesel engine operated with diesel fuel and ethanol blend.* Transactions of the Canadian Society for Mechanical Engineering, 2009. **34**(1): p. 93-104.
56. Sekmen, P. and Z. Yılbaşı, *Application of energy and exergy analyses to a CI engine using biodiesel fuel.* Mathematical and Computational Applications, 2011. **16**(4): p. 797-808.
57. Sayin, C., et al., *Energy and exergy analyses of a gasoline engine.* International journal of energy research, 2007. **31**: p. 259–273.

APPENDIX A Ruggerini RF91 performance curves